1-1-2009

A Numerical Study On Active Film Cooling Flow Control Through The Use Of Sister Holes

Marc J. Ely
Ryerson University

A NUMERICAL STUDY ON ACTIVE FILM COOLING FLOW CONTROL THROUGH THE USE OF SISTER HOLES

by

Marc J. Ely
B.Eng Aerospace Engineering
Ryerson University

A thesis
Presented to Ryerson University

In partial fulfillment of the
Requirements for the degree of

Masters of Applied Science
in the program of
Aerospace Engineering

Toronto, Ontario, Canada, 2009

This Page Intentionally Left Blank

Author's Declaration

I hereby declare that I, Marc Ely, am the sole author of this thesis titled "A Numerical Study on Active Film Cooling Flow Control Through the Use of Sister Holes".

I authorize Ryerson University to lend this thesis to other institutions or individuals for the purpose of scholarly research.

Marc J. Ely

I further authorize Ryerson University to reproduce this thesis by photocopying or by other means, in total or in part, at the request of other institutions or individuals for the purpose of scholarly research.

Marc J. Ely

This Page Intentionally Left Blank

Abstract

A NUMERICAL STUDY ON ACTIVE FILM COOLING FLOW CONTROL THROUGH THE USE OF SISTER HOLES

Masters of Applied Science
2009

Marc J. Ely
Aerospace Engineering
Ryerson University

The research contained herein studied the effect of sister holes on film cooling. This novel technique surrounds a primary injection hole by two or four smaller sister holes to actively maintain flow adhesion along the surface of the blade. A numerical evaluation using the realizable k-ε turbulence model led to the determination that the use of sister holes significantly improves adiabatic effectiveness by countering the primary vortical flow structure. Research was performed to determine the optimal hole configuration, arriving at the conclusion that placing sister holes slightly downstream of the primary injection hole improves the near-hole effectiveness, while placing sister holes slightly upstream of the primary hole improves downstream effectiveness. Similar results were found in evaluating both long and short hole geometries with a significantly less coherent flow field arising from the short hole study. However, on the whole, the sister hole approach to film cooling was found to offer viable improvements over standard cooling regimes.

This Page Intentionally Left Blank

Acknowledgements

The author would like to thank his supervisor, Dr. Bassam Jubran, for his support and insight through the process of completing this thesis and publishing its related papers. His helpful thought provoking insight continually brought fresh ideas and inspiration to this project.

Thanks are also due to the author's girlfriend, Cassie, and parents, Sharon and Ted, for their love, support, and most of all, patience, over the two years it took to complete this work.

A special thank you goes out to the author's lab mates, Marcel Leon de Paz and Mohammed Gandhi whom offered a broad knowledge base and great friendship to help the author through the research process.

Finally, the author would like to thank the Natural Science and Engineering Research Council of Canada and the Government of Ontario for their support in funding this research. Additional thanks also go out to the High Performance Computing Virtual Laboratory for their funding support as well as their tremendous resources.

This Page Intentionally Left Blank

Table of Contents

List of Tables

This Page Intentionally Left Blank

Table of Figures

Nomenclature

Alphabetical

A	Area
C	Closure Coefficient
D	Diameter
DR	Density Ratio
E	Distance from Injection Hole to Back of Plenum
G_b	Generation of Turbulent Kinetic Energy due to Buoyancy
H	Plenum Height
K	Thermal Conductivity
L	Length
M	Blowing Ratio
P	Pitch
S	Strain-Rate Tensor
T	Temperature
V	Velocity
e	Internal Energy
f	Body Forces
h	Height
k	Turbulent Kinetic Energy
p	Pressure
t	Time
$u_{i,j,k}$	Velocity in Tensor Notation
$u'_{i,j,k}$	Turbulent Fluctuation
$x_{i,j,k}$	Position in Tensor Notation
y^+	Normalized Distance yu_*/ν
z	Coordinate in the Lateral Direction

Greek

ε	Dissipation Rate of Turbulence Kinetic Energy
λ	Second Viscosity
η	Adiabatic Effectiveness
μ	Kinematic Viscosity
ρ	Density
σ	Nonequilibrium Parameter
τ	Surface Stress
ν	Eddy Viscosity

Subscripts

aw	Adiabatic Wall
c	Coolant
t	Turbulent
∞	Freestream

This Page Intentionally Left Blank

1 Introduction

Film cooling of gas turbine blades has become the industry standard for maintaining reasonable blade temperatures as gas turbine technology continues to advance. Turbine efficiency and throughput is greatly improved with increasing rotor inlet temperature. This temperature often exceeds the metallurgical limit of the turbine blades making the use of film cooling necessary. The study of film cooling has evolved significantly over the past fifty years ranging from simple techniques to complex novel cooling techniques attainable as a result of advanced manufacturing techniques. A comprehensive discussion on film cooling techniques and novel approaches is found in Section 2.0 of this report.

Research has demonstrated that cylindrical holes offer relatively good performance when placed in optimized configurations. These holes are primarily advantageous due to their ease of manufacturing and availability in the current industry. The research herein outlines a novel approach to film cooling deemed "sister holes". Here, two or four holes of half the primary hole diameter bind the primary injection hole in an attempt to maintain flow adhesion along the surface of the blade over a wide range of operating parameters. As will be discussed, the primary rationale for instituting advanced film cooling techniques is due to flow separation at high coolant to freestream velocity ratios. By coordinating the hole position in such as way that the flows interact favourably with one-another, the primary flow can effectively be brought to the surface of the blade, improving cooling performance. The sister hole approach is a novel technique that has been instituted to maximize cooling effectiveness while minimizing aerodynamic mixing, a factor that is often overlooked in studies of novel cooling techniques.

Film cooling techniques are analyzed on a number of fronts. Most prominently, this research will focus on an evaluation of the adiabatic film cooling effectiveness along the centreline and in the lateral direction. However, these results must be evaluated simultaneously with those of the flow field in order to illustrate the effect of these holes on the entire computational domain. Certain cooling techniques can significantly improve adiabatic effectiveness while simultaneously increasing aerodynamic losses. To evaluate this, a cut-plane is taken down the centreline of the plate to evaluate the flow structure. Further flow structure analysis will ensue with an evaluation of the primary vortex pair at various locations downstream of the primary hole. To conclude the result analysis, an evaluation of the streamwise vorticity for each of the cooling techniques evaluated in this research will be shown. Such an

analysis illustrates the swirling nature of the flow and precisely how the sister holes interact with one-another along the plate wall.

At the time of publication, the research held herein has been converted into several scholarly sources. The first such submission was to ASME Turbo Expo 2008 in Germany where a paper entitled "A Numerical Study on Increasing Film Cooling Effectiveness Through the Use of Sister Holes" [1] was presented and published in the conference proceedings. More recently, a paper entitled "A Numerical Study on Improving Large Angle Film Cooling Through the Use of Sister Holes" [2] has been accepted for publication at Numerical Heat Transfer: Part A. Finally, a third paper entitled "A Numerical Evaluation on the Effect of Sister Holes on Film Cooling and the Surrounding Flow Field" [3] has been submitted to Heat and Mass Transfer and is currently awaiting review.

The current study is divided into eight sections. Section 1 introduces the topic of film cooling and outlines the layout of the forthcoming analysis. Section 2 contains a detailed literature review, providing an overview of classical film cooling trends as well as modern advanced techniques. Section 3 contains a discussion on the geometries and simulation parameters used in the current study, leading directly into Section 4 which contains a discussion on the numerical approach used in this work. Sections 5 through 7 contain the results for each geometry studied; half-plane, long-hole, and short-hole. It is in these sections that a great deal of understanding into the sister hole technique will be developed. Finally, Section 8 contains the conclusions and recommendations for future research derived from this work. Back matter in the report contains two appendices which outline the primary algorithms used to extract the raw thermal data and develop it into the results contained herein.

2 Literature Review

Research into film cooling of gas turbine blades has been researched extensively for nearly sixty years. While significant advancements have been made in this time, the most notable of these have occurred within the past two decades. In this short time, research has progressed from simple cylindrical cooling holes to complicated novel geometries thanks in part to modern manufacturing techniques. The following discussion will provide an overview of film cooling research, stemming from primitive techniques through to bleeding edge technologies.

2.1 Slot Holes

Early research into film cooling focused on the use of slot holes. Flows emanating from holes of this shape have been shown to provide the optimal balance of high film cooling effectiveness and low aerodynamic losses [4]. Unfortunately, research has shown that due to their elongated nature, the material integrity of the blade is severely diminished, making these holes infeasible in practical situations [5]. However, results from these studies often act as an important benchmarking tool for new cooling techniques. In particular, some of the most novel cooling techniques make use of cylindrical and shaped holes that arise from a trench within, in a technique known as trenched hole film cooling.

One of the most thorough evaluations on the effects of slots on film cooling performance was performed by the group of Jia et. al [6]. Their research simulated slot holes at inclination angles of 30°, 60°, and 90° to determine their effect at both low and high inclination angles. Through both experimental and numerical means, their group studied the flow field arising from these holes to determine their validity as well as to discuss the accuracy of modelling these flows numerically. Their study made use of the RSM turbulence model in an attempt to improve upon the simplifications of RANS-based two-equation models. The experimental and numerical results were found to be within a reasonable margin of one-another, both demonstrating that for inclination angles less than or equal to 40° the slot flow remained fully attached to the surface of the blade while at angles upwards of this, a distinct separation region downstream of the hole existed [6].

2.2 Cylindrical Holes

As more research groups demonstrated that slot cooling was not a practical cooling regime, an increasing number of groups began to study the use of simple cylindrical angle cooling holes. It has been

widely accepted that adequate cooling coverage can be achieved by inclining coolant holes between 20° and 40° to the horizontal. More specifically, inclination angles near to 35° offer the most ideal performance for simple angle injection cylindrical hole film cooling [7]. Unfortunately, on the highly curved surfaces of a turbine blade, such low inclination angles are often not plausible making larger angle holes necessary.

In an attempt to better understand the flow field emanating from holes of varying inclination angle, the group of Yuen et. al [8] evaluated film cooling performance at inclination angles of 30°, 60°, and 90° for both low and high blowing ratios. As one would expect, at low blowing ratios, the 30° injection angle offered the highest overall effectiveness due to attached flow over the entire domain. However, as the blowing ratio was increased, the higher angle injections offered better protection from the mainstream flow, downstream of the injection hole. This characteristic is most easily attributed to jet lift-off, as the near-hole region continued to be better protected by the low angle hole. However, as the jets reattach following separation, they are shown to mix less with the freestream than the fully attached low-angle injection, leading to higher effectiveness values [8]. However, it should be noted that as blowing ratios increased, the vertical momentum of the large-angle injection holes increased simultaneously, enlarging the separation region. In turn, this created a significant unprotected region downstream of the holes making large angle holes less favourable than low-angle holes in practice [8].

While shown to provide less than ideal coverage, research into these large angle holes has been necessary to accommodate for realistic blade geometries. As such, Kohli and Bogard [9] performed a study using rectangular injection holes inclined at 55° to the horizontal. These highly angled holes were used to better simulate the curved surface of a turbine blade. In doing so, their study continued to make use of a flat plate rather than a curved airfoil, a technique widely adopted when analyzing novel cooling techniques. The effectiveness values and flowfield that arose from this study were reminiscent of shallower injection holes; however it was noted that at high blowing ratios, these holes offered significantly lower effectiveness than their shallow counterparts due to increased mixing with the mainstream [9].

Similarly, Nasir et al. [10] released a study building upon the results of Kohli and Bogard [9] by using compound angle injection under the same operating conditions. That is, their holes were inclined in both the streamwise and lateral directions to optimize cooling performance. Their study found that, as

with shallow angle injection, adding a compound angle improved adiabatic effectiveness over all blowing ratios. However, it should be noted that this improvement in effectiveness came at the cost of higher heat transfer coefficients, which is generally undesirable in film cooling regimes [10].

The research group of Ahn et al. [11] studied the effect of hole orientation on film cooling performance. Their research evaluated oppositely oriented cooling holes placed in four unique geometries ranging from in-line to staggered. As expected, the arising flow fields were truly diverse with very little predictability. The flow field was dominated by the primary counter-rotating vortex pair as was evidenced by the asymmetric nature of the flowfield [11]. Ultimately, this study concluded that staggering these oppositely oriented holes negatively impacted the cooling performance of the blade due to the upwash of the upstream hole's primary vortex pair. Due to the opposite orientation, rather than countering the primary vortex pair, the flow was drawn further from the surface [11].

2.3 Modern Applications of Classic Techniques

As was previously discussed, slot hole film cooling is, to date, the most effective means of film cooling. However, due to its elongated shape, material integrity losses dictate that it is infeasible to use in practical cooling regimes. In order to take advantage of slot hole cooling properties while maintaining blade integrity, Sargison et al. [12] proposed a novel cooling technique named 'Console'. Console is of particular interest because in essence, it is simply an array of shaped holes. Where this technique differs is that at the ejection point, these holes come together to become an elongated slot-like entity. Their results dictate that Console's performance is second only to slot cooling with minimal mainstream mixing [12]. With that said, it should be noted that the effectiveness of this technique is only realized when an array of holes are used.

Further to this, groups including Baheri et al. [13] have recently begun studying the effects of placing coolant holes within a narrow trench. As with Console [12], the motive is to mimic slot cooling performance most closely while minimizing integrity losses. The study of Baheri et al. [13] evaluated cylindrical holes, shaped holes, and their trenched counterparts over a curved airfoil surface. Their results indicated that, as expected, shaped holes outperform the standard cylindrical holes. Notably, placing a trench around these holes improves the overall performance by filling the trench with coolant prior to spilling into the mainstream. As a result, the transition of the coolant into the mainstream was less dramatic and more reminiscent of slot film cooling [13].

As shown, simple cylindrical hole film cooling can lead to limitations that can often seem insurmountable. To improve upon these designs, research groups have been developing new novel techniques for film cooling. With advancing manufacturing techniques, the ability to shape coolant holes has become a reality. The study of Kanani et al. [14] focused on the impact of laterally-diffused simple angle coolant holes. Their research, which made use of the RSM turbulence model, indicated that the laterally diffused holes offer improved performance over standard cylindrical holes due to less penetration into the mainstream. Subsequently, the diffused exit area causes the coolant to spread, improving lateral coverage [14].

Further to this research, the study of Bell et al. [15] proposed that laterally diffused compound angle holes offered the most optimal cooling performance over other shaped holes at blowing ratios in the range of $0.7 \leq M \leq 1.8$ [15]. In a similar fashion to the study of Kanani et al. [14] these holes are highly advantageous because they reduce the degree to which the flow must bend when entraining on the hot mainstream flow, ultimately leading to better flow adhesion. As well, due to the spread at the hole exit, lateral diffusion is significantly increased further improving performance [15].

2.4 Multi-Jet Arrangements

As was demonstrated in the work of Sargison et al. [12], the flow emanating from an array of holes can drastically differ from that of a single hole. Roy [16] numerically evaluated the flow arising from an array of cylindrical coolant jets. Of particular interest was his evaluation of pitch-to-diameter ratios (P/D), a discussion on the spanwise spacing of adjacent jets. His research noted that by reducing the P/D ratio between adjacent holes, the flow became increasingly more attached to the surface of the plate, improving effectiveness and lateral spread. This phenomenon was attributed to the primary counter-rotating vortex pair being countered by an oppositely rotating pair of the adjacent jet [16]. This is of particular interest in the current study where the P/D ratio between single and sister holes is less than unity.

The sister hole concept was first put forth by the research group of Javadi et al. [17] whom proposed a simplified version of the models evaluated in the present study. Their research made use of a primary injection hole of diameter D bound by two smaller jets of diameter 0.5D slightly downstream to arrive at their "triple jet" approach to film cooling [17]. In their study, the holes were rectangular in nature and injected perpendicularly to the mainstream, a less than ideal orientation for optimum effectiveness.

Initial results indicated that the addition of these holes dramatically improved film cooling effectiveness over standard single hole cooling [17]. They noted that the use of this technique offered the most substantial improvements in the near-hole region as a result of a smaller separation bubble and region of flow reversal. More recent research by the group of Javadi et. al [18] attributed the performance gains of the triple jet technique to the additional CRVPs generated by the bounding jets. Their counter-rotating nature effectively minimized the primary vortex structure to maintain flow adhesion and increase lateral spreading [18].

Further to this research, Dhungel [19] and Heidmann [20] performed analyses on a technique deemed "anti-vortex holes". The anti-vortex hole technique made use of a primary cylindrical cooling hole with anti-vortex holes originating along its development length [19]. In agreement with the work of Javadi et al. [17, 18], both Dhungel [19] and Heidmann [20] found that the addition of these secondary holes improved effectiveness by reducing the impact of the primary vortex pair. Further, Heidmann [20] performed a parametric study to determine the optimum position of the secondary holes. His research demonstrated that, particularly at high blowing ratios, positioning the secondary holes directly adjacent to the primary jet offered the most optimal cooling performance [20].

The research group of Kusterer et al. [21, 22] focused on double-jet ejection (rather than triple jet studies previously discussed). Similar results were observed in their studies indicating the effectiveness of the use of multiple holes over single hole cooling. In particular, they evaluated the effect of staggering the holes to improve performance at moderate to high blowing ratios in the range of $1.0 \leq M \leq 1.5$. On the whole, their study found that staggered oppositely oriented holes provide the most improved effectiveness over standard film cooling [21]. Interestingly, while their research demonstrated that the primary counter-rotating vortex pair was minimized by the addition of a secondary hole, they found that at high blowing ratios with sufficiently large separation between holes in the spanwise direction, the hot mainstream can penetrate the boundary layer, reducing the effectiveness of the approach [22].

2.5 Hole and Plenum Geometry

Thus far, discussions have focused on film cooling techniques. However, it is equally as important to discuss the geometries upon which these techniques are derived.

Film cooling hole length-to-diameter ratio significantly has been shown to appreciably impact the performance of a cooling technique. The research of Burd et al. [23] and Lutum et al. [24] have shown that in considering all geometrical constraints, the development length of a coolant hole most significantly impacts performance. Notably, Burd et al. [23] evaluated the effects of plenum geometry, plenum feed, and L/D ratio in an attempt to analyze their effect on cooling performance. Their research indicated that plenum geometry negligibly affected performance while hole length and plenum feeding method impacted the results more appreciably. Long holes were shown to perform more optimally than short holes at high blowing ratios but offered similar performance at low blowing ratios. Additionally, the use of a counter flow plenum, whereby the coolant flow enters the plenum in the opposite direction of the freestream, provides better effectiveness than use of a co-flow plenum. Interestingly, when compared against an unrestricted bottom fed plenum, the counter-flow plenum was shown to offer better overall performance [23].

The study of Lutum et al. [24] focused exclusively on the impact of L/D ratios on cooling performance. Their study evaluated 35° injection film cooling at L/D ratios between 1.75 and 18. Complementing the previous work of Goldstein et al. [25], Lutum demonstrated that at large L/D ratios ($L/D > 5$) effectiveness was negligibly impacted with increasing L/D. In contrast, as $L/D \rightarrow 0$, the flow became increasingly underdeveloped, leading to significant freestream mixing and lower overall effectiveness [24].

The research group of Azzi et al. [26] simulated the effect of variable length-to-diameter ratio numerically. In particular, their study evaluated $1.5 \leq L/D \leq 8$ using the standard k-ε turbulence model with the Bergeles modification (which significantly improves the accuracy of the results for adiabatic effectiveness [27]). The use of this turbulence model warranted excellent results, indicating that short holes are detrimental to lateral spreading as a result of the underdeveloped flow that arises from the holes. This flow tends to dissipate quickly offering minimal blade coverage.

These results play a key role in film cooling research to date. Detailed literature surveys indicate that very little research exists in the field of short hole film cooling; however, its applicability is monumental. In modern turbine blades, it is common to find very low L/D ratios, providing minimal room for flow development. At the time of publication, the most prominent research group studying the effects of short holes on film cooling was that of Hale, Plesniak, and Petersen [28-31]. Of particular interest in the

current study is the work of Hale [28] who performed a detailed analysis on short-hole film cooling ejecting into a crossflow.

Short-hole film cooling is defined as holes with a length-to-diameter ratio less than or equal to unity [29]. These holes are more prone to generate complicated vortex structures including shear layer vortices, horseshoe vortices, wake vortices, and counter-rotating vortex pairs [29]. The research of Hale [28] was the first comprehensive study to evaluate the flow field arising from short holes fed by a narrow plenum. His study evaluated two inclination angles with variable hole lengths with particular emphasis on short holes oriented at 35° to the horizontal with L/D = 1.16. The narrow plenum of this study was unique due to its height of H/D = 1 creating highly turbulent flow within. This geometry was simulated with both co- and counter-flow plenums to determine the most optimal configuration. It was found that, as discussed in Lutum et al. [24], at such low L/D ratios, there is very little flow cohesion leading to an erratic flow field [28]. However, this is improved with the addition of a counter-flow plenum which generates a more defined counter rotating vortex pair [28], validating the research of Burd et. al [23] Although intrinsically undesirable, the creation of a well formed CRVP allows for better active control of the flow through novel cooling techniques.

Further to this research, Peterson and Plesniak [29-31] focused on the effects of plenum feeding techniques. Their research demonstrated that the counter-flow plenum outperforms the co-flow plenum as a result of in-hole vortices that lead to the cohesiveness of the primary vortex pair [30]. This discussion naturally progressed into an evaluation of short holes fed by the two plenum types at a range of blowing ratios. As one would expect, due to the less cohesive nature of the co-flow plenum, at high blowing ratios, geometries fed by a co-flow plenum penetrate further into the mainstream than their counter-flow counterparts [31].

The study of Harrington et al. [32] focused on numerical simulations of short hole film cooling. Making use of the RNG k-ε model, their study evaluated the performance of an array of perpendicularly ejected holes with L/D = 1. Their study illustrated the significance of hole L/D ratio and also indicated that the RNG k-ε was able to predict, with good accuracy, the flow at low blowing ratios. At high blowing ratios, further refinement was necessary to provide adequate results; however, on the whole, these results bode well for the k-ε model in predicting complex flow regimes [32].

2.6 Flow Physics

Film cooling flow is dominated by a pair of vortices denoted the primary counter-rotating vortex pair (CRVP). This pair of vortices rotates in a sense such that they push the coolant flow into the mainstream and drag the mainstream flow towards the surface of the blade. Logically, designs attempt to minimize these pairs or counter them with oppositely oriented CRVP's. The study of Kurosaka [33] focused on the impact of shaped holes on film cooling flow physics. His results offered a great deal of understanding as to the effectiveness of these cooling techniques. Performing an analysis of shaped holes under differing orientations, it was found that by orienting the hole laterally and driving its shape towards a slot-like design offered the best performance and lateral spread as a result of the spanwise separation of the vortex pair. Since the vortices are not given the opportunity to interact, jet lift-off is delayed, leading to an optimized cooling technique [33].

Bernsdorf et al. [34] performed a detailed analysis evaluating the flow physics of film cooling with varying blowing ratios, inclination angles, density ratios, and momentum flux. Their results visualize the thickening boundary layer with increasing blowing ratio as well as the large primary kidney vortex structure that arise at such blowing ratios [34]. These results illustrate how the primary CRVP is detrimental to flow adhesion, pulling the coolant away from the blade and pushing the hot mainstream towards it. Similarly, by studying the streamwise vorticity, Bernsdorf et. al [34] demonstrates the asymmetric nature of the flow while demonstrating the counter rotating nature of the primary vortex structure.

Further, the degree of turbulence intensity can play a key role in defining the effectiveness of a film cooling technique. Mayhew et al. [35] studied the effect of low and high turbulence intensities on low and high blowing ratio flows to determine the performance impact of this parameter. Their research indicated that low turbulence intensities proved detrimental to high blowing ratios while high turbulence intensities proved detrimental to low blowing ratios [35]. These results were attributed to conformity of the mainstream flow. At low blowing ratios, the highly non-uniform turbulent mainstream mixes aggressively with the coolant to draw it away from the blade. In contrast, at high blowing ratios, low turbulent mainstream flow remains attached to the surface of the blade with no means to force the coolant to the surface of the blade [35].

2.7 Numerical Considerations

Numerical film cooling studies are of particular difficulty due to the complex nature of the flow as the coolant entrains on the mainstream. Significant velocity and temperature gradients pose a unique obstacle that many researchers have attempted to overcome.

Research into turbulence models for film cooling flows have evaluated the use of techniques including algebraic, RANS, RSM, LES, DES, and even DNS turbulence models [36, 37]. Algebraic models are the most simplified, solving a single equation, generally not providing an accurate representation of the complex mixing of the flowfield. RANS solvers offer a wide range of models, all with varying strengths and weaknesses. These models solve two equations that can generally be defined as a kinetic energy equation and a dissipation equation to solve the flow. Further, LES and DES techniques aim to use a more advanced approach in solving the largest eddies while solving the smaller scale turbulence with either a subgrid scale solver or a RANS approach [38]. Finally, DNS solvers make no assumptions in its solution approach, solving the flowfield in its entirety. This technique is highly disadvantageous due to the tremendous resources it demands. To date, very little research has been performed on DNS for film cooling but a detailed study has been performed by Muldoon et al. [39] whom developed their own solver to simulate these complex flows.

To date, no research group has been able to propose the most optimal turbulence model for all film cooling regimes. Due to the complex nature of the flow, simplified RANS turbulence models often struggle to accurately model the flow while advanced models such as LES, DES, and DNS are either too computationally intensive or insufficiently defined to proceed with their use.

Research validating the use of the standard k-ε model was found in the research of Kalita et. al [40]. His research focused on numerical simulations of a simple planar jet ejecting into a crossflow. In agreement with the work of Ajersch et al. [41], Kalita et. al [40] found that the velocity decay along the x-axis was sufficiently predicted; however, the boundary layer profile (a function of flow mixing and vortex production) was poorly predicted. This trend matches the widely accepted understanding of the relatively poor modeling of swirling flow within the standard k-ε model, a trend which is improved upon in the realizable k-ε model. It should be noted that while the k-ε model predicted results that were slightly askew from the experimental results, the low computational requirements make this model very appealing.

Further, the group of Ajersch et al. [41] performed a detailed analysis of an array of rectangular jets ejecting perpendicularly into a crossflow, simulated using a heavily customized k-ε model. The standard solver has been widely accepted for decades as a good entry point into a novel technique. Their research demonstrated the strengths and weaknesses of this model as it was found to adequately model the basic characteristics of the flow, but struggled to depict the complicated near hole vortices with sufficient accuracy [41].

To date, very few studies have focused on the effects of turbulence modeling on hole length. Two studies have numerically evaluated short-hole film cooling, that of Harrington et al. [32] and Iourokina [42]. While the study of Harrington et al. [32], discussed previously, focused on short-hole film cooling through the use of RANS turbulence modeling, the work of Iourokina [42] studied the impact of LES on this film cooling regime. Their research heavily tailored the solution scheme to adapt to the short-hole model by enlarging the scope of their sub-grid scale solver; however, their study brought about excellent results at significant computational cost [42].

The recent work of Harrison and Bogard [44] studied commonly used RANS turbulence models in film cooling. Their research was intended to place these models under scrutiny to determine which offers the highest accuracy in effectiveness and heat transfer predictions. To span a range of turbulence models, their study evaluated the standard k-ω turbulence model, the realizable k-ε turbulence model, and the RSM-SST turbulence model with near-wall modeling. The RSM-SST model was found to provide the highest accuracy in heat transfer coefficient modeling; however, the added computational cost was unnecessary in evaluating the film cooling effectiveness as it offered negligible variations from the other two models [44] The standard k-ω model marginally improved upon the lateral predictions of the realizable k-ε model while the opposite was true along the centreline [44]. On the whole, the use of any of the three models is sufficient for preliminary film cooling analyses.

One technique that has generated some interest in recent years is that of detached eddy simulations (DES). Large Eddy Simulations solve all large eddies fully and make use of complex subgrid scale solvers to analyze smaller scale turbulence. Detached Eddy Simulations make use of the LES approach in the freestream and merge the solution with a RANS based turbulence model in the subgrid range (in the case of film cooling, along the boundary layer) [38]. The research of Roy et. al [45] made use of such model with the Spalart-Allmaras model used within the boundary layer. Their first approach made use of

a half-plane model with symmetry boundary conditions, leading to highly generic results. However, further research into this approach made use of a full geometry without a symmetry plane generating a flowfield that was asymmetric and more indicative of actual performance [36]. While this approach is of great interest to maintain solution accuracy while driving down computational cost, its relative immaturity makes it a challenging candidate for analyzing novel cooling techniques.

2.8 Contributions to Scholarly Research

The research contained herein has been proposed to offer a definitive solution to the optimal jet placement for multi-jet studies. As the discussion in Section 2 has indicated, several research groups have studied a variety of applications with little consistency. By evaluating geometries that are more applicable to actual turbine geometries and fully achievable with modern manufacturing techniques, the current study proposes an understanding into the physics which make each secondary hole location most optimal. Through an analysis of the flowfield, improvements in effectiveness are better understood and pave the way for future research to focus on further optimizing the design geometry.

This Page Intentionally Left Blank

3 Design Geometry and Simulation Parameters

The focus of the research conducted herein was to evaluate the effect of sister holes on film cooling. As a result, it was necessary to examine several unique geometries in an attempt to determine the most optimal design candidate. By first analyzing the effectiveness of sister holes at various inclination angles, the study was able to proceed with more complicated sister hole orientations in a complete analysis of long-hole and short-hole film cooling.

The following section will discuss the various geometries utilized in this study. Additionally, the section will conclude with an overview of the simulation parameters used in the current evaluation.

3.1 Geometries

The half-plane geometries evaluated in this study stemmed from the work of Javadi et. al [17]. The original intention of the shallow-angle design was to improve upon their study by changing the holes from rectangular to cylindrical and inclining them at 35° to the horizontal, compared to their 90° inclination. The second half-plane model made use of the same geometry but increased the inclination angle to 55° to evaluate more realistic turbine conditions, as seen in the work of Kohli et al. [9]. For the purpose of simplicity, these geometries will be denoted as the shallow-angle and large-angle geometries, respectively.

The half-plane geometries made use of a primary hole diameter of D = 12.7mm and sister holes of diameter 0.5D. To mimic the work of Javadi et al. [17], 5D was allotted prior to the primary hole to allow for flow development while 30D downstream of the primary hole was allotted for the flow to settle, allowing ample opportunity to evaluate the flowfield. The sister holes were located at 0.75D downstream of the primary injection hole and were situated at ±0.75D about the centreline of the plate. Note that the geometry was designed about a plane of symmetry to reduce computational cost and was given a width of 1.5D. For the purpose of consistency, no plenum was used in the current evaluation, and the flow was given 5D to develop before ejecting into the mainstream. Below, Figure 1 contains the top and side views of the shallow-angle half-plane geometry.

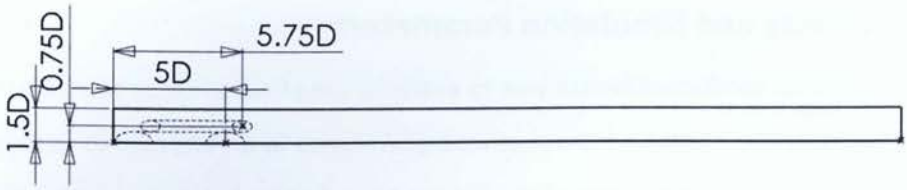

(a) Top View – Shallow-Angle Model (35°)

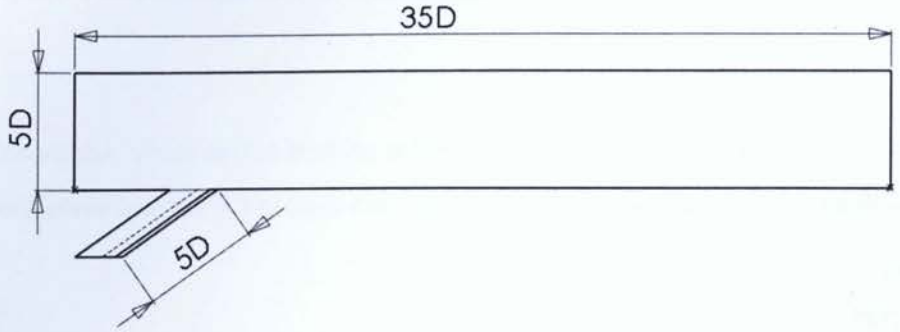

(b) Side View – Shallow-Angle Model (35°)

Figure 1: Half Plane Geometry

The research group of Leylek and Zerkle [46] has demonstrated the importance of a plenum in improving film cooling effectiveness. However, it should be noted that such flows are not indicative of realistic film cooling regimes. Generally, film cooling flow in an actual gas turbine is underdeveloped and highly turbulent; characteristics that are more common without the use of such plenum. Further to this, Goldstein et al. [25] and Lutum et. al [24] have shown that increasing the L/D ratio above 5 offers negligible variations in film cooling performance, indicating that the assumptions used in the work of Javadi et al. [17] are valid and are representative of realistic gas turbine conditions.

Beyond a comparison of hole inclination angle, the current research was focused on two key performance criteria. The first was that of hole L/D ratio, where a comparison of long-hole (L/D = 5) and short-hole (L/D $\approx$ 1) performance was evaluated. The second was finding the optimal sister hole orientation for maximizing film cooling effectiveness while minimizing interaction with the mainstream flow. These two drivers led to four design geometries that were evaluated for both long and short hole film cooling flows.

The four base geometries stemmed from the original half-plane models previously discussed. In a similar fashion, these geometries were designed with a flow development allotment of 5D prior to the centre of the primary injection hole, 30D allotted downstream of the injection hole, and sister holes placed at

0.75D up/downstream and ±0.75D to each side of the primary hole. In stark contrast, to allow for simulation of an array of jets, these geometries were designed in full with a width of 3D. In order to make use of one grid for all simulations, each hole was defined separately to allow for each to be easily opened (allowing coolant through) or closed (considered part of the flat plate). A top view of the four geometries are given below, where the active holes are highlighted in red, note that for clarity, the primary injection hole remains white even though it is open for each of the geometries.

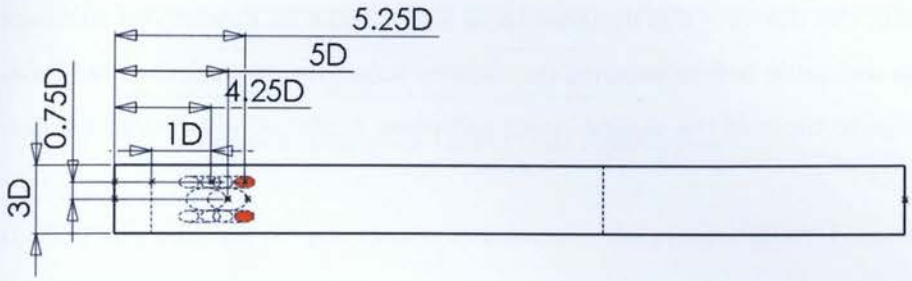

(a) Top View – Downstream Holes

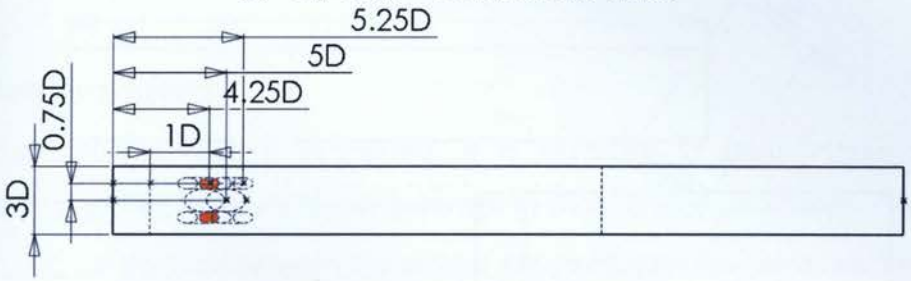

(b) Top View – Upstream Holes

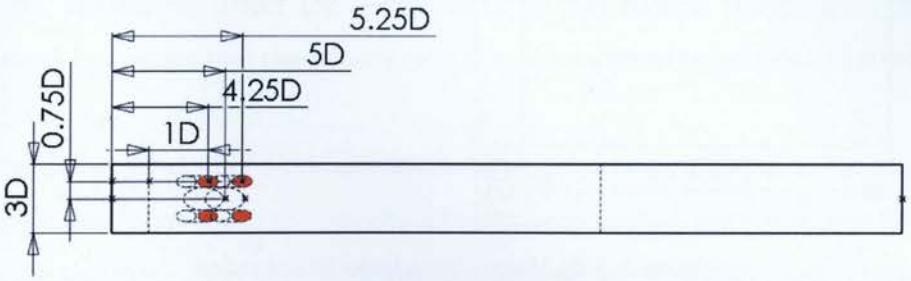

(c) Top View – Upstream/Downstream Holes

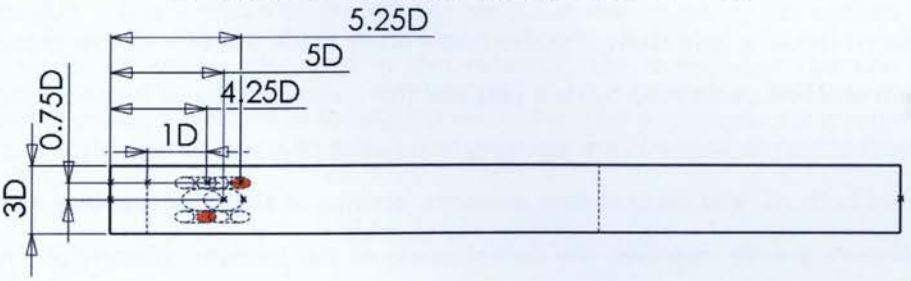

(d) Top View – Left/Right Holes

Figure 2: Sister Hole Geometries - Top View

The long and short hole studies differ most prominently in their hole length and how the coolant is fed through their coolant holes. Unlike the half-plane studies, both of these made use of a plenum to feed their coolant holes. The long hole plenum was designed as a settling chamber which was bottom fed in such a way to most closely mimic the work of Bell et. al [15]. Bell et al. [15] performed a film cooling study with a plenum of 23D X 17D X 23D (their plenum is much wider than that of the current study due to the overall width of their geometry). Upon investigating the plenum sizing of several research groups, their model was found to be a reasonable average and was modified slightly for the current research. In the present study, the chamber was designed to be 20D x 15D x 3D allowing for sufficient room for the flow to develop and settle before entering the coolant holes. The plenum then fed holes 5D in length, identical in design to those of the shallow-angle half-plane model. A side view of the geometry is given in Figure 3.

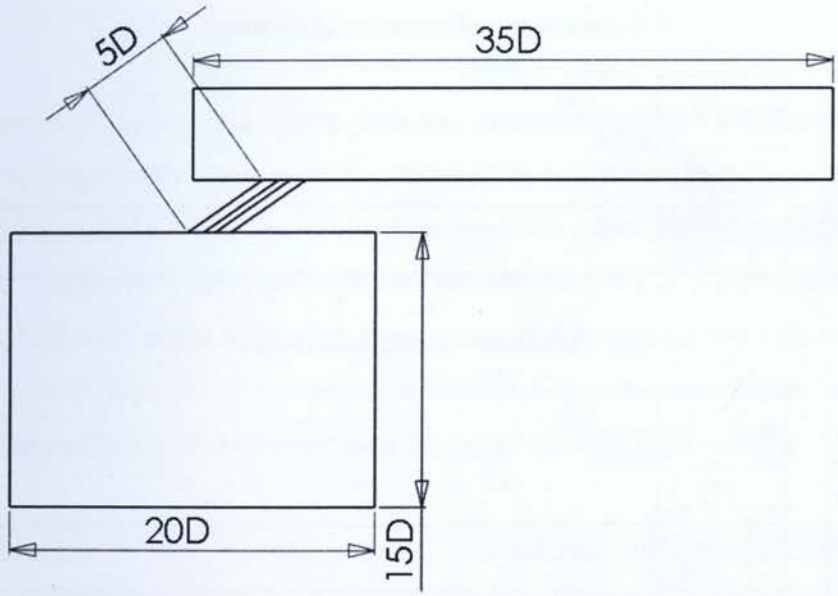

Figure 3: Side View - Long Hole Geometries

To compare against the long hole study, the short-hole study made use of a narrow plenum. The use of a narrow plenum was first performed by Hale [28] and then subsequently by Petersen and Plesniak [29-31] whom argue that narrow plenums are more representative of actual turbine blade geometries. Their studies evaluated both co- and counter-flow plenums, arriving at the understanding that the use of a counter-flow plenum greatly improves the cohesiveness of the primary counter-rotating vortex pair, driving film cooling effectiveness [31]. The geometry here was designed with a height-to-diameter (H/D) ratio of 1 and a spacing of back wall to centre of the injection hole (E/D) of 1. Also of note is the length

of the holes, which here, have been modeled as L/D = 1.16 to mimic the work of Hale [28]. Figure 4 contains a side view of the short-hole geometries.

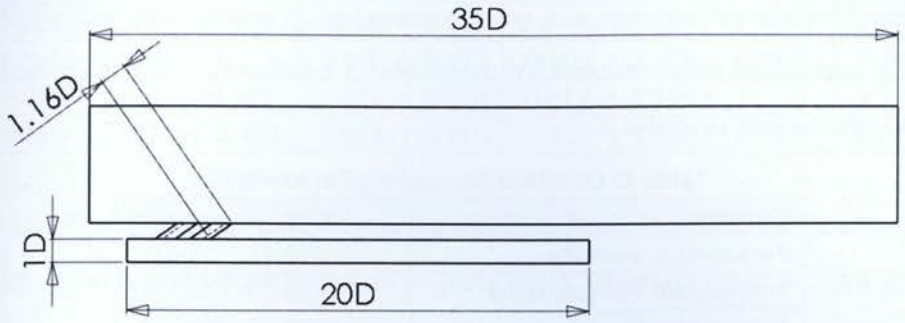

Figure 4: Side View - Short Hole Geometries

The above discussion fully outlined the geometries evaluated in the present study. Following this, it was possible to define the simulation parameters.

3.2 Simulation Parameters

Before introducing the simulation parameters, it is necessary to discuss three flow defining characteristics. Film cooling flows are largely governed by three related parameters. First, the density ratio, $DR = \rho_c / \rho_\infty$, is the ratio between the coolant and freestream flow densities. Variations in the density ratio can significantly affect the performance of film cooling techniques. For standard jet operation, research has shown that the density ratio should lie within the bounds of 1≤DR≤2 [47].

The density ratio allows for the definition of the other two governing parameters. The blowing ratio, M, is a function of the density ratio and the velocity ratio between coolant and freestream flows. This is the ratio by which the simulations performed herein are measured and is widely used in this field. Further, the momentum flux, I, is a function of the density ratio and the square of the coolant to freestream velocity ratio. While not widely discussed in this research, the momentum flux can be used as a quantitative tool to evaluate when flow separation will occur. These concepts are given mathematically in Equations 1 and 2.

$$M = DR\left(V_c / V_\infty\right) \quad \textbf{(1)}$$

$$I = DR\left(V_c / V_\infty\right)^2 \quad \textbf{(2)}$$

Generally, the momentum flux indicates that separation regions become evident in the range of $0.4<I<0.8$ [47].

Each of the geometries shared common simulation parameters to ensure consistency between results. The blowing ratio was varied between M=0.2 through M=1.5 by altering only the coolant velocity. The simulation constants are given in Table 1.

Table 1: Constant Simulation Parameters

Property	Value	Units
Freestream Velocity	10	[m/s]
Freestream Temperature	353.15	[K]
Freestream Density	0.9997	[kg/m^3]
Coolant Temperature	293.15	[K]
Coolant Density	1.204	[kg/m^3]
Operating Pressure	101 325	[Pa]

As discussed, for realistic flow regimes, density ratios should lie in the range of $1 \leq DR \leq 2$. This has been satisfied here with a density ratio of DR=1.204, well within the acceptable range.

Although the blowing ratios were held constant through all studies, the velocity of the coolant flow that was fed to the system varied based on inlet geometry. For instance, by calculating the mass flux, $\dot{m} = \rho A V$, one can clearly see that the coolant velocity through the long hole plenum must be significantly lower than that of the narrow plenum to maintain the same mass flux flow through the coolant holes.

In this analysis, it is important to note that the mass flux through each hole was designed to meet the blowing ratio being evaluated. That is, for the single hole M=0.2 case, the local blowing ratio at the exit of the coolant hole was M=0.2. For the sister hole case (regardless of design) at the same blowing ratio, the local blowing ratio at the exit of each hole was M=0.2. As such, dependent on geometry, with the sister holes active, the new technique makes use of 1.5 (2-sister holes) or 2 (4 sister holes) times more coolant than a standard single hole at the same blowing ratio. However, it will be shown that the single hole coolant at the same overall blowing ratio would not perform nearly as effectively as the sister hole case. Ultimately, although this means that the overall blowing ratio increases, the results will dictate that there is good merit to this analysis.

Below, Table 2 contains the coolant inlet velocities for each geometry.

Table 2: Inlet Velocities

[m/s]	Single Hole			Downstream			Upstream		Up/Downstream		Left/Right	
M	Half	Long	Short	Half	Long	Short	Long	Short	Long	Short	Long	Short
0.2	1.660	0.0217	0.435	1.660	0.0435	0.869	0.0435	0.869	0.0652	1.304	0.0435	0.869
0.5	4.151	0.0543	1.087	4.151	0.109	2.173	0.109	2.173	0.163	3.260	0.109	2.173
1.0	8.301	0.109	2.173	8.301	0.217	4.346	0.217	4.346	0.326	6.520	0.217	4.346
1.5	12.452	0.163	3.260	12.452	0.326	6.520	0.326	6.520	0.489	9.779	0.326	6.520

In addition to the flow conditions indicated previously, to satisfy the realizable k-ε turbulence model, turbulent length scales had to be defined at all velocity inlets. To define these, a simplification assuming unbound external flow at the boundaries allowed for the length scales to be defined as $L = 0.05h$. The properties associated with the turbulence model are given in Table 3.

Table 3: Turbulence Properties

Flow	Intensity [%]	Length Scale [mm]
Freestream	2	3.175
Plenum	1	0.635

Note that the turbulence intensities used in this study were selected to most closely mimic past research and for their applicability to experimental research.

Post processing focused most prominently on an analysis of the adiabatic effectiveness of each of the geometries. Adiabatic effectiveness is a measure of how well the coolant protects the surface of the blade by a ratio of differences between wall and freestream to coolant and freestream temperatures and is given in Equation 3. Further, laterally averaged effectiveness is calculated by selecting discrete x/D locations and numerically integrating their adiabatic effectiveness values at a range of z/D (spanwise) points as shown in Equation 4.

$$\eta = \frac{T_\infty - T_{aw}}{T_\infty - T_c} \tag{3}$$

$$\bar{\eta} = \frac{1}{L}\int_L \eta \, dz \tag{4}$$

3.2.1 Sensitivity Analyses

Further to the simulations discussed thus far, to validate the use of the computational grid, it was necessary to perform a detailed sensitivity analysis to ensure that the solution was reasonably accurate. To do so, each grid was benchmarked against other well-referenced research with similar geometries.

All long hole shallow angle studies were benchmarked against the research of Sinha et al. [48]. The geometry of the current study was virtually identical to their work aside from the coolant hole length, which was longer in the current study. In order to match the results of their research, the simulations were run with identical simulation parameters of Sinha et al. [48] which are found in Table 4.

Table 4: Simulation Parameters – Sinha et al. [48]

Property	Value	Units
Freestream Velocity	20	[m/s]
Freestream Temperature	300	[K]
Freestream Density	1.18	[kg/m^3]
Coolant Temperature	250	[K]
Coolant Density	1.41	[kg/m^3]
Blowing Ratio	0.5	

It is important to note that the solution techniques employed in Section 4.3 were held constant throughout the simulations. Changing these could alter the perception of validity of the grids making the analysis inconclusive.

Although only a marginal component of the forthcoming analysis, it was pertinent to perform a similar analysis for the long hole large angle study. Here, two works were viable for comparison, with the work of Kohli et al. [9] offering the most similarities between current and prior research. Here, the hole shape was the only difference between simulations, with the work of Kohli et al. [9] making use of rectangular injection holes, while the current study evaluated cylindrical cooling holes. Similarly, the operating parameters used in these simulations are given in Table 5.

Table 5: Simulation Parameters - Kohli et al.[9]

Property	Value	Units
Freestream Velocity	19.81	[m/s]
Freestream Temperature	298.15	[K]
Freestream Density	1.18	[kg/m^3]
Coolant Temperature	188.15	[K]
Coolant Density	1.88	[kg/m^3]
Blowing Ratio	0.5	

Finally, the short-hole studies also required a similar analysis be performed. The research of Hale [28] provided a good foundation and comparison point for these simulations. The underlying problem with his research was the lack of focus on thermal effects. Rather, his interest lay primarily in analyzing the flow field emanating from these holes. Nevertheless, an analysis was performed using the parameters of Table 6.

Table 6: Simulation Parameters - Hale [28]

Property	Value	Units
Freestream Velocity	10	[m/s]
Freestream Temperature	298.15	[K]
Freestream Density	1.18	[kg/m^3]
Coolant Temperature	317.75	[K]
Coolant Density	1.11	[kg/m^3]
Blowing Ratio	0.5	

This Page Intentionally Left Blank

4 Computational Methodology

The complicated flow physics of film cooling flow can often be difficult to simulate numerically. Much effort has gone into determining the most applicable numerical approach to best represent experimental results. There are a number of factors that play a significant role in determining the validity of a numerical technique including grid quality, turbulence model, and solution technique, and the proper combination of these can deliver excellent results [49].

4.1 Turbulence Model

As was alluded to previously, the design of the grid was largely dependent on the choice of turbulence model. For the sake of computational cost as well as for its demonstration of relative accuracy, the realizable k-ε turbulence model was selected for the simulations performed herein. The k-ε turbulence model is one of several Reynolds-Averaged Navier-Stokes (RANS) turbulence models which takes the Navier-Stokes equations and simplifies them by assuming several closure coefficients such that the equations can be solved without further input on the incoming flowfield.

In its most familiar form, the basic set of conservation equations include continuity, momentum, and energy, given in Equations 5 through 7 [38].

$$\frac{\partial \rho}{\partial t} + \frac{\partial}{\partial x_k}(\rho u_k) = 0 \tag{5}$$

$$\rho \frac{\partial u_j}{\partial t} + \rho u_k \frac{\partial u_j}{\partial x_k} = -\frac{\partial p}{\partial x_j} + \frac{\partial}{\partial x_j}\left(\lambda \frac{\partial u_k}{\partial x_k}\right) + \frac{\partial}{\partial x_i}\left[\mu\left(\frac{\partial u_i}{\partial x_j} + \frac{\partial u_j}{\partial x_i}\right)\right] + \rho f_i \tag{6}$$

$$\rho \frac{\partial e}{\partial t} + \rho u_k \frac{\partial e}{\partial x_k} = -p \frac{\partial u_k}{\partial x_k} + \frac{\partial}{\partial x_j}\left(K \frac{\partial T}{\partial x_j}\right) + \lambda\left(\frac{\partial u_k}{\partial x_k}\right)^2 + \mu\left(\frac{\partial u_i}{\partial x_j} + \frac{\partial u_j}{\partial x_i}\right)\frac{\partial u_j}{\partial x_i} \tag{7}$$

However, RANS equations heavily simplify Equation 6 into the following form [38].

$$\rho \frac{\partial u_j}{\partial t} + \rho u_k \frac{\partial u_j}{\partial x_k} = -\frac{\partial p}{\partial x_j} + \frac{\partial}{\partial x_j}\left(2\mu S_{kj} - \rho \overline{u_k' u_j'}\right) \tag{8}$$

Between Equations 6 and 8, one can see the significant simplifications made in the RANS approach to turbulence modeling. It is in these simplifications that the most fundamental differences lie between RANS models and more advanced models such as LES and DNS. However, these advanced models are still in their relative infancy and require significant computational cost, driving the hesitancy towards their use in the current study.

The standard k-ε model was first proposed by Spalding and Launder [50] and has gone through a multitude of iterations to arrive at its current form. There are also a significant number of variants all designed to serve unique purposes from low Reynolds number flows to flows with freestream and crossflow interactions, as is the case in the current study. The realizable k-ε model was designed to satisfy this purpose, and it does so effectively.

The realizable k-ε model, proposed by Shih et al [43], refined the dissipation rate and eddy-viscosity equations, to make the k-ε turbulence model applicable to flows with blowing and strong gradients. The revised equations used in this model also significantly improve the model's axisymmetric jet spreading abilities making it a prime candidate for film cooling applications. Equations 9 through 11 outline the solution scheme for this model.

$$\frac{\partial}{\partial t}(\rho k)+\frac{\partial}{\partial x_j}(\rho k u_j)=\frac{\partial}{\partial x_j}\left[\left(\mu+\frac{\mu_t}{\sigma_k}\right)\frac{\partial k}{\partial x_j}\right]-\rho\varepsilon+\tau_{ij}\frac{\partial u_i}{\partial x_j} \quad \textbf{(9)}$$

$$\frac{\partial}{\partial t}(\rho \varepsilon)+\frac{\partial}{\partial x_j}(\rho \varepsilon u_j)=\frac{\partial}{\partial x_j}\left[\left(\mu+\frac{\mu}{\sigma_\varepsilon}\right)\frac{\partial \varepsilon}{\partial x_j}\right]+\rho C_1 S_\varepsilon-\rho C_2\frac{\varepsilon^2}{k+\sqrt{\nu\varepsilon}}+C_{1\varepsilon}\frac{\varepsilon}{k}C_{3\varepsilon}G_b+S_\varepsilon \quad \textbf{(10)}$$

$$\nu_T=C_\mu\frac{k^2}{\varepsilon} \quad \textbf{(11)}$$

One further improvement over the standard k-ε model arises from the fact that the closure coefficient, C_μ, is no longer constant. Rather, it is a variable that can change dependent on flow condition, further improving the viability of the model [43].

Two equation models solve wall boundary layers differently than their more advanced counterparts. Whereby direct numerical simulations solve the flow regime in its entirety, RANS turbulence models make use of wall functions or near-wall modeling techniques to evaluate the complicated phenomena in

the near-wall region. The use of wall functions models the near-wall region empirically, requiring low nodal density in this region. In particular the wall nodes must lie within the non-dimensional distance of $5 < y+ < 50$ [51]. However, wall functions can often overlook critical features of the flowfield which could critically impact the solution.

Near-wall modeling (also known as a two-layer solution) solves the entire computational domain by applying the law of the wall in the near-wall region and building it into the freestream where the base solver takes over. The use of such grids requires y^+ values in the neighbourhood of 1, which can dramatically increase the computational cost of the model. However, research has shown that this model offers excellent film cooling performance making it desirable in the present study.

4.2 Solution Approach & Convergence Criteria

To minimize computational cost, air was modeled as an incompressible ideal gas. The selection of such approach was wholly applicable since the local Mach number always remained at least one order of magnitude smaller than the critical Mach number for compressibility effects.

The use of multi-core processing power allowed for the use of higher order solvers than would otherwise have been employed. The momentum, energy, and turbulence model equations were solved using the QUICK solution scheme. The QUICK scheme makes use of the weighted-average of the second-order upwind scheme and combines the results with that of central interpolation of the variable in question to arrive at a solution [52]. This approach is particularly successful when evaluating hexahedral grids, and since the current mesh was made up of hexahedral elements, it was a prime candidate for this approach. Further, the pressure-velocity coupling was solved using the SIMPLEC solution scheme with skewness correction, while the remaining solvers were simulated using the second-order upwind technique.

The convergence criteria were set such that the weighted residuals between successive iterations not exceed 10^{-4} for any solution parameter. Due to the complicated nature of the flow, the aggressive default under-relaxation factors in FLUENT® [53] were modified on a per-case basis to artificially slow the solution in order to arrive at an adequately converged solution. Doing so led to convergence within 1000 iterations for the half-plane models, up to 4000 iterations for the short hole models, and up to 6000 iterations for the long hole models.

4.3 Grid Generation Technique

In developing the computational grid, it was of the utmost importance to generate a grid that would produce results indicating that the solution was grid independent. To achieve such a result, a coarse base grid was generated and three more refined grids were generated by increasing the node count per edge by 10%. To compare the results, simulations were run using identical operating parameters to determine the deviation between solutions.

Studies including that of Yavuzkurt et al. [49] have illustrated the importance of proper grid generation for film cooling techniques. In particular, it was noted that tetrahedral grids often do not predict the mixing of film cooling regimes adequately. Improved results have been found using a hexahedral approach as seen in Lu [54] illustrating its applicability to complicated film cooling phenomena.

Due to the nature of the turbulence model, it was necessary that the wall y^+ value be close to 1, indicating that the grid in this region be very dense to accommodate for the full solution through the viscous sublayer. Similarly, the regions slightly up- and downstream of the holes are generally regions of significant flow mixing and interaction. This was a driving factor for increased mesh density in these regions as well. Further regions were meshed such that the overall node count could be optimized without exceeding a stretch factor of 1.1.

The near-hole region of the shallow-angle half plane model is shown in Figure 5, while the long and short-hole grids are shown in Figures 6 and 7. Note that GAMBIT® [53] was used to generate all computational grids developed in the current study.

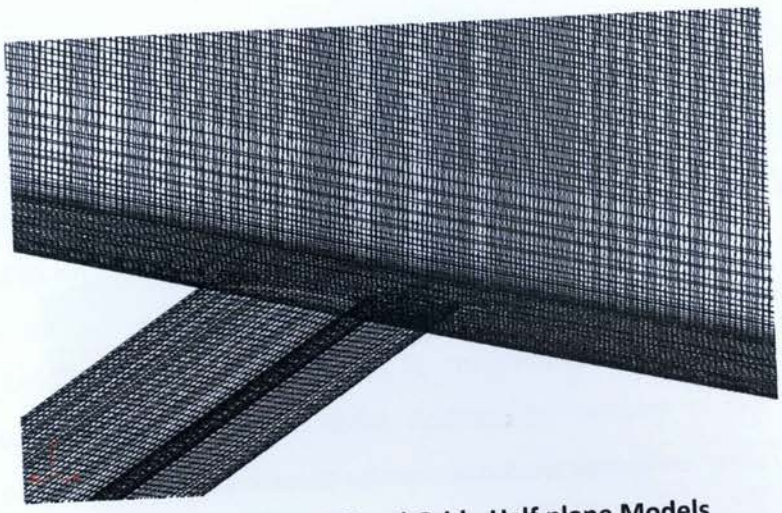

Figure 5: Computational Grid - Half plane Models

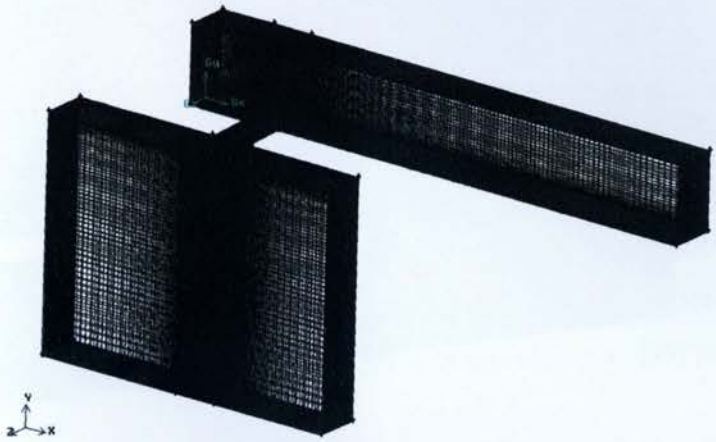

(a) Computational Domain

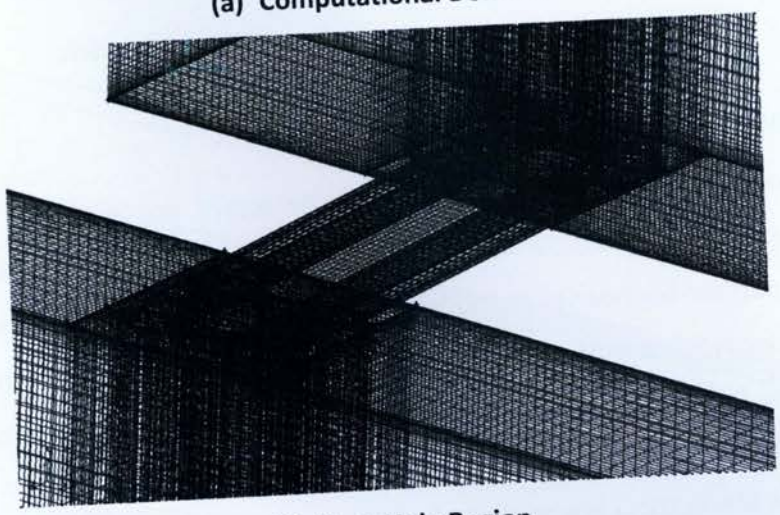

(b) Near-Hole Region

Figure 6: Computational Domain - Long Hole Models

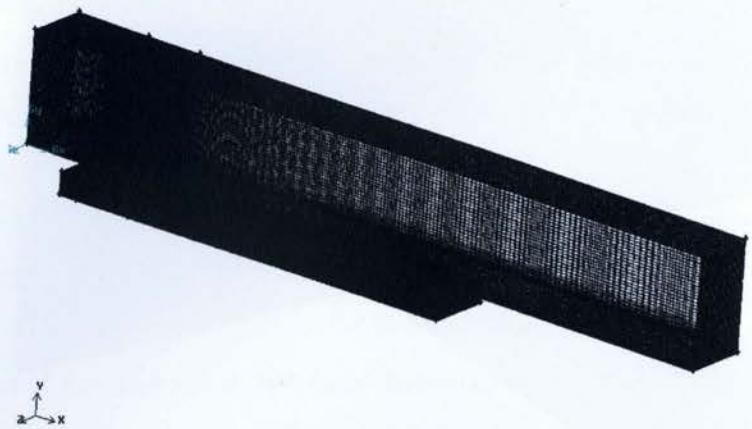

(a) Computational Domain

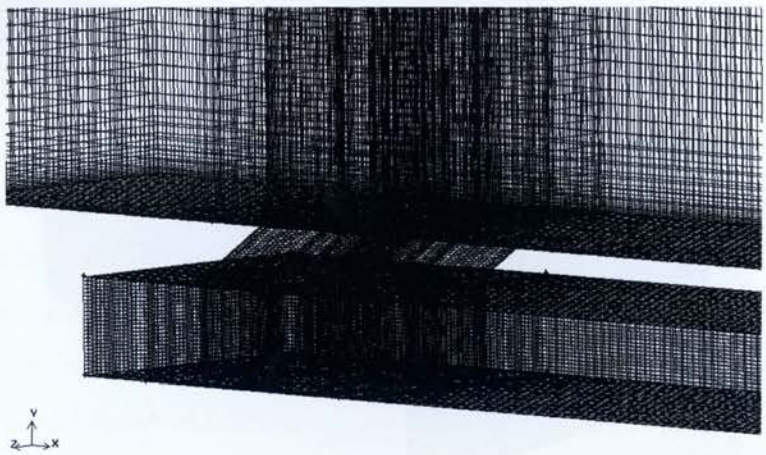

(b) Near-Hole Region

Figure 7: Computational Domain - Short Hole Models

4.4 Computational Domain

Appropriately defining the boundary conditions is a necessary and nontrivial task in numerical simulations. Due to the incompressible nature of these simulations, it was possible to make use of velocity inlets and outflow boundaries to model the flow. Velocity inlets allow the user to specify a temperature and velocity while outflow boundaries require no user input, forcing the solver to iterate the solution along the boundary. It should be noted that outflow boundaries are most acceptable when the exiting flow is fully developed. Due to the length of the flow field, this assumption is valid; however a comparison between the outflow boundary and pressure outlet boundary (with freestream backflow conditions) illustrated negligible variations between solutions, indicating that the use of the outflow boundary was acceptable.

All wall surfaces were defined as adiabatic walls. By setting the wall heat flux to zero, it was ensured that there would be no heat loss through any of these surfaces. Finally, two further conditions were used at the left and right bounding walls of the plate and plenum. The half-plane study made use of a symmetry boundary along the centre-plane of the geometry. The use of such a boundary condition minimized computational cost in preliminary studies. The comparative long and short hole studies made use of periodic boundary conditions to the left and right of the bounding sister holes as well as on the coinciding faces of the plenum. Doing so allowed for the simulation of an array of jets rather than a single hole as studied in the half-plane model. Additionally, removal of the symmetry boundary condition lifted the restriction of a symmetric solution about the centreline, which is a necessity for the evaluation of the left/right case.

The following figures contain the computational domains for the half-plane, long hole, and short hole cases. Each has been colour coded to indicate where each boundary condition is applied. Here, velocity inlets are coloured green, outflow boundaries are coloured red, adiabatic walls are purple, and periodic and symmetry boundary conditions are coloured yellow. Also, although not truly a separate entity, the coolant holes have been coloured blue as they can be individually manipulated between interior and wall boundaries dependent on simulation. Note that similar boundary conditions have been utilized with great success in the works of Lu [54], Azzi et al. [26], and Nemdili et al. [55] justifying their use in the current simulations

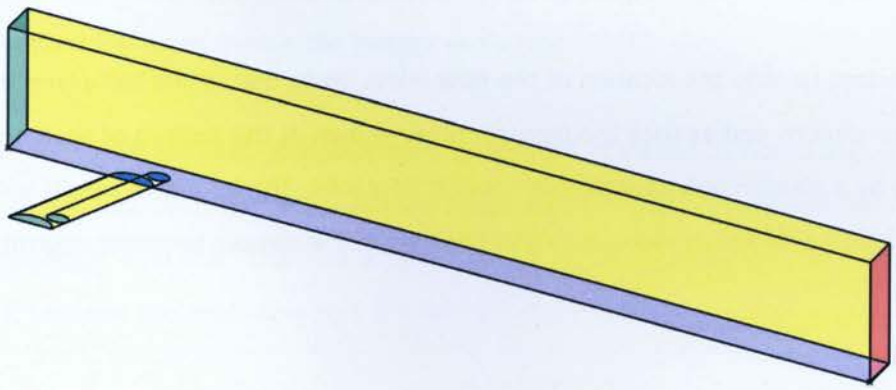

(a) Half-Plane Models

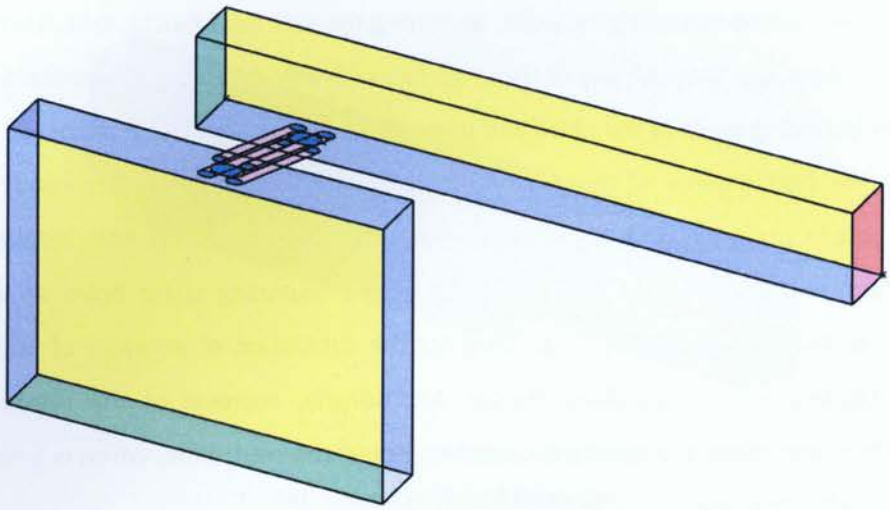

(b) Long Hole Models

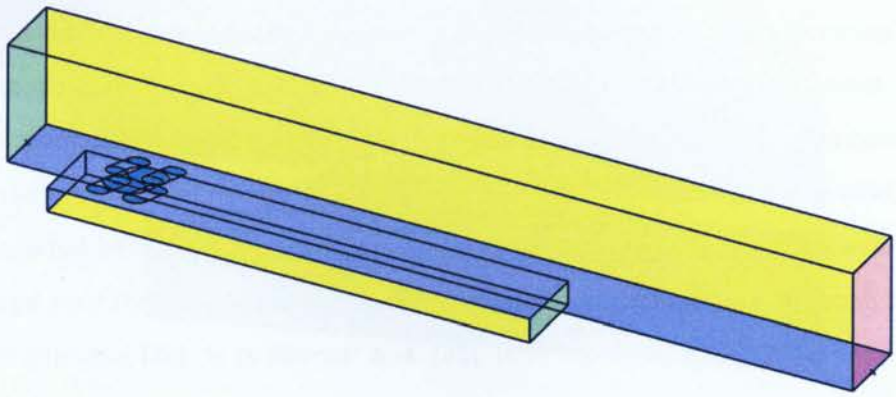

(c) Short Hole Models

Figure 8: Computational Domains

Here, it is important to note the location of the flow inlets. Note that in the half-plane model, the flow enters each hole directly and as such the flow inlets are shown as the bottom of each hole. In contrast, the models fed by a plenum only contain one coolant flow inlet. The long-hole case is bottom-fed while the short-hole case is side-fed in such a way that the flow in the plenum becomes oppositely oriented to the freestream.

5 Half-Plane Models

The study of half-plane models was originally intentioned as a point of reference for the research found in sections 5 and 6 of this thesis; however, it quickly turned into a more thorough evaluation. The work performed in this section primarily served two purposes: determining the basic applicability of sister hole film cooling and comparing the effect of sister holes of varying inclination angles.

The following discussion will be broken into a discussion on grid sensitivity and will then proceed into a discussion on adiabatic effectiveness where the benefits of the addition of downstream sister holes will be evaluated and compared between shallow (35)° and large (55°) angle injection holes.

5.1 Sensitivity Analysis

The sensitivity analysis component of this work was performed to ensure that the grid was generating sensible accurate measurements of the complicated flow field that is film cooling. For each case, a benchmarking study was used to validate the numerical results. As discussed earlier, the shallow (35°) angle model was compared against the research of Sinha et. al [48]. This group performed experimental simulations with geometrical conditions similar to those evaluated in the current study. As a result, it was expected to note significant similarities between studies.

The large (55°) angle case was benchmarked against the study of Kohli et al. [9]. Their research group made use of seemingly similar geometry to the current study but evaluated rectangular injection holes rather than the cylindrical holes used in the current evaluation.

For this analysis, four grids for each geometry were generated. It should be noted that, interestingly, to obtain a grid independent solution for the shallow-angle study, the grid count was notably lower than that of the large-angle injection. This was a direct result of complicated mixing in the downstream region. Figure 9 contains the centreline and laterally averaged adiabatic effectiveness for the shallow-angle study.

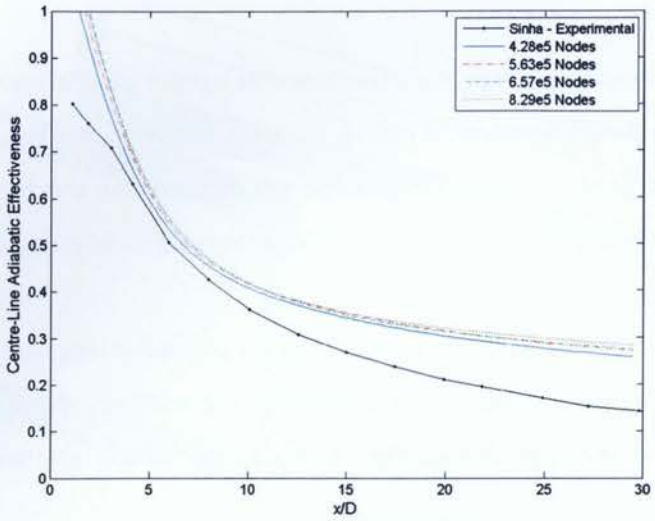

(a) Centreline Effectiveness

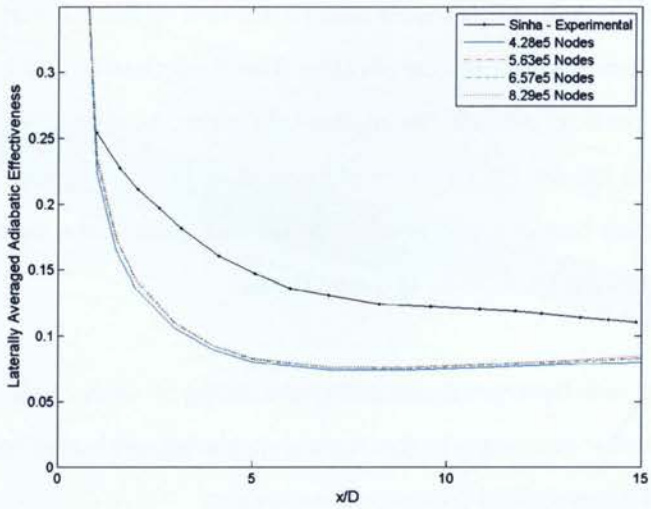

(b) Laterally Averaged Effectiveness

Figure 9 : Sensitivity Analysis – Shallow (35°) Angle

The centreline case shows excellent data matching while the laterally averaged case illustrates that the trends are matched with significant under-prediction of the flow. These differences, relative to the experimental work, can be attributed to two primary factors. Most prominently, the use of the realizable k-ε turbulence model is the most likely culprit. Additionally, the use of longer holes, in the current study, than the baseline case could also have driven the deviations. However, further justification of the turbulence model deviations will be discussed shortly.

Figure 10 contains the sensitivity analysis for the large-angle injection against the work of Kohli et al. [9].

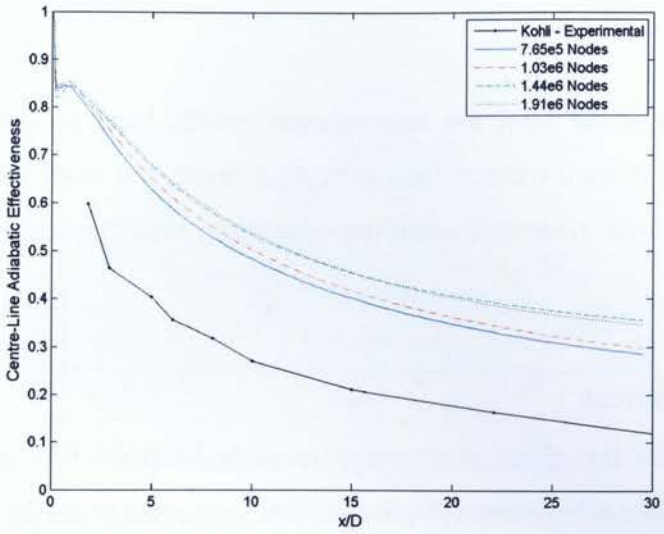

(a) Centreline Effectiveness

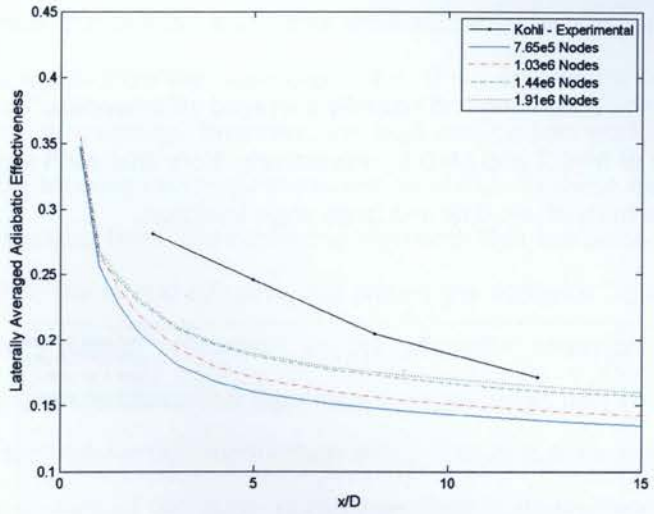

(b) Laterally Averaged Effectiveness

Figure 10: Sensitivity Analysis – Large (55°) Angle

As one would expect, the trends between the large and shallow angle analyses are highly similar. The lateral results match the experimental with a higher degree of accuracy than the centreline results, while both matched trends adequately. Although there is a notable deviation between experimental and computational results, other similar research has shown the same deviations and has been able to adequately correlate them to a variation as a result of the turbulence model. The work of Na et al. [56] compared their numerical work to that of the work of Kohli et al. [9]. Their trends indicated similar

discrepancies with an over-prediction of centreline effectiveness and an under-prediction of lateral effectiveness, leading to the identification of the turbulence model as the most likely culprit for these deviations.

However, even with deviations from the experimental results, both geometries demonstrate grid independent results by the third most refined grid. As a result, the shallow-angle simulations were carried out with the 6.57×10^5 node grid while the large-angle simulations were carried out with the 1.44×10^6 node grid.

5.2 Adiabatic Effectiveness

To most astutely evaluate the effect of downstream sister holes on film cooling performance, an evaluation of the adiabatic effectiveness for the shallow and large angle injections will ensue. The following figures will illustrate the baseline single and sister hole cases for each of the four blowing ratios evaluated.

Figures 11 and 12 contain the centreline and laterally averaged effectiveness for shallow and large-angle injection at blowing ratios of M=0.2 and M=0.5, respectively. Note that each image contains both single hole and sister hole results for both shallow and large angle injection.

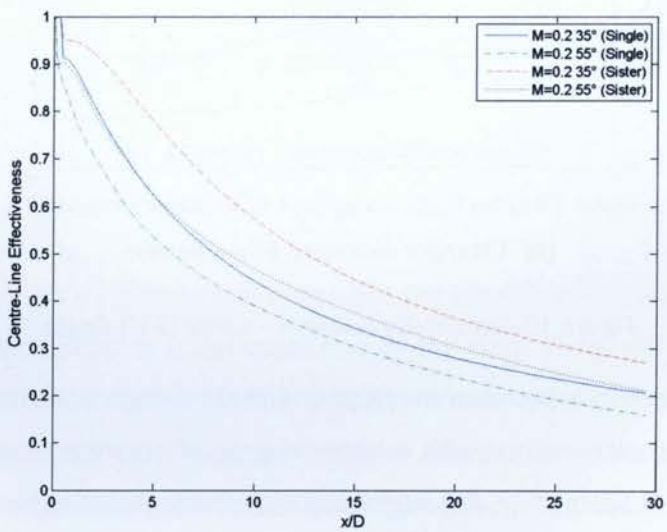

(a) Centreline Effectiveness

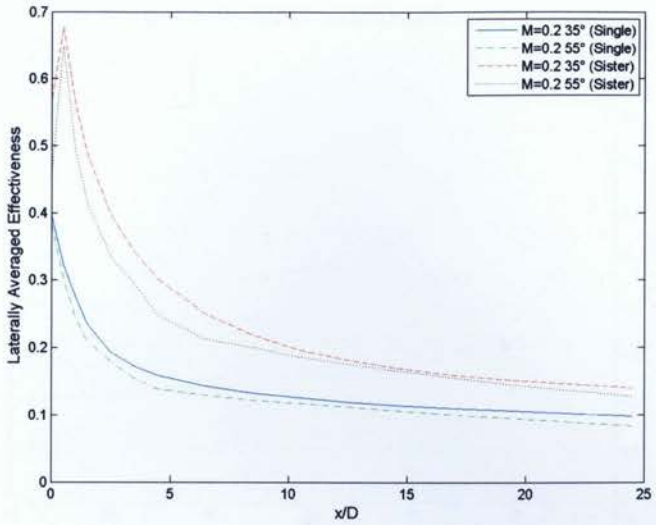

(b) Laterally Averaged Effectiveness

Figure 11: Adiabatic Effectiveness – Half Plane (M=0.2)

Interesting results arise immediately when examining the above Figures. Firstly, at the lowest blowing ratio of M=0.2, as expected, the shallow-angle case provided better protection along the centreline and laterally in the near-hole region than the large-angle case. This is largely due to reduced dissipation as a result of its lower vertical momentum. However, the high vertical momentum of the large-angle case works in its favour as the blowing ratio was increased to M=0.5. In these cases, the near-hole region provides an interesting analysis. Here, the centreline illustrates that the plate is better protected by the low inclination angle, while the lateral effectiveness argues the opposite. This indicates that the higher inclination angle provides better protection in the spanwise direction of the plate; however, downstream, the large angle injection offers significant improvements over the small angle as a result of flow separation. Due to the high vertical momentum of the flow as it arises from the injection holes, the flow separates from the surface of the plate, reattaching further downstream – increasing the overall effectiveness in this region.

Figures 13 and 14 contain the M=1.0 and M=1.5 blowing ratio cases for the current geometry.

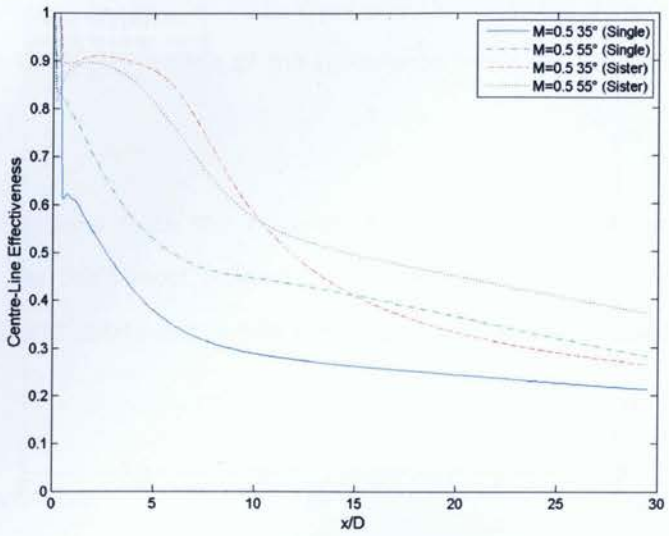

(a) Centreline Effectiveness

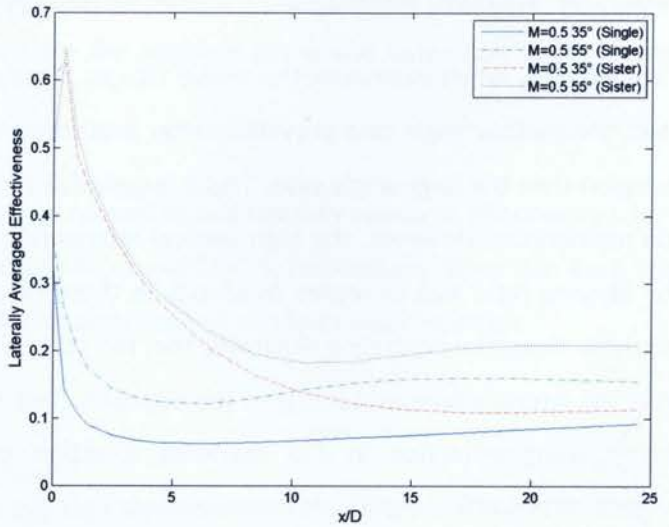

(b) Laterally Averaged Effectiveness

Figure 12: Adiabatic Effectiveness – Half Plane (M=0.5)

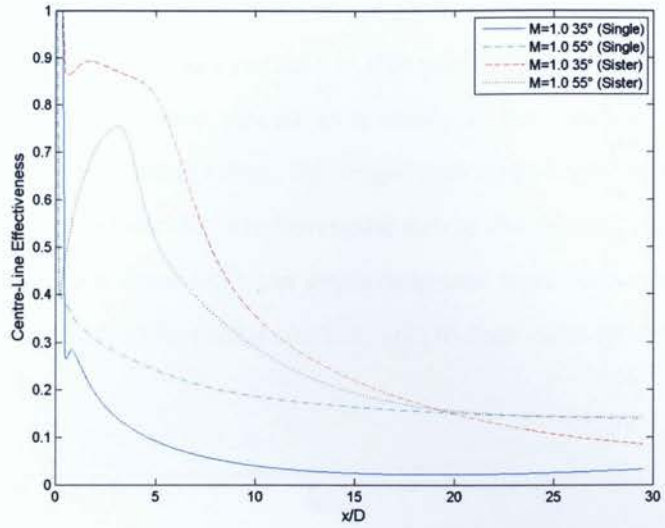

(a) Centreline Effectiveness

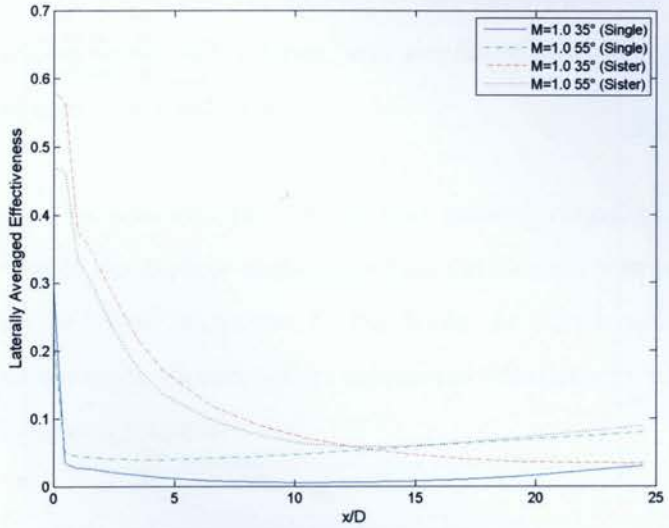

(b) Laterally Averaged Effectiveness

Figure 13: Adiabatic Effectiveness – Half Plane (M=1.0)

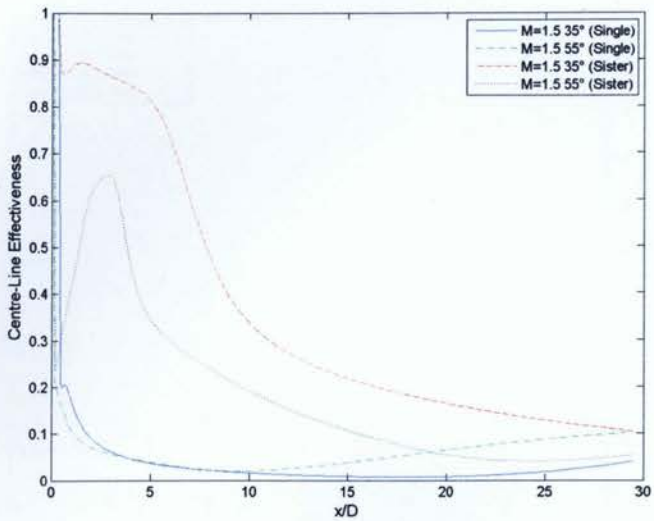

(a) Centreline Effectiveness

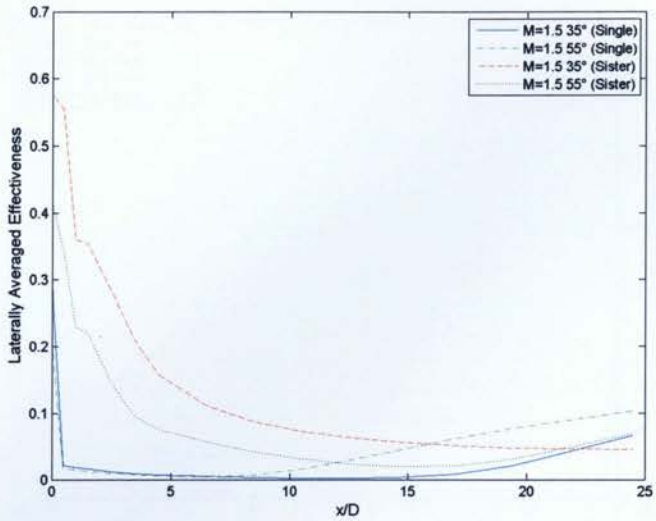

(b) Laterally Averaged Effectiveness

Figure 14: Adiabatic Effectiveness – Half Plane (M=1.5)

These higher blowing ratio cases offer an interesting comparative to the low blowing ratio cases. Although the reattachment region is still evident in the large angle cases, as the blowing ratio increases, this region moves increasingly downstream of the primary injection hole. Due to the length of time the flow is separated from the blade, the flow mixes heavily with the mainstream, decreasing the overall effectiveness of the technique. Alternately, although the shallow angle dissipates quite heavily shortly downstream of the primary hole, these holes offer a more uniform flow field with better overall cooling performance.

As expected, the sister holes offer significantly improved performance over the standard single hole case at all blowing ratios. The effects are most notable in the near-hole region particularly at high blowing ratios, as the coolant is naturally more spread as a result of the location of the sister holes. It is interesting to note that at high blowing ratios, the single hole large-angle injection case surpasses the sister hole cases far downstream from the ejection point due to the reattachment of its separated flow. Unlike the large-angle sister hole simulation, the single hole case does not suffer from the same degree of vertical momentum as a result of less total coolant. This in turn leads to less flow mixing and better overall effectiveness.

5.3 Conclusion

The results contained in the analysis above indicate that the sister hole cooling technique offers a viable alternative to simple single hole cooling. The technique has been shown to offer significant coolant improvements, particularly at high blowing ratios, and should be evaluated further to determine its viability under a variety of operating conditions.

The results in the present section indicate that at low blowing ratios, the large angle approach marginally outperforms that of the shallow-angle, but offers significantly improved performance further downstream as the separated flow reattaches to the blade. At high blowing ratios, more notable deviations arise as the shallow angle injection offers substantial effectiveness improvements in the near-hole region over its large angle counterpart.

In considering the results of the present analysis, the low angle injection was selected for the remaining studies. Since blowing ratios are usually in the vicinity of $M \geq 1$, it was important to optimize the technique for this condition. Additionally, the simplifications made in the half-plane model, most notably the lack of a plenum and use of a symmetry plane, may have adversely impacted the results of the present analysis. As a result, the following analyses make use of more highly developed geometries including plenums and fully designed freestream regions.

This Page Intentionally Left Blank

6 Long Hole Models

Long holes have been the prime focus of film cooling research to date. A multitude of numerical and experimental studies have all shown that fully developed flow emanates from coolant holes in a fairly predictable manner. However, these long holes have been shown to vary in effectiveness based on plenum design, dictating that much is still unknown about the field of film cooling.

Primarily, this analysis will allow for the comparison between long and short holes with their respective plenum types to demonstrate the change in flow structure and, as a result, film cooling effectiveness for each geometry.

6.1 Sensitivity Analysis

As with the half-plane models, it was necessary to illustrate that the solution obtained in the long hole study was in fact grid independent. To do so, a comparison was run with only the primary hole active. This allowed for a comparison against the research of Sinha et al. [48] to maintain consistency.

The most relevant means of comparison is that of adiabatic effectiveness. Both the centreline and laterally averaged adiabatic effectiveness for the sensitivity analysis are found in Figure 15.

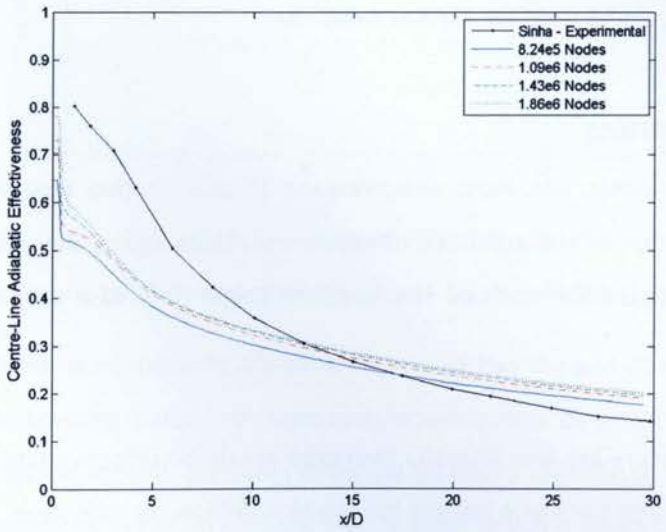

(a) Centreline Effectiveness

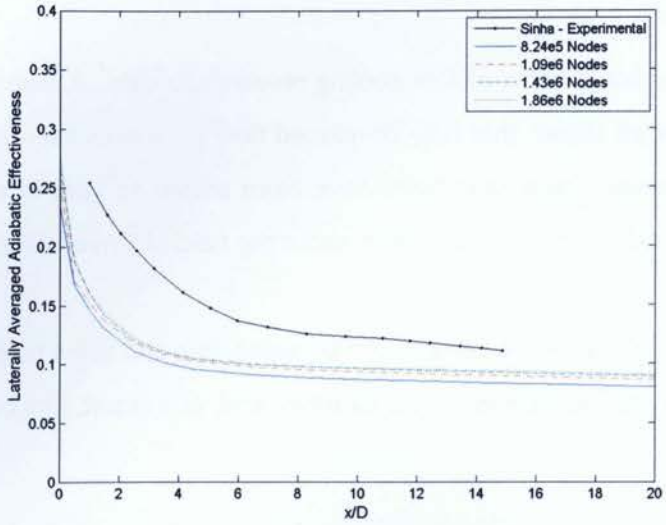

(b) Laterally Averaged Effectiveness

Figure 15: Sensitivity Analysis - Long Hole

These figures indicate that while the solution is clearly grid independent, the centreline results are over-predicted while the lateral results are under-predicted. Once again, this can be directly attributed to the use of the realizable k-ε turbulence model. As illustrated in Section 5.1, Na et al. [56] demonstrated similar discrepancies with roughly the same percentage over and under prediction against experimental results. As such, it can be argued that the results from the 3rd most refined grid with 1.43x10^{6} nodes was sufficiently refined and could be used for further solutions.

6.2 Adiabatic Effectiveness

As with the half-plane models, the most direct means of quantitative analysis of each film cooling technique was an evaluation of the adiabatic effectiveness. Once again, these will be broken down by blowing ratio and each figure will include the baseline single hole case coupled with its sister hole counterparts.

Figure 16 contains the centreline and laterally averaged adiabatic effectiveness for the M=0.2 blowing ratio while Figure 17 contains the same images for the M=0.5 blowing ratio case.

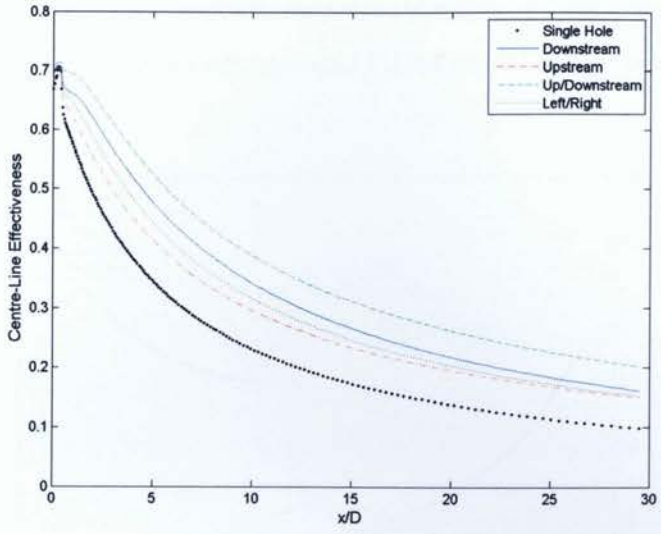

(a) Centreline Effectiveness

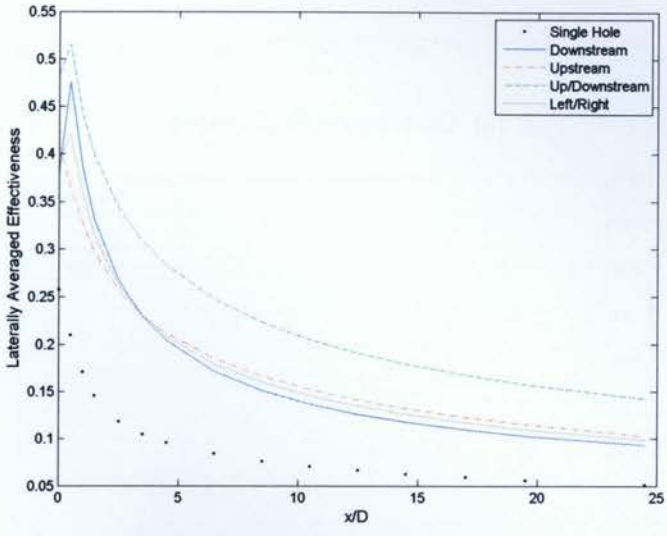

(b) Laterally Averaged Effectiveness

Figure 16: Adiabatic Effectiveness - Long Hole (M=0.2)

As one would expect there is no notable lift-off with any of the designs at the low blowing ratio of M=0.2. At such a low blowing ratio the upstream/downstream design offers optimal coverage, particularly noted in its lateral spread. Similarly, it should be noted that the designs with only two sister holes offer negligible deviations between one-another; a point which is important due to the significant coolant cost of operating four sister holes. At the M=0.5 blowing ratio, there is a small separation bubble primarily evident in designs with downstream holes; however, the flow quickly reattaches and performance is restored. Interestingly, as the solution progresses downstream, the case with downstream-only holes offers the poorest performance of the cooling candidates.

Figure 18 contains the centreline and laterally averaged effectiveness for the M=1.0 blowing ratio while Figure 19 contains the same results for the M=1.5 blowing ratio case.

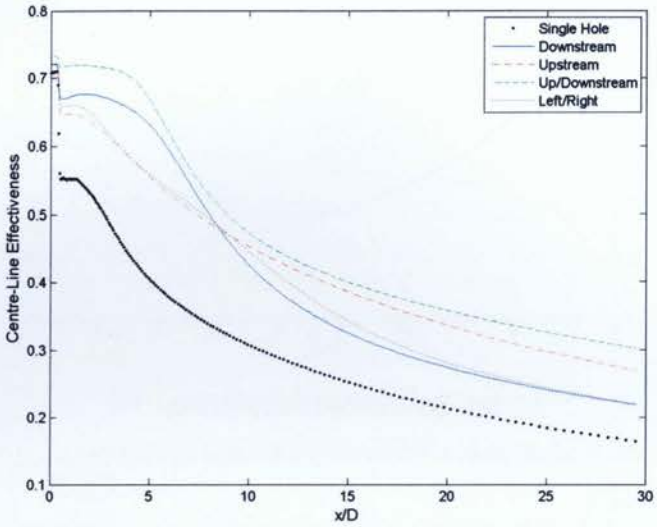

(a) Centreline Effectiveness

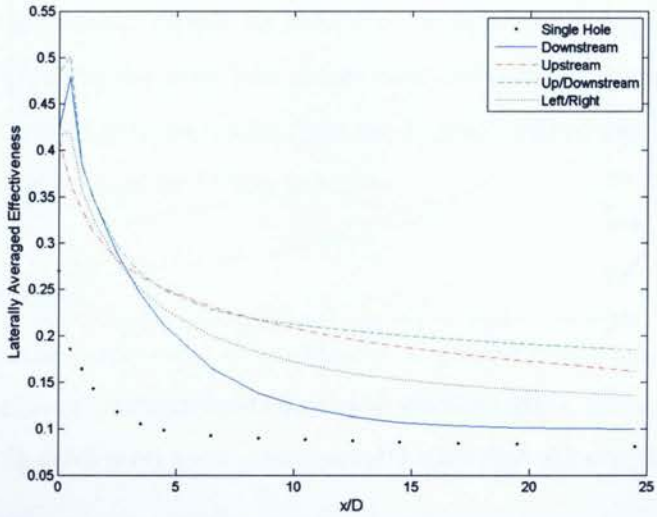

(b) Laterally Averaged Effectiveness

Figure 17: Adiabatic Effectiveness - Long Hole (M=0.5)

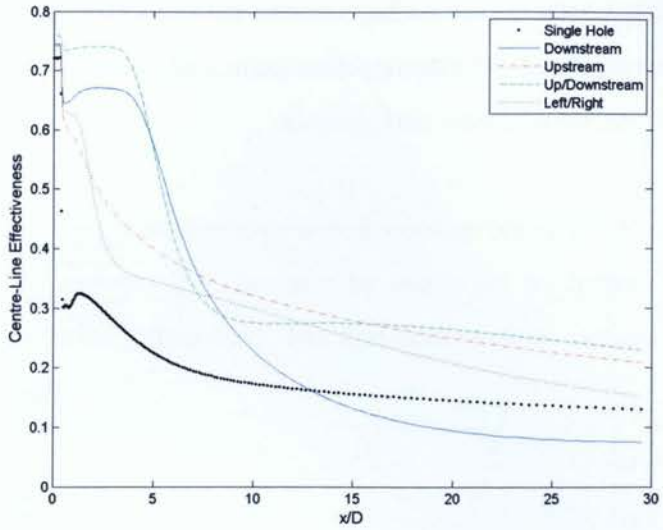

(a) Centreline Effectiveness

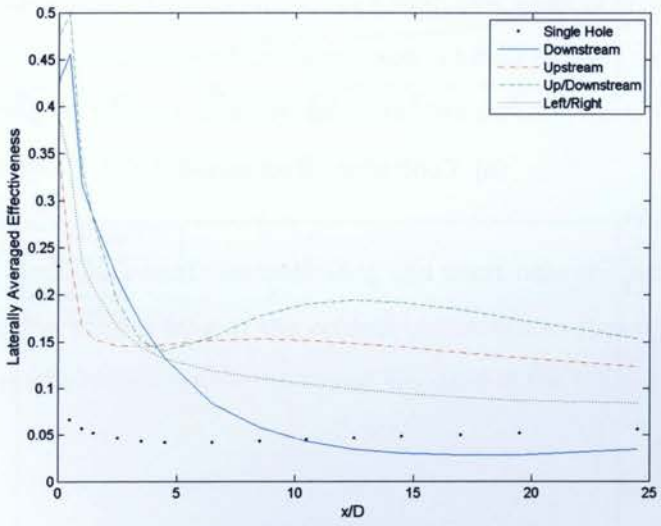

(b) Laterally Averaged Effectiveness

Figure 18: Adiabatic Effectiveness - Long Hole (M=1.0)

At these higher blowing ratios the results from the centreline and lateral analyses become increasingly complex. It is here that the discrepancies between sister hole designs become increasingly notable. At M=1.0 the downstream-only holes provide the most notable benefits in the near-hole region. Unfortunately, this advantage dissipates quickly becoming less effective than the single hole case for x/D>10. This can be attributed to the increased momentum of the flow leading to a primary coolant stream that does not fully reattach to the wall. In contrast, the cases with upstream holes performed better over the entire computational domain. This characteristic was due to the upstream jets

interacting with the primary coolant flow, forcing it to the surface of the blade. Further improvements are noted due to the jets lifting off at their ejection point and reattaching downstream, leading to improvements in both up- and downstream performance.

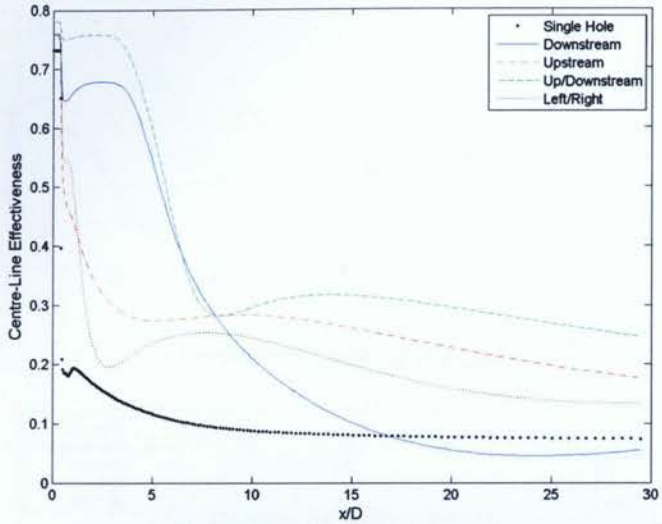

(a) Centreline Effectiveness

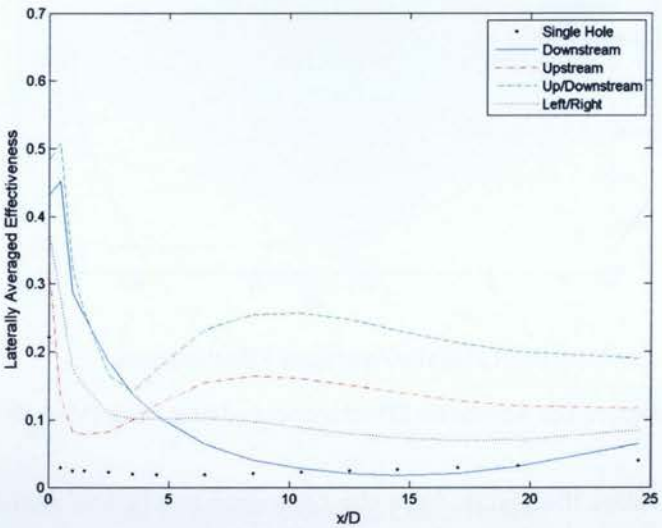

(b) Laterally Averaged Effectiveness

Figure 19: Adiabatic Effectiveness - Long Hole (M=1.5)

Similar results were obtained at the blowing ratio of M=1.5. Aside from the near-hole region which is still best protected by the downstream case, the geometries with upstream holes provided the best coolant protection over the entire computational domain. Interestingly, as one would expect, the

separation region, as a result of jet ejection at the high blowing ratio of M=1.5, is very notable. However, the use of sister holes reduces this effect significantly, leading to a solution with little separation and reduced dissipation.

While quantitative results help indicate how well a cooling technique is performing, there are a multitude of qualitative approaches that can also be evaluated to determine the impact a cooling technique has on the surrounding flow field. The first such analysis will evaluate the effect cooling techniques have on jet lift-off.

6.3 Primary Jet Lift-Off

The following section will illustrate the effect of sister holes of varying orientation on the entrainment of the coolant on the hot mainstream flow. As previously noted, as a result of high vertical momentum, the primary flow often separates from the surface of the plate at high blowing ratios. The addition of two additional counter-rotating vortex pairs dramatically alter the solution (as will be discussed in Section 6.4), leading to a more cohesive flowfield.

The jet lift-off and flow structure results for both long and short hole studies make use of a common temperature colour key. The scale is blue at the coldest temperatures (the coolant stream) and red at the hottest temperatures (the mainstream). The colour key used in the following analyses is provided in Figure 20.

Figure 20: Temperature Colour Key

To evaluate jet lift-off, a cut plane down the centreline of the plate was analyzed for flow reversal and temperature magnitude. The following figures contain the cut-plane flowfield at blowing ratios of M=0.2, 0.5, 1.0, and 1.5 for each of the five geometries. Figures 21 and 22 contain the separation for the M = 0.2 and M=0.5 blowing ratio cases.

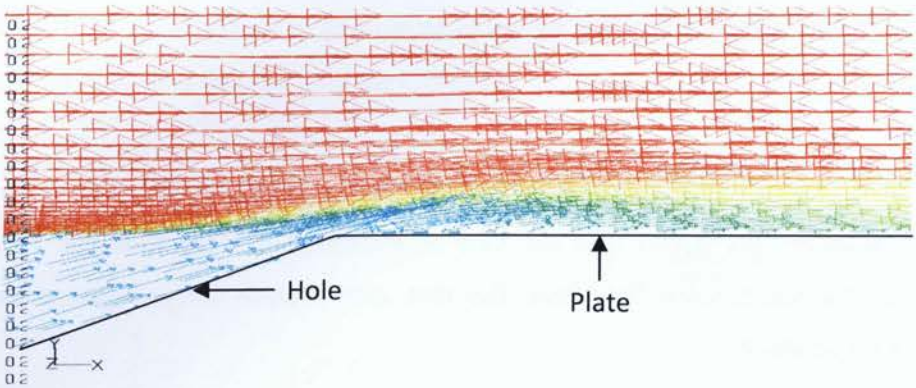

(a) Single Hole

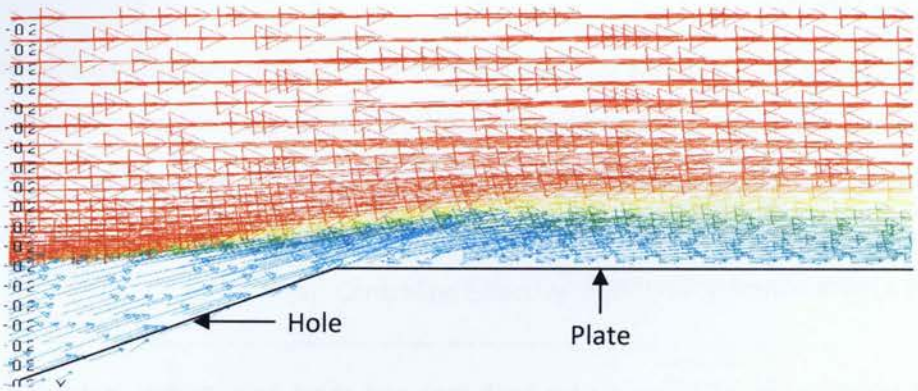

(b) Downstream Sister Holes

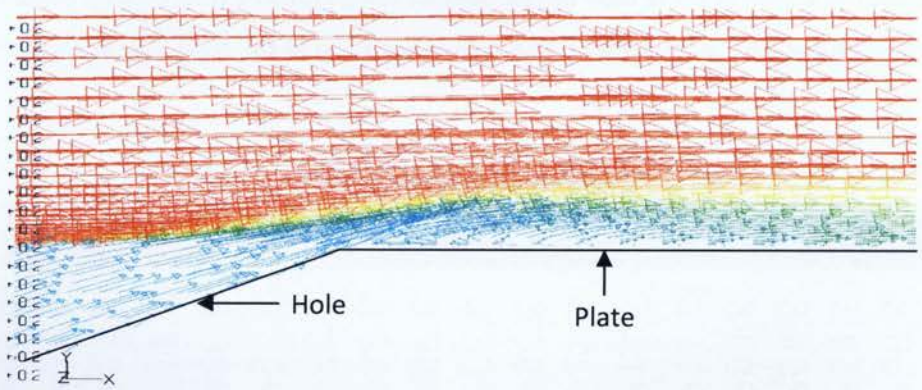

(c) Upstream Sister Holes

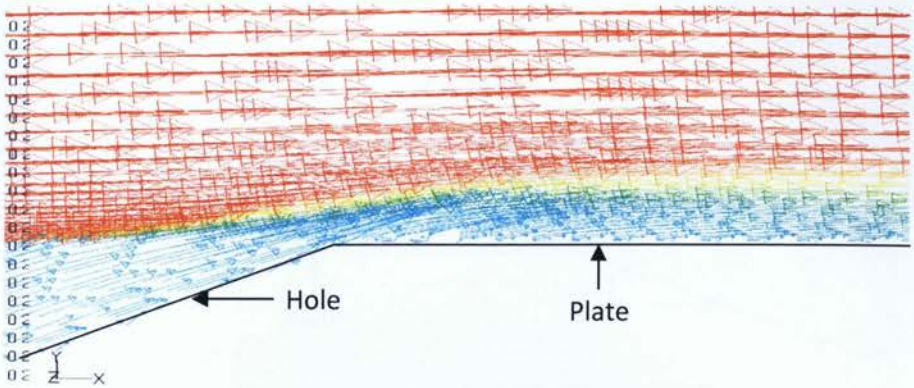

(d) Upstream/Downstream Sister Holes

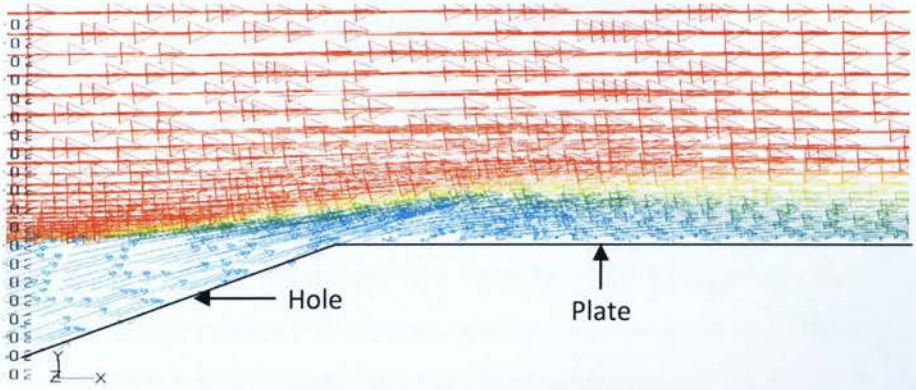

(e) Left/Right Sister Holes

Figure 21: Jet Lift-Off - Long Hole (M=0.2)

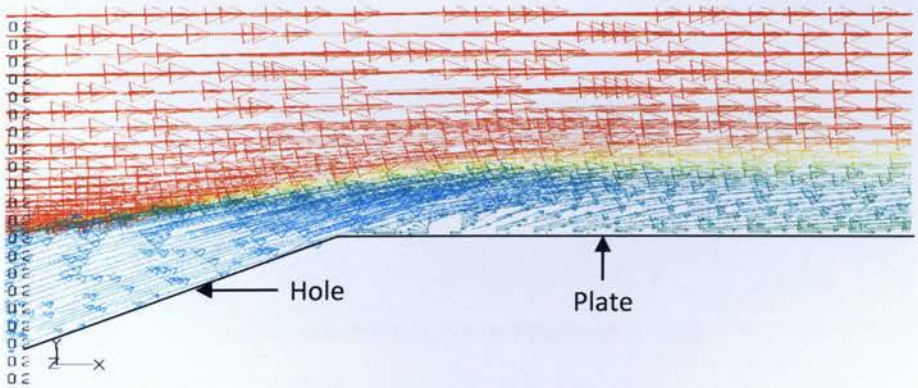

(a) Single Hole

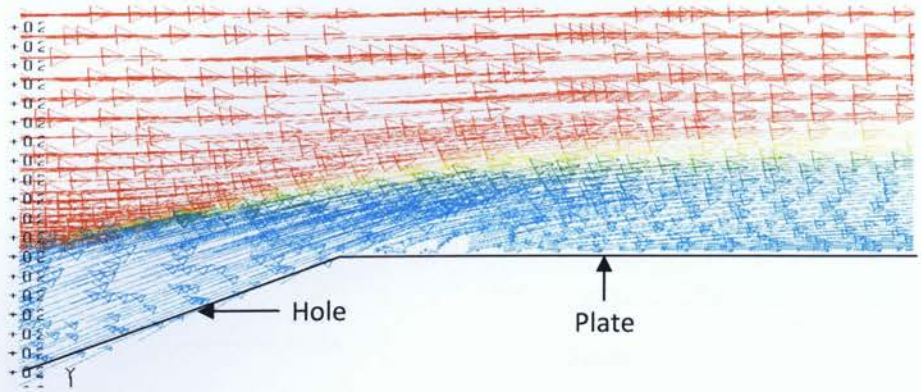

(b) Downstream Sister Holes

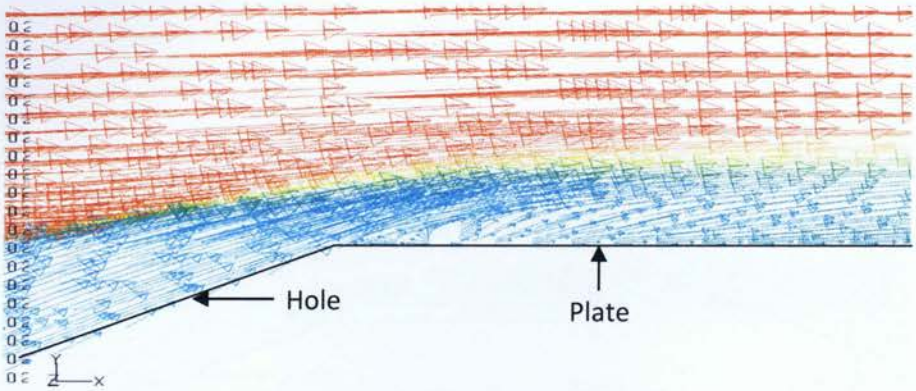

(c) Upstream Sister Holes

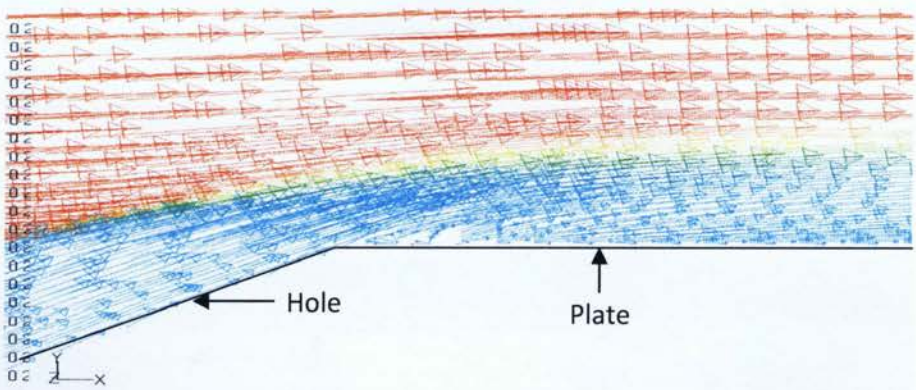

(d) Upstream/Downstream Sister Holes

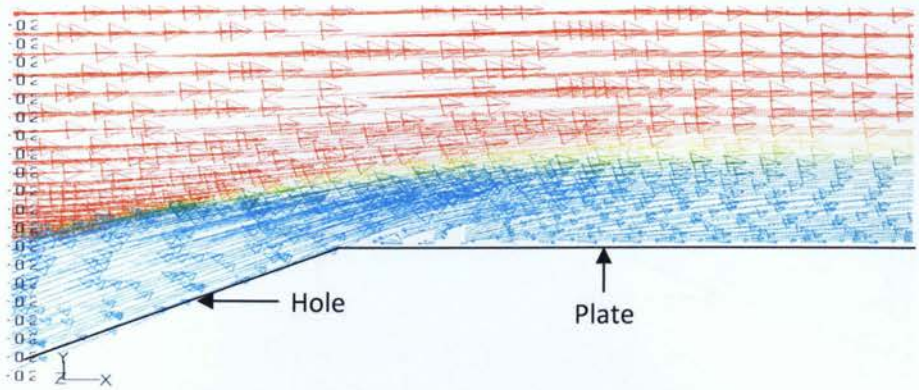

(e) Left/Right Sister Holes

Figure 22: Jet Lift-Off - Long Hole (M=0.5)

The previous figures illustrate two interesting trends. The first is that, as noted in the effectiveness analysis, there is no separation or reversal region for the lowest blowing ratio of M=0.2. However, at M=0.5 there is a slightly reversed region which is not significantly improved by the addition of the sister holes in any configuration. That being said, the velocity vectors, coloured relative to their static temperature, indicate a step change in temperature when sister holes in any orientation are added to the solution, indicating better overall protection from the freestream.

While the low blowing ratio cases were of little interest from a practical standpoint, Figures 23 and 24 which contain the M=1.0 and M=1.5 blowing ratio cases provide a more interesting analysis.

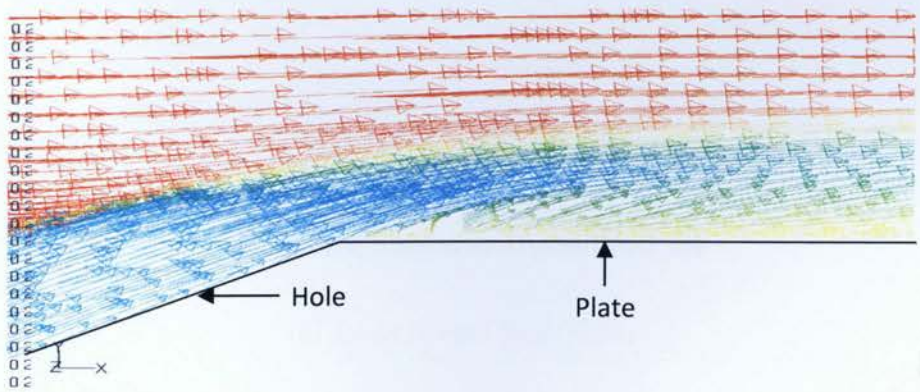

(a) Single Hole

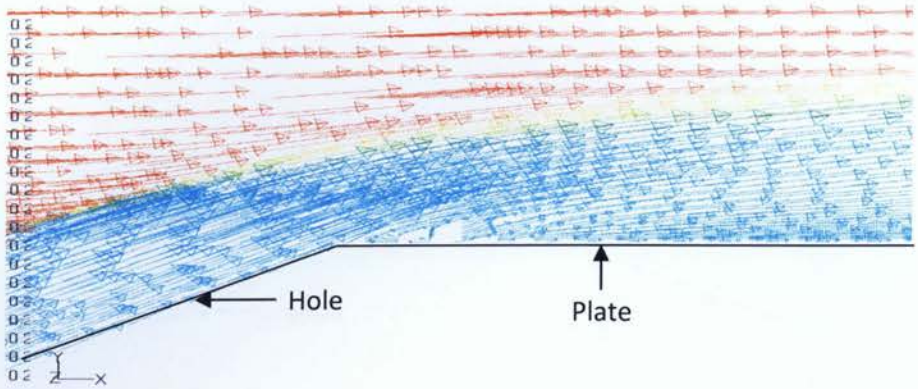

(b) Downstream Sister Holes

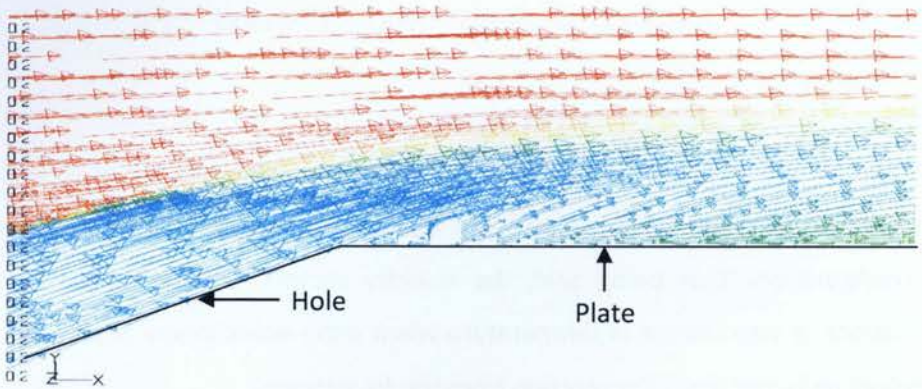

(c) Upstream Sister Holes

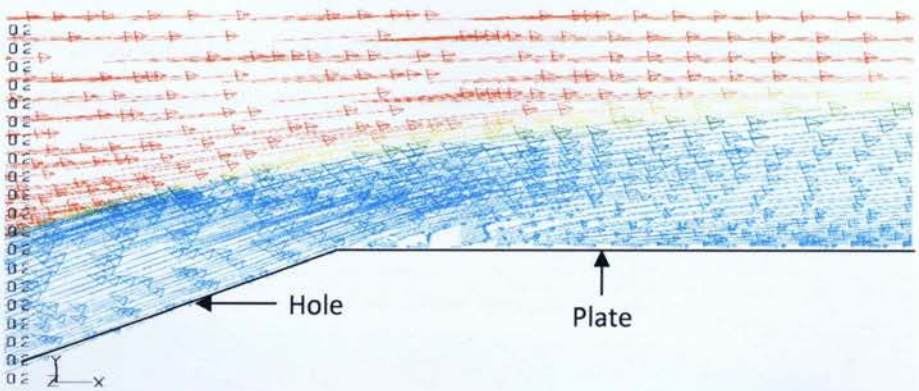

(d) Upstream/Downstream Sister Holes

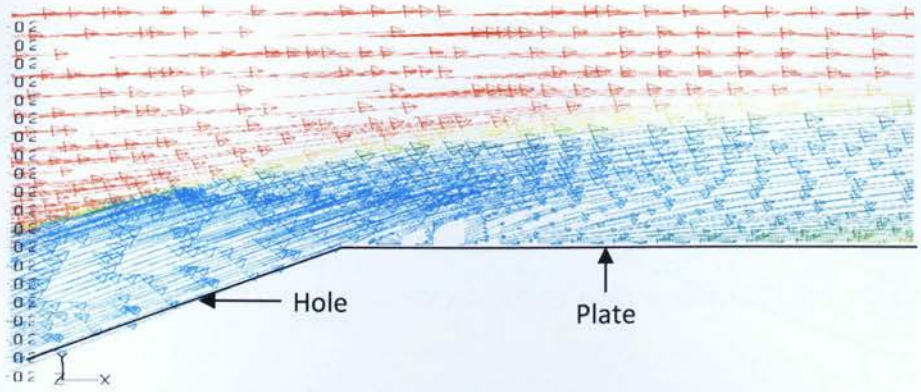

(e) Left/Right Sister Holes

Figure 23: Jet Lift-Off - Long Hole (M=1.0)

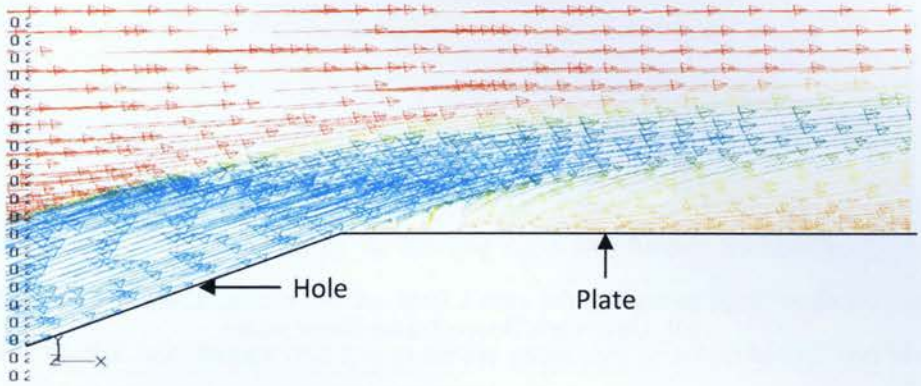

(a) Single Hole

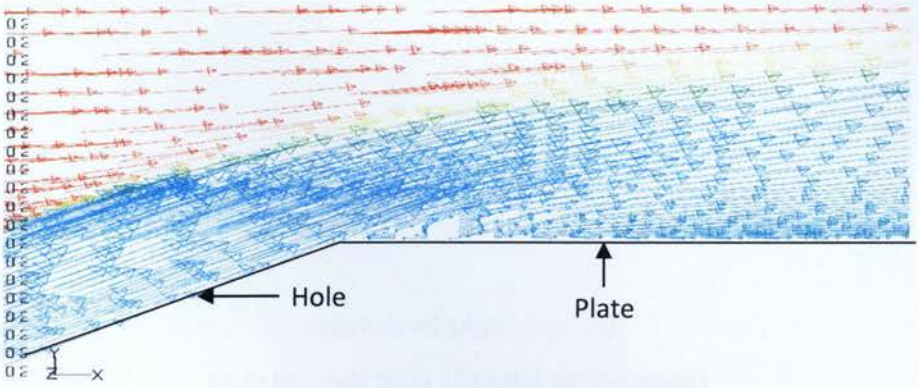

(b) Downstream Sister Holes

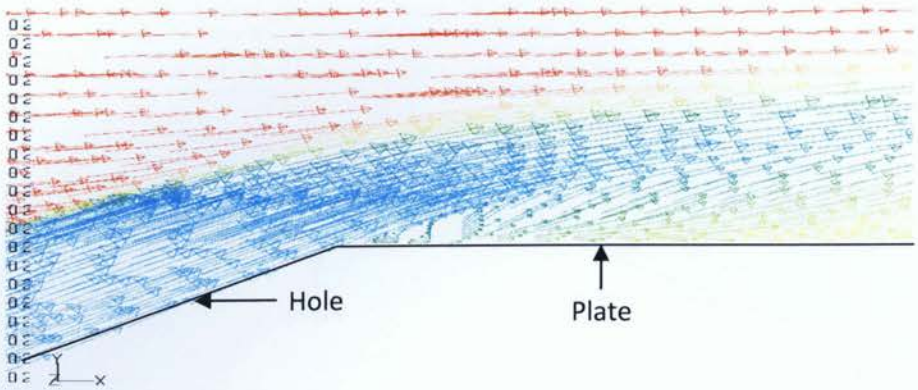

(c) Upstream Sister Holes

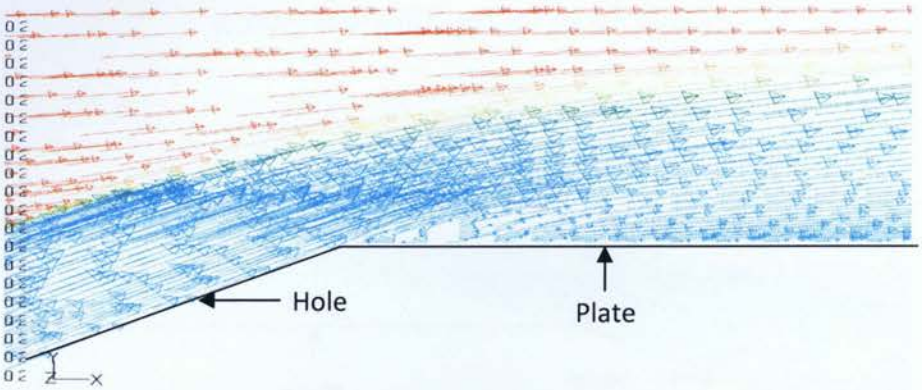

(d) Upstream/Downstream Sister Holes

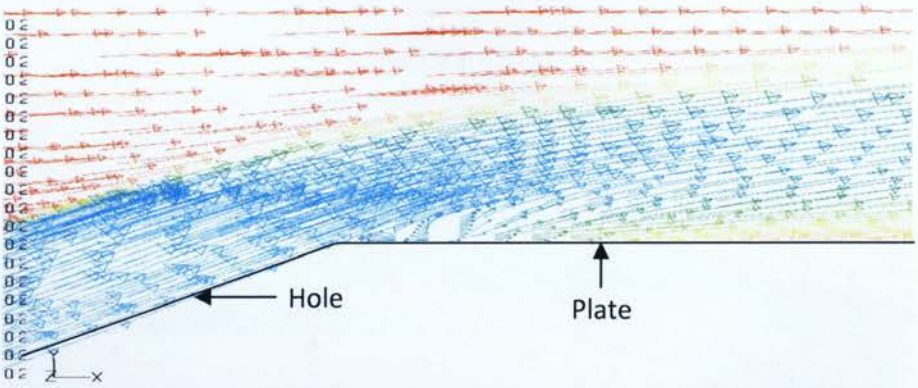

(e) Left/Right Sister Holes

Figure 24: Jet Lift-Off - Long Hole (M=1.5)

Here, both blowing ratios illustrate a separation region where the flow is reversed and separated from the surface of the blade. Aside from the reverse-faced velocity vectors, one also notes the vectors pointed upwards away from the plate indicating no adhesion to the surface of the blade. The figures indicate that the addition of downstream holes provides the most improved near-field flow as indicated in the adiabatic effectiveness results of Section 6.2. Similarly, Figures 23(c) and 24(c) demonstrate why

the upstream holes provide better coverage downstream of the injection hole. Since the flow has lifted off the surface of the plate, the near-hole region loses protection to permit for better protection of the downstream region.

Although an analysis of jet-liftoff provides some insight into the flowfield, a more thorough analysis of the flowfield at various x/D locations is necessary to completely understand the effects of the sister holes.

6.4 Primary Flow Structure

Research has shown that the primary vortex structure (CRVP) has the largest impact on film cooling effectiveness of any of the vortex structures that occur in such complicated mixing flows. As a result, the following analysis evaluates the flow at x/D = 0, 1, 2, and 3 to understand the mixing that occurs and how the primary vortex structures interact to promote flow adhesion.

The results in this section are segregated by blowing ratio and further by hole geometry. Figures 25 through 29 contain the flow structure for the M=0.2 case while Figures 30 through 34 contain the flow structure for the M=0.5 case. Notice that it is generally applicable to group M=0.2 and M=0.5 results as they demonstrate similar trends, while M=1.0 and M=1.5 demonstrate their own similar trends.

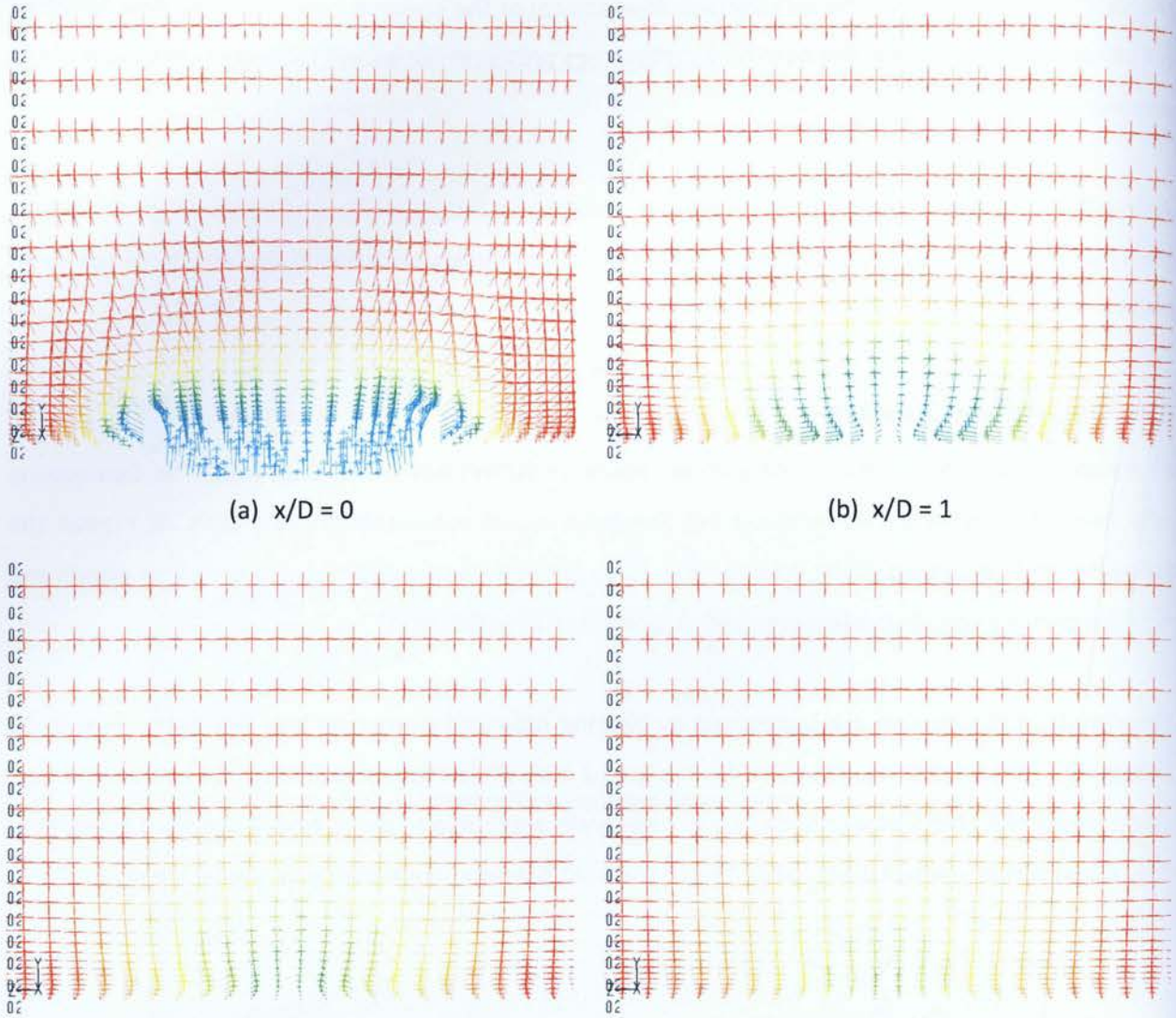

(a) x/D = 0

(b) x/D = 1

(c) x/D = 2

(d) x/D = 3

Figure 25: Flow Structure – Single Hole (M=0.2)

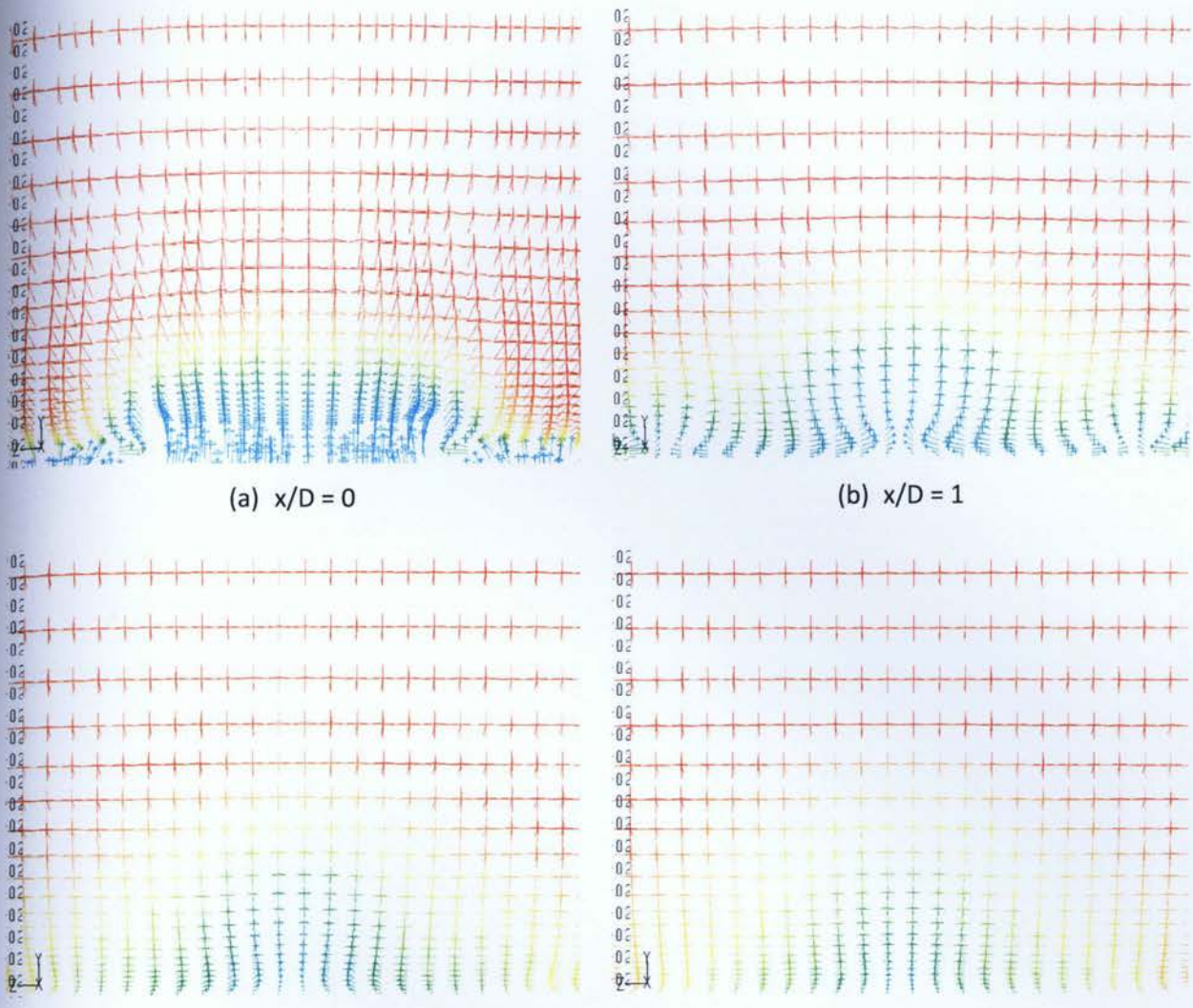

(a) x/D = 0

(b) x/D = 1

(c) x/D = 2

(d) x/D = 3

Figure 26: Flow Structure – Downstream Sister Holes (M=0.2)

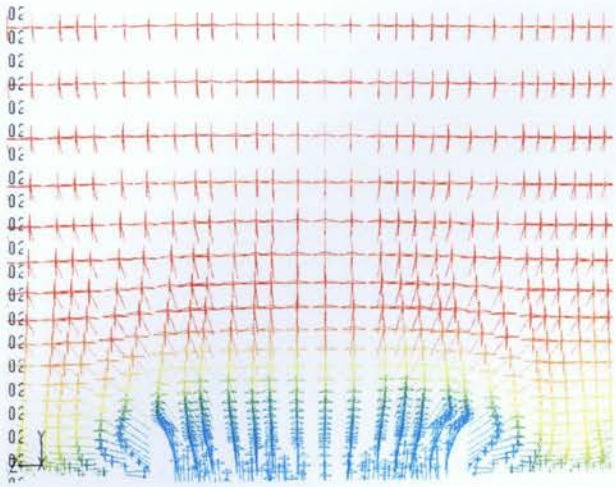

(a) x/D = 0

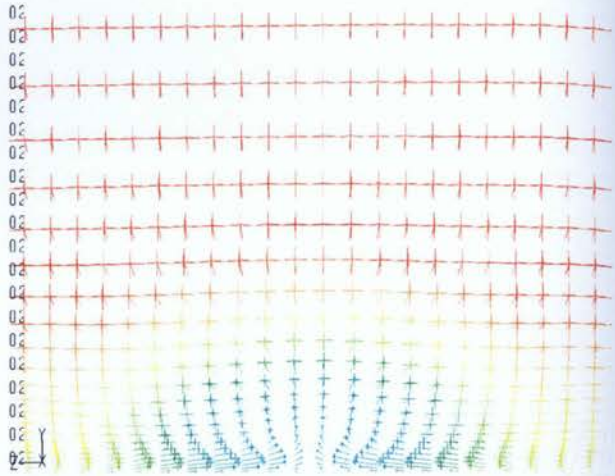

(b) x/D = 1

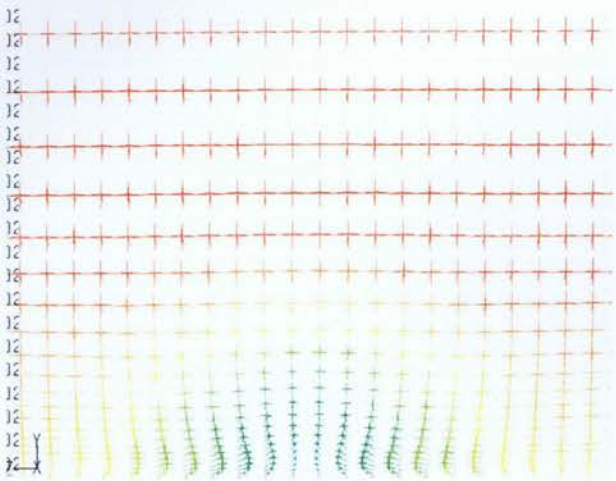

(c) x/D = 2

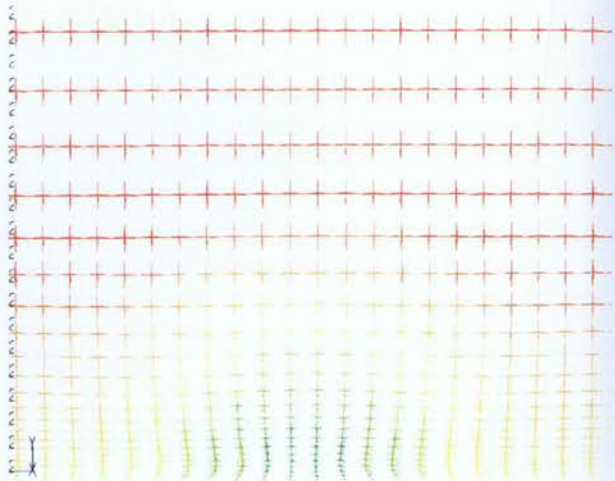

(d) x/D = 3

Figure 27: Flow Structure – Upstream Sister Holes (M=0.2)

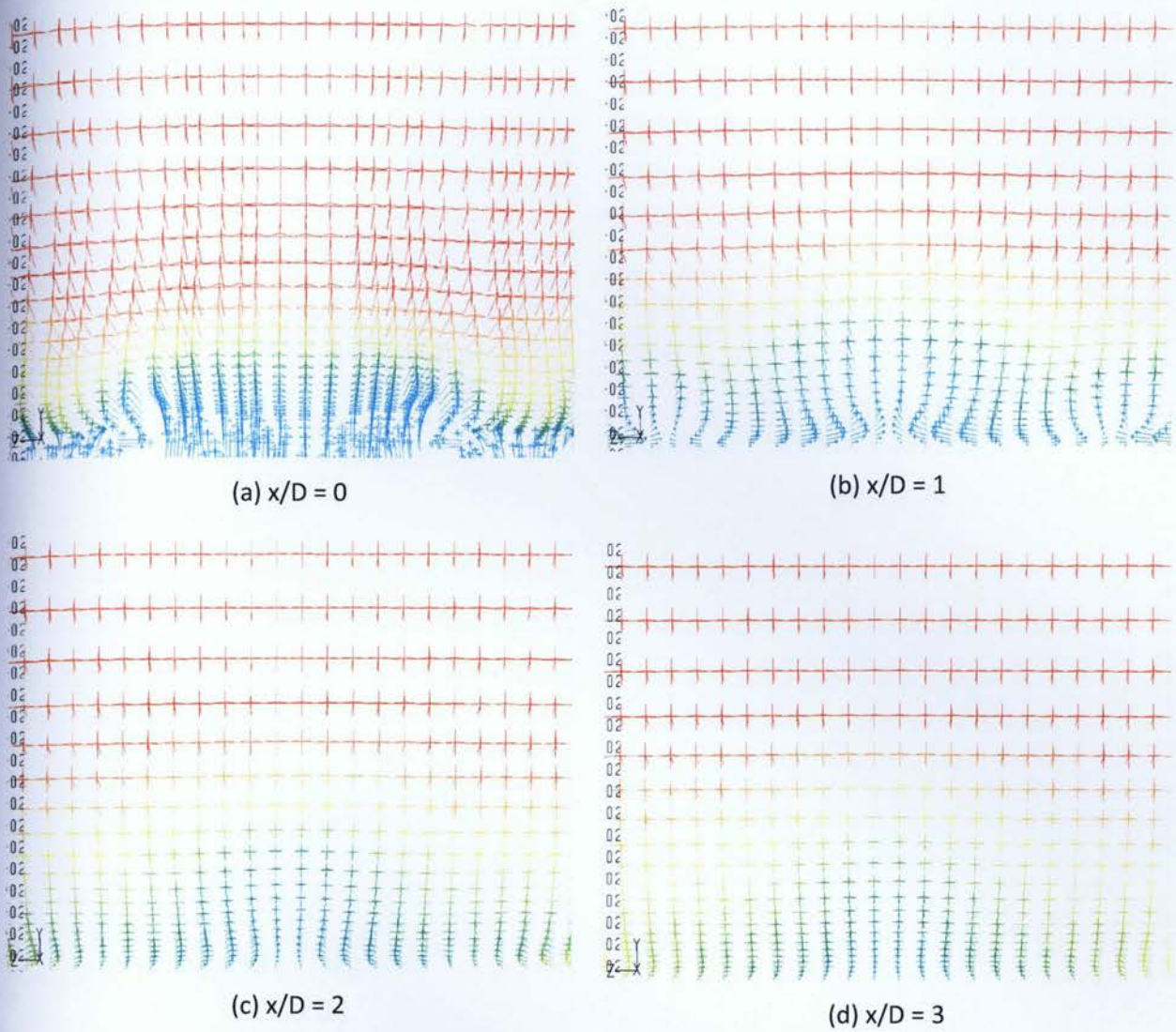

(a) x/D = 0

(b) x/D = 1

(c) x/D = 2

(d) x/D = 3

Figure 28: Flow Structure – Downstream/Upstream Sister Holes (M=0.2)

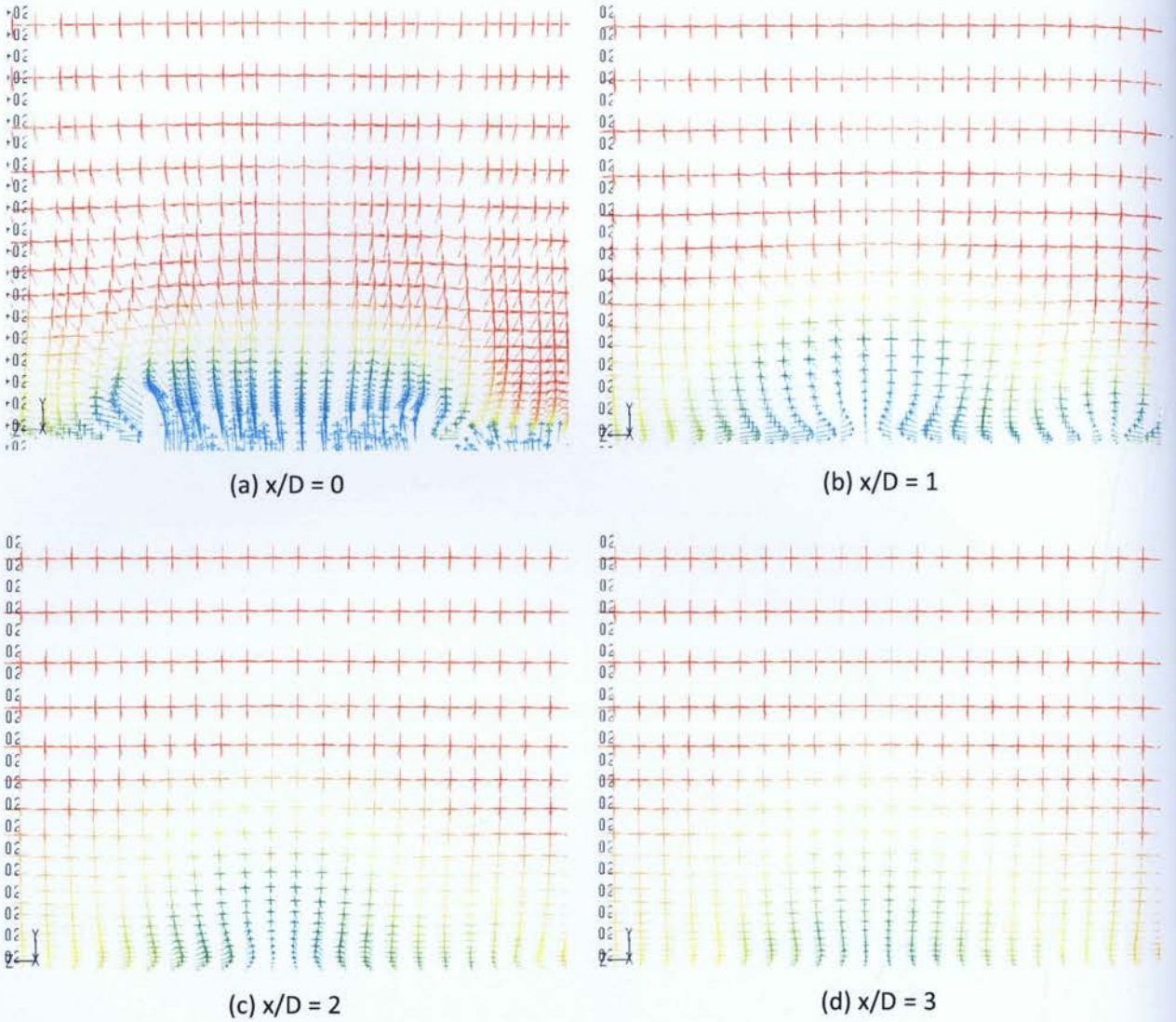

(a) x/D = 0

(b) x/D = 1

(c) x/D = 2

(d) x/D = 3

Figure 29: Flow Structure – Left/Right Sister Holes (M=0.2)

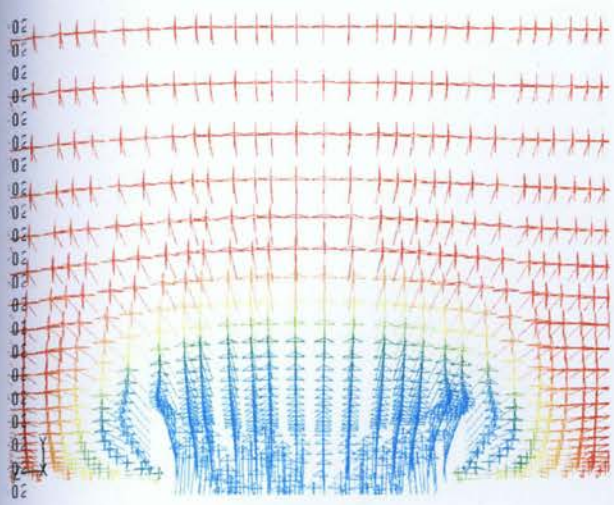

(a) x/D = 0

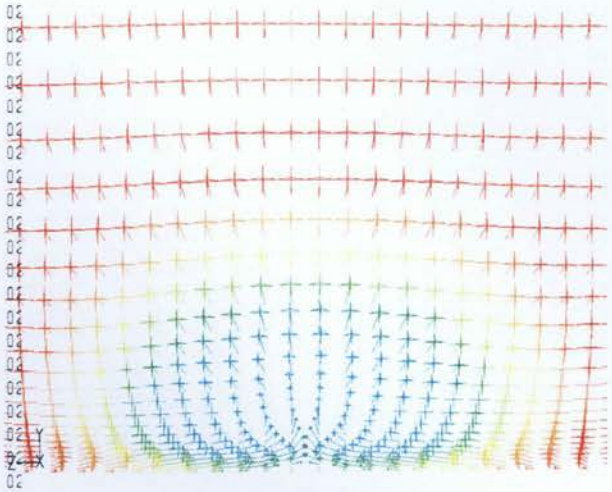

(b) x/D = 1

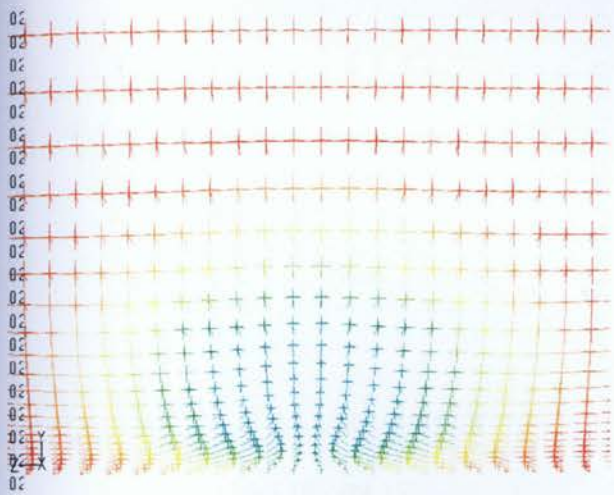

(c) x/D = 2

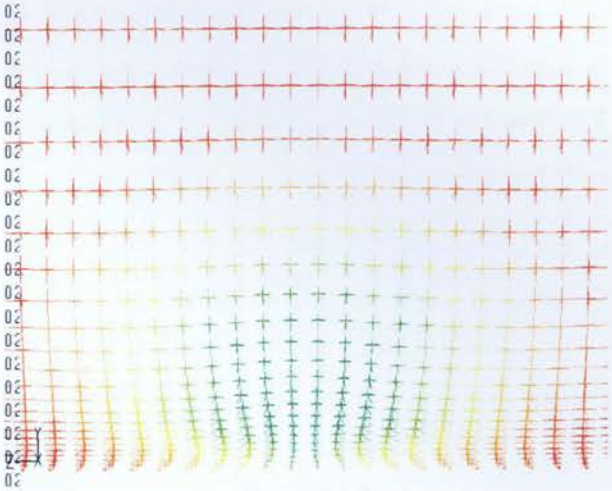

(d) x/D = 3

Figure 30: Flow Structure – Single Hole (M=0.5)

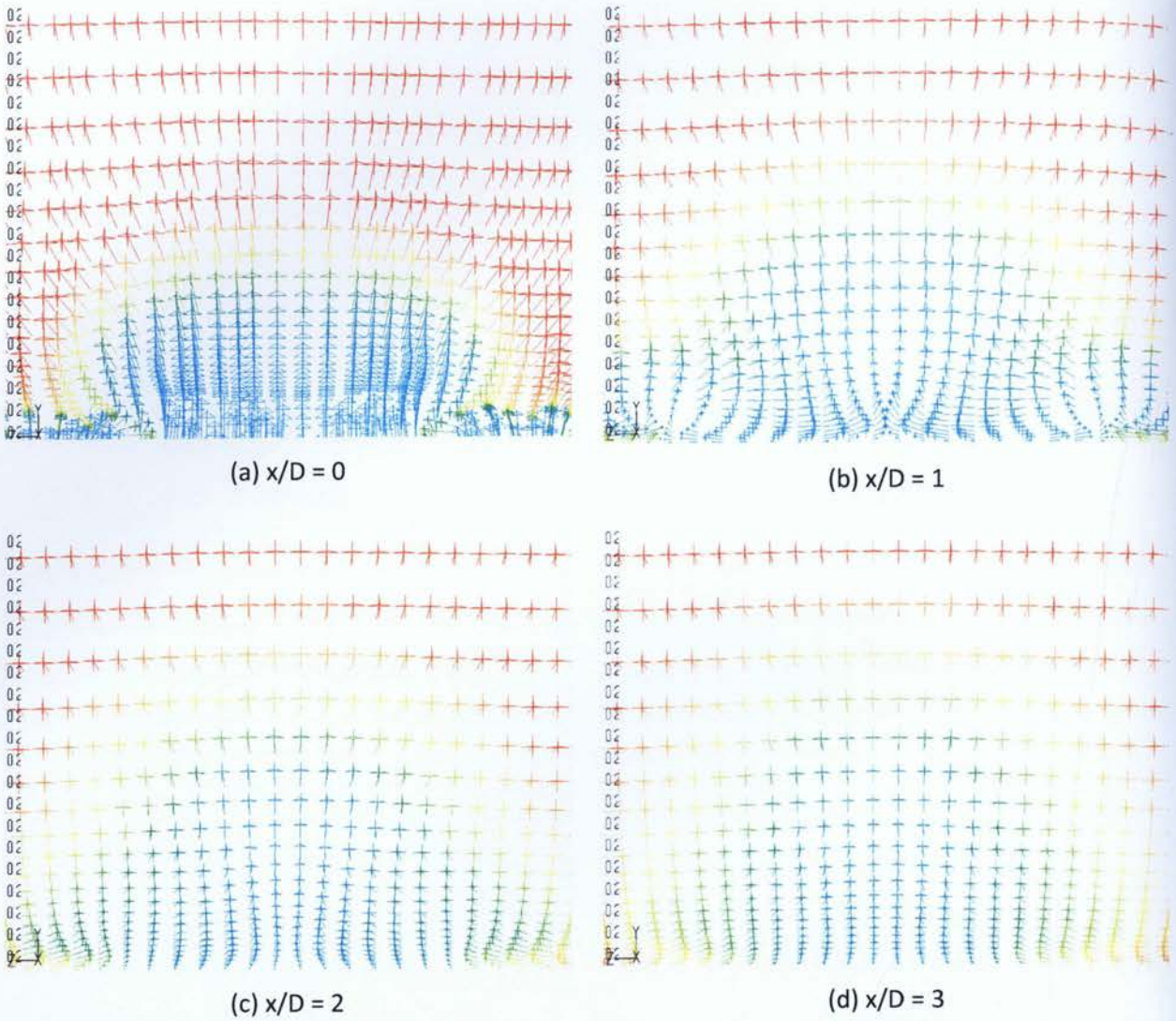

(a) x/D = 0

(b) x/D = 1

(c) x/D = 2

(d) x/D = 3

Figure 31: Flow Structure – Downstream Sister Holes (M=0.5)

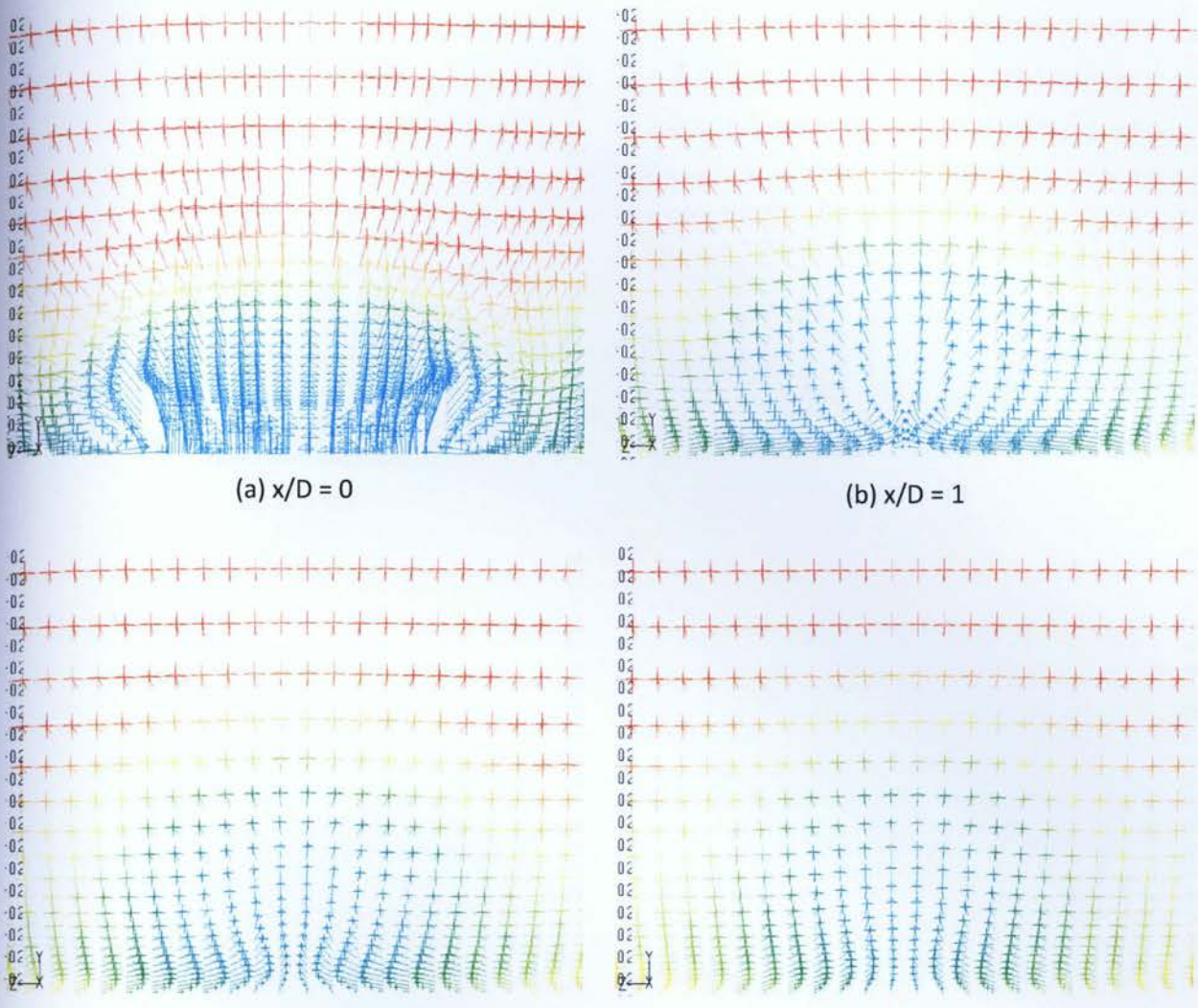

(a) x/D = 0

(b) x/D = 1

(c) x/D = 2

(d) x/D = 3

Figure 32: Flow Structure – Upstream Sister Holes (M=0.5)

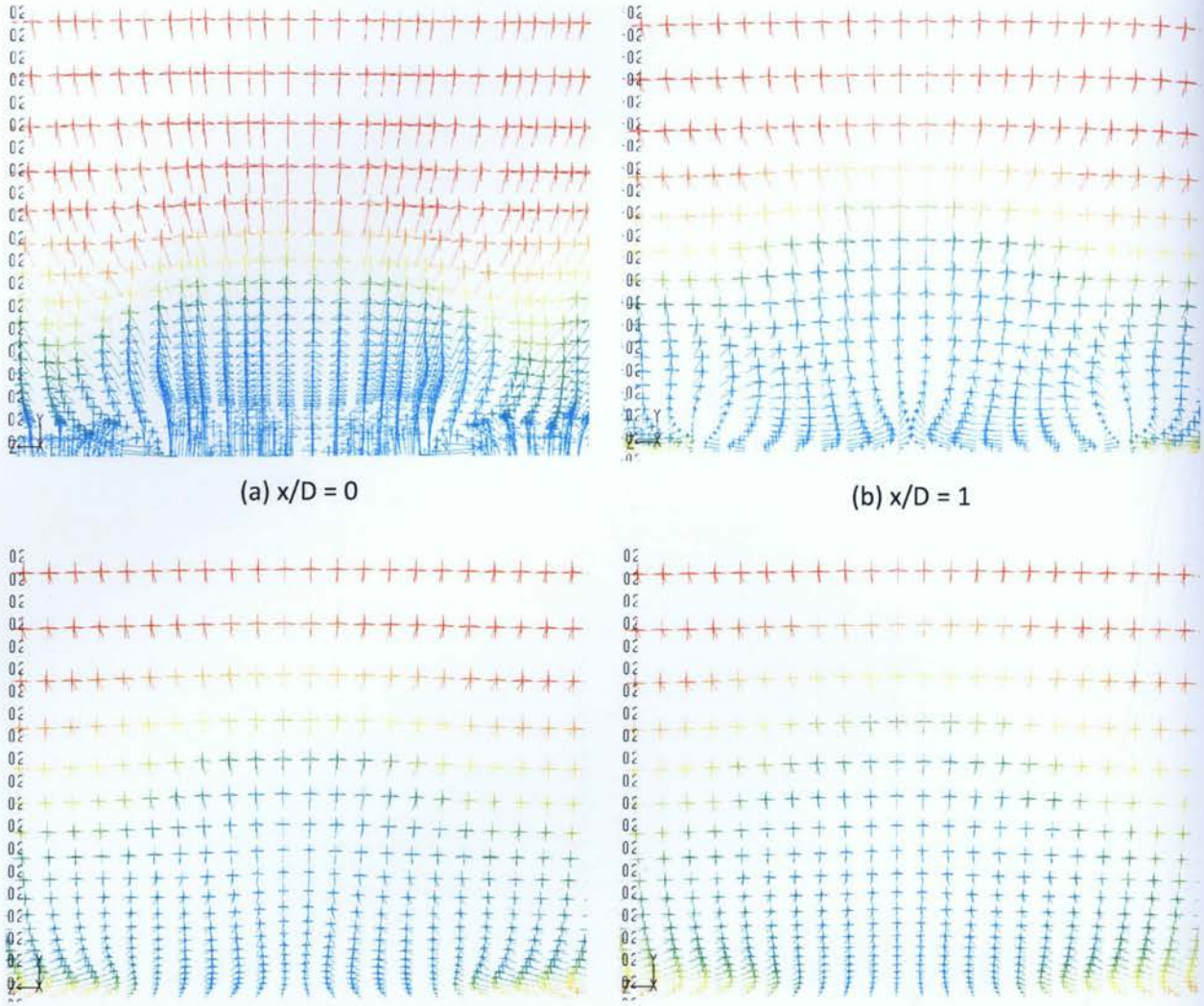

(a) x/D = 0

(b) x/D = 1

(c) x/D = 2

(d) x/D = 3

Figure 33: Flow Structure – Upstream/Downstream Sister Holes (M=0.5)

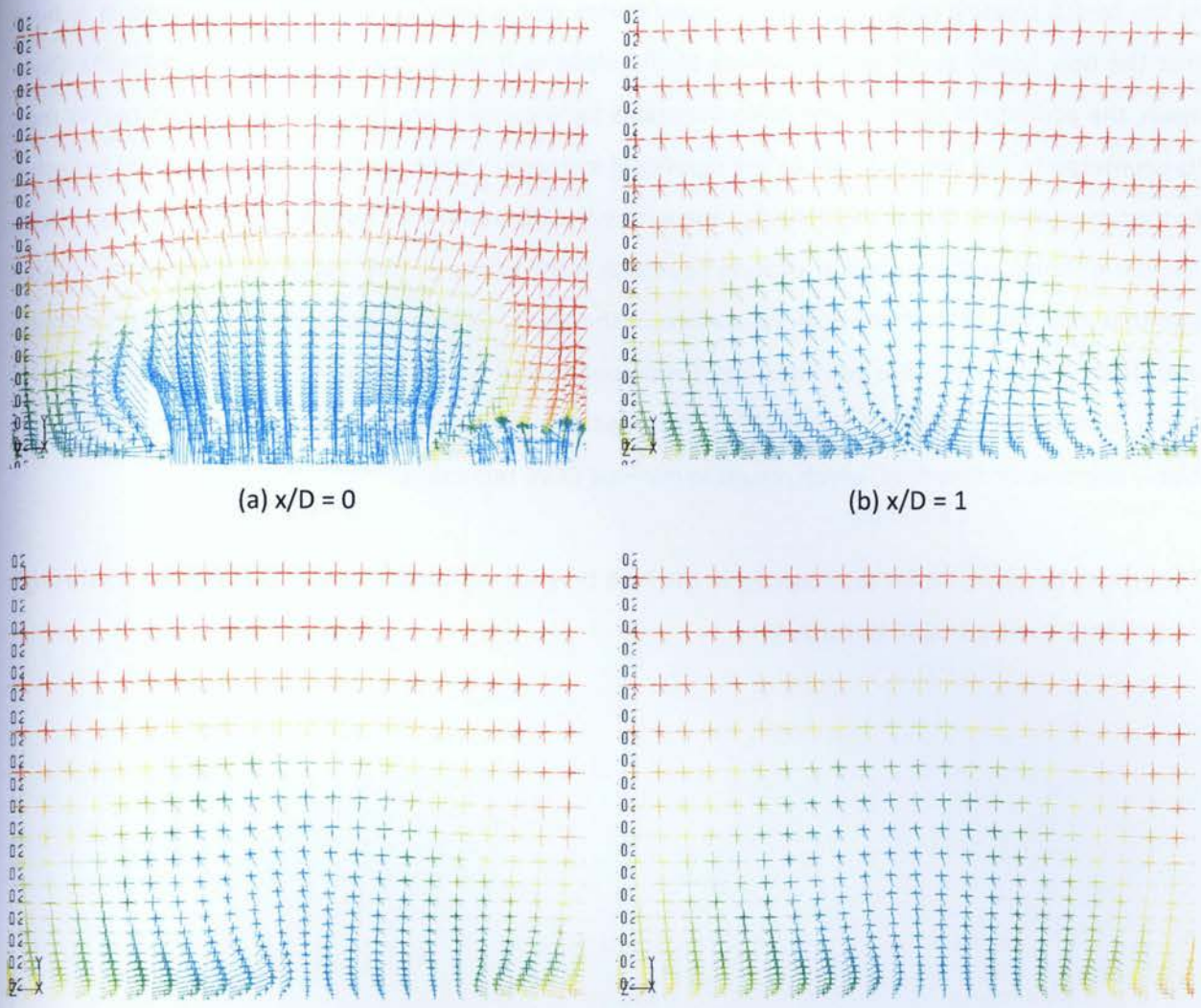

(a) x/D = 0

(b) x/D = 1

(c) x/D = 2

(d) x/D = 3

Figure 34: Flow Structure – Left/Right Sister Holes (M=0.5)

At such low blowing ratios there is not a significant degree of cohesion to the flow. One will notice that as the solution moves downstream the swirl that occurs becomes less notable as the velocity vectors level-off and become parallel to the surface of the blade. At the lowest blowing ratio of M=0.2, the baseline case with a single hole operable shows very little mixing but also indicates negligible lateral spread. As was noted in the symmetry plane case, the addition of downstream holes significantly improves near-hole coverage and spread, improving the adiabatic effectiveness without pushing the coolant too far into the mainstream.

At the M=0.5 blowing ratio, the kidney-shaped vortex pair is significantly more pronounced. It is here that the flow begins to lift off the surface of the blade as it spins, mixing with the mainstream. Once again, the addition of downstream holes maintains significantly more flow adhesion in this region than its counterparts, but one must notice the significant increase in highly vortical flow causing less cohesion further downstream. It is at this blowing ratio where the upstream-only holes begin to show their effect. The use of holes in the upstream location counteracts the primary CRVP, replacing it with a favourable pair that pulls the coolant towards the surface of the blade. As one expects, the use of both upstream and downstream holes also provides improved cooling, but the penalty in coolant mass flux is non-trivial. Finally, the left-right case, while offering moderate effectiveness results, shows its pitfalls in the highly asymmetric flow field, which results in minimal CRVP reduction.

The results become further pronounced in the high blowing ratio cases of M=1.0 in Figures 35 through 39 and M=1.5 in Figures 40 through 44.

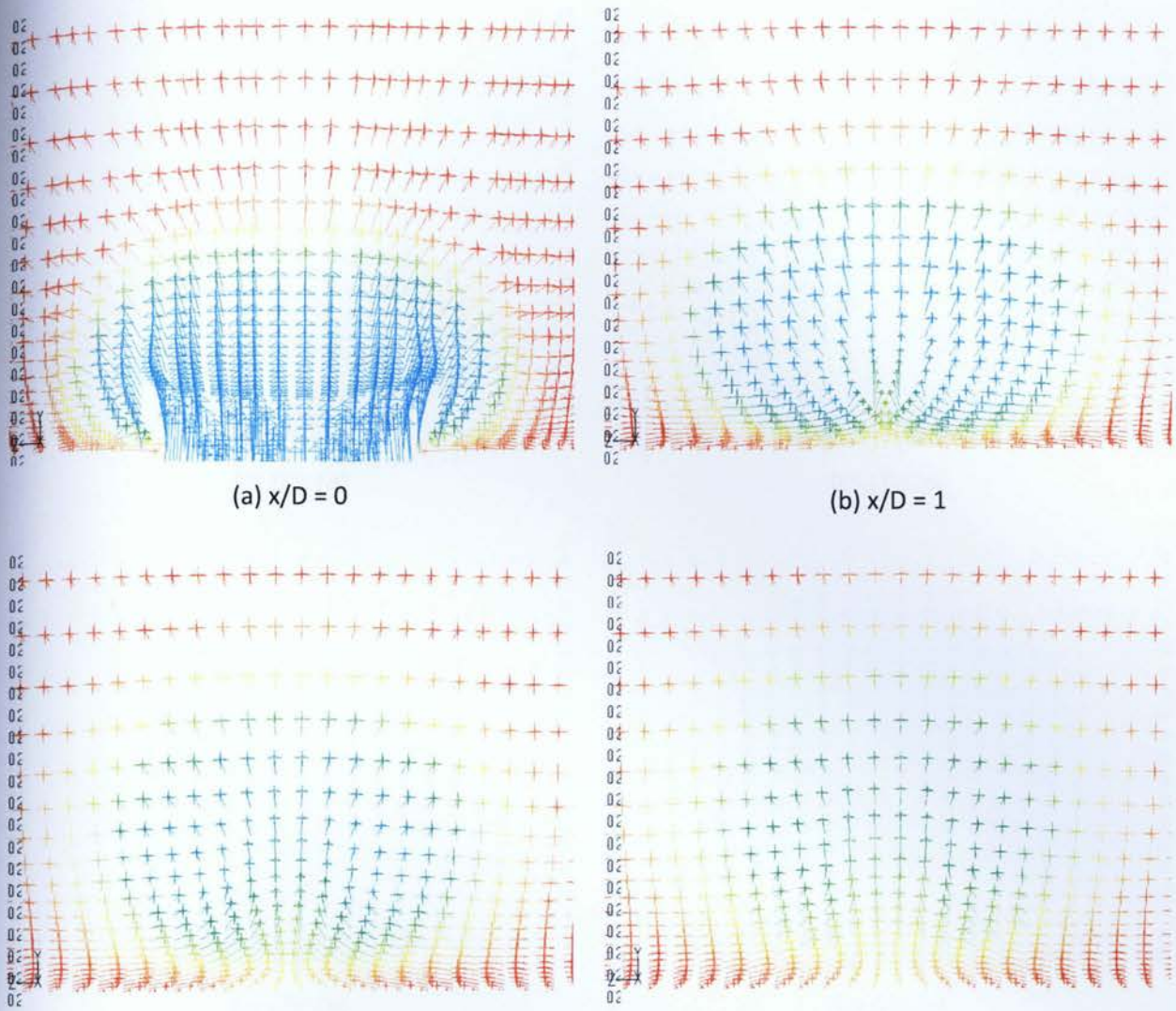

(a) x/D = 0

(b) x/D = 1

(c) x/D = 2

(d) x/D = 3

Figure 35: Flow Structure – Single Hole (M=1.0)

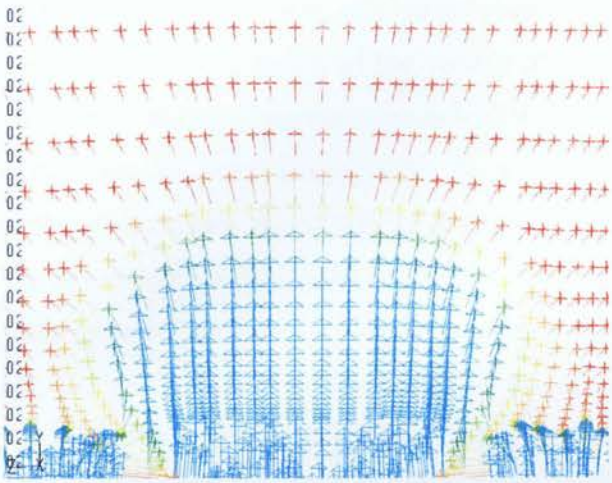

(a) x/D = 0

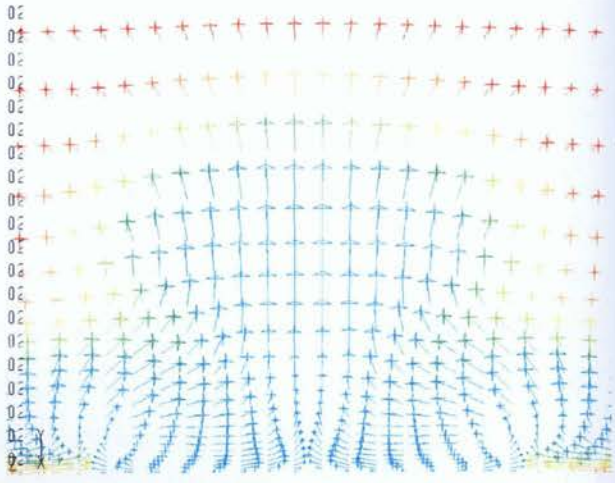

(b) x/D = 1

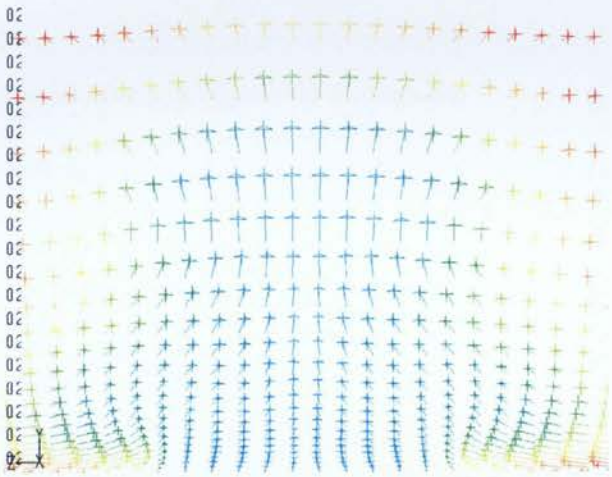

(c) x/D = 2

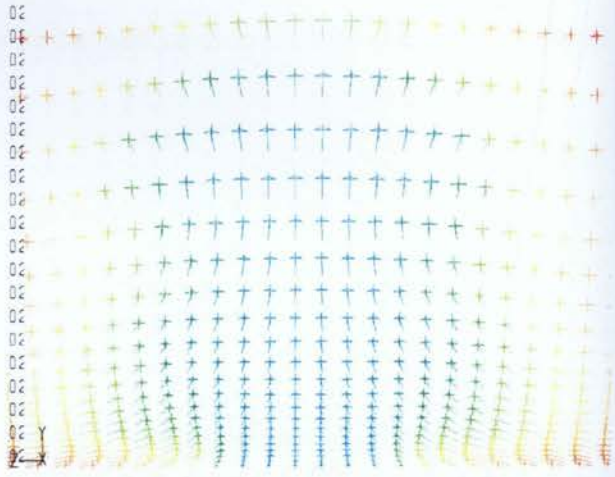

(d) x/D = 3

Figure 36: Flow Structure – Downstream Sister Holes (M=1.0)

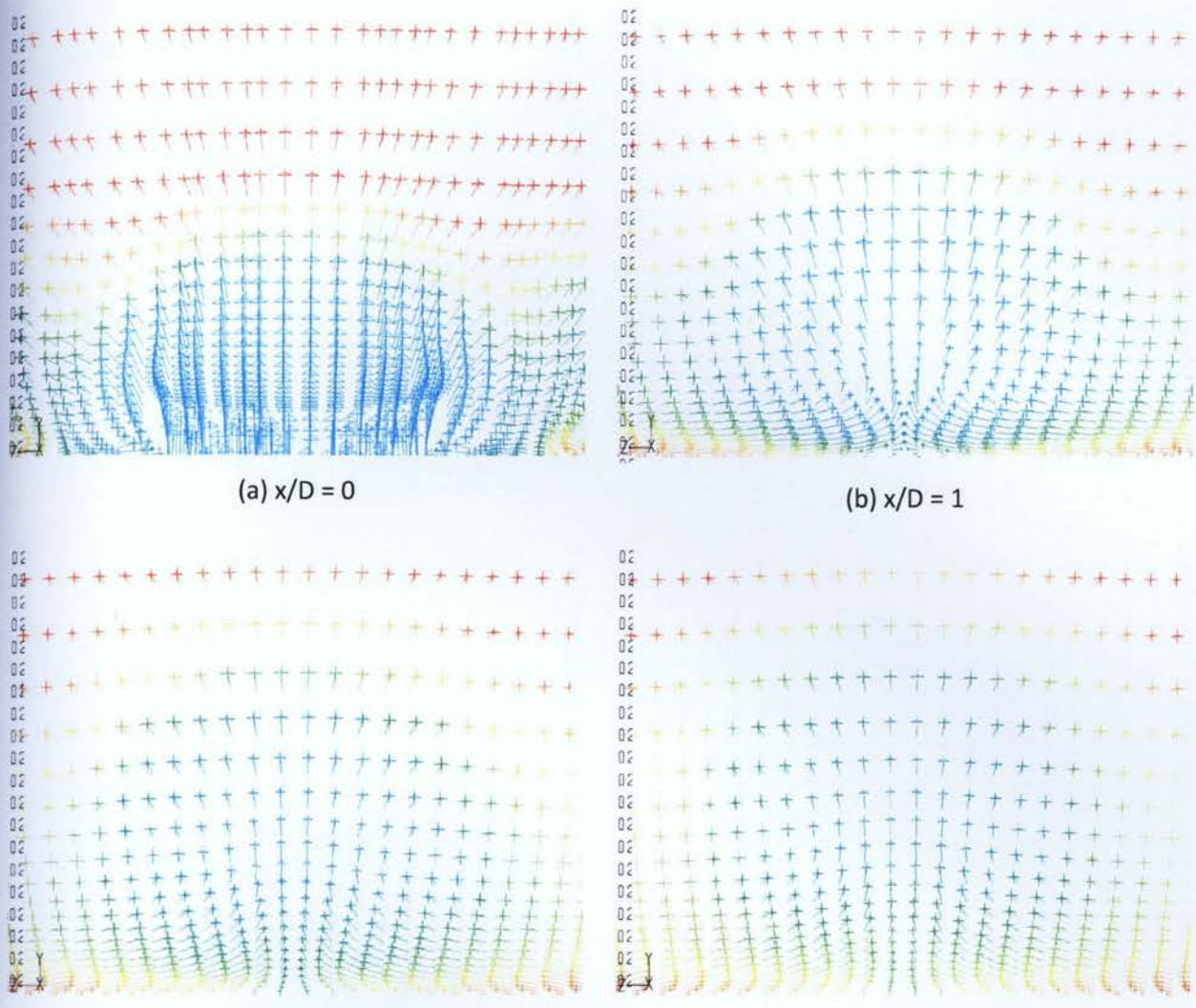

(a) x/D = 0

(b) x/D = 1

(c) x/D = 2

(d) x/D = 3

Figure 37: Flow Structure – Upstream Sister Holes (M=1.0)

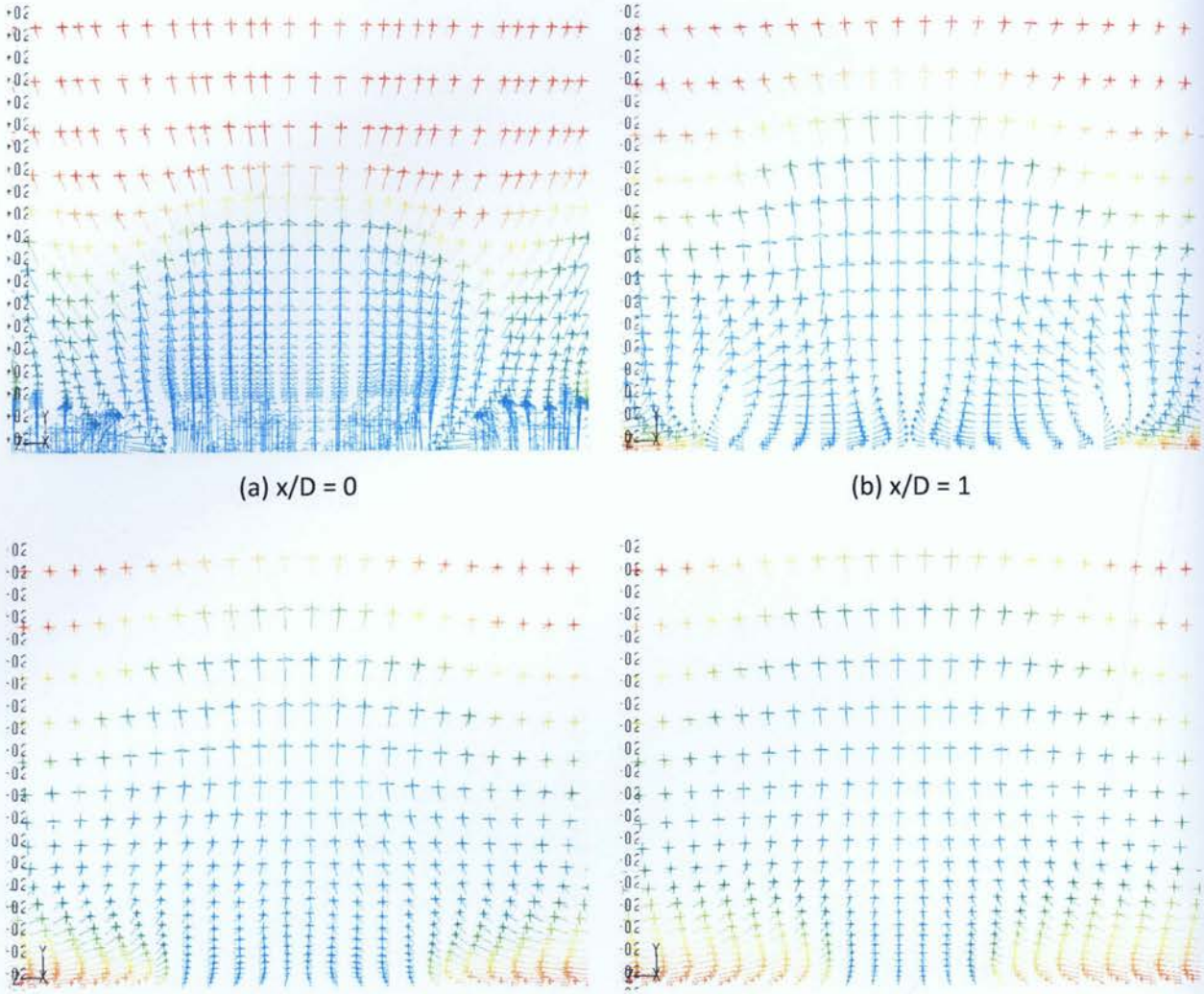

(a) x/D = 0

(b) x/D = 1

(c) x/D = 2

(d) x/D = 3

Figure 38: Flow Structure – Upstream/Downstream Sister Holes (M=1.0)

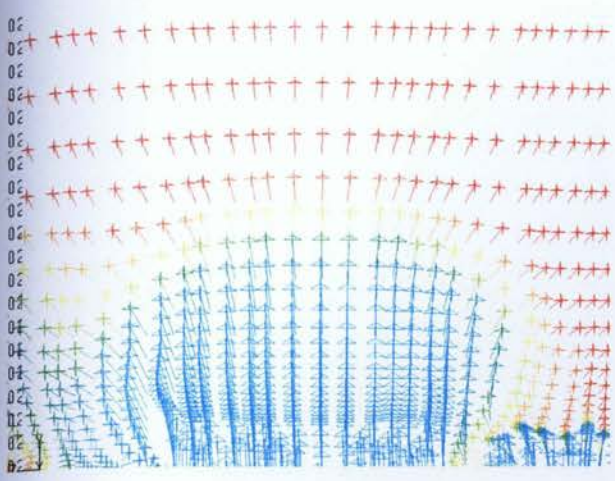

(a) x/D = 0

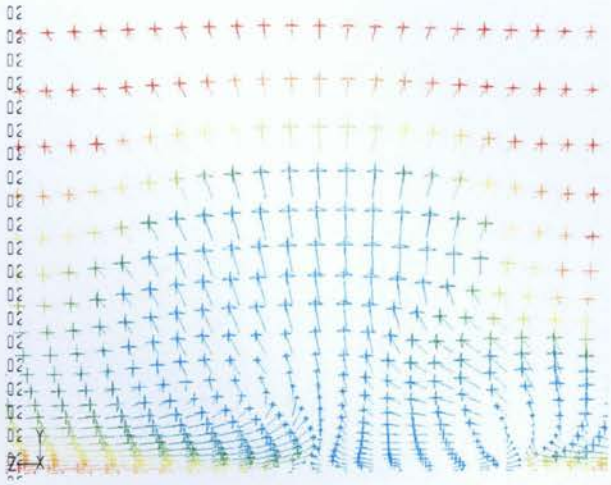

(b) x/D = 1

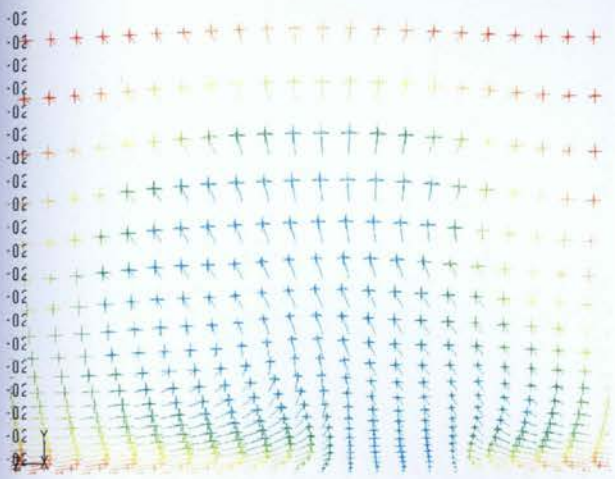

(c) x/D = 2

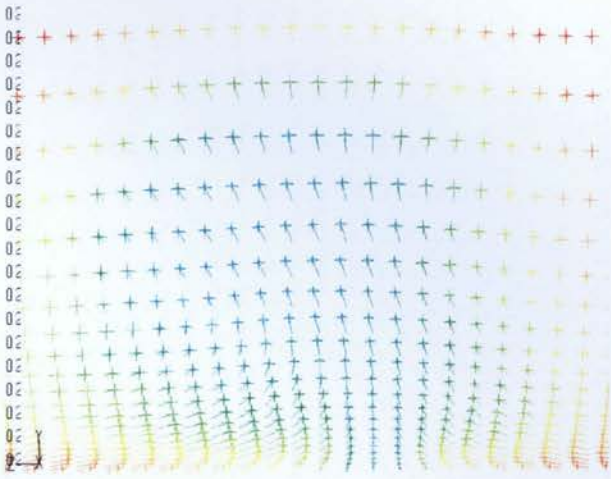

(c) x/D = 3

Figure 39: Flow Structure – Left/Right Sister Holes (M=1.0)

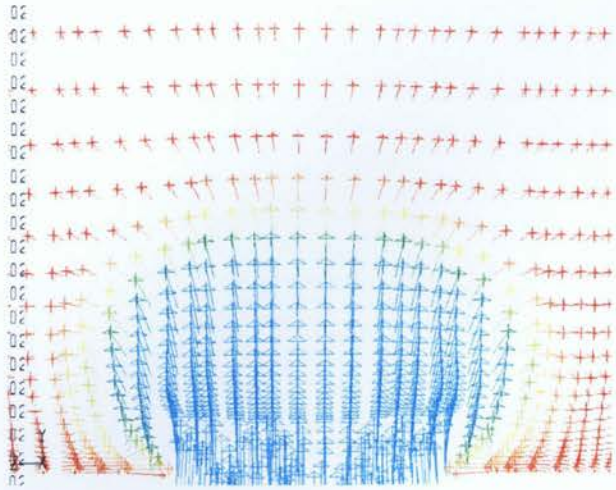

(a) x/D = 0

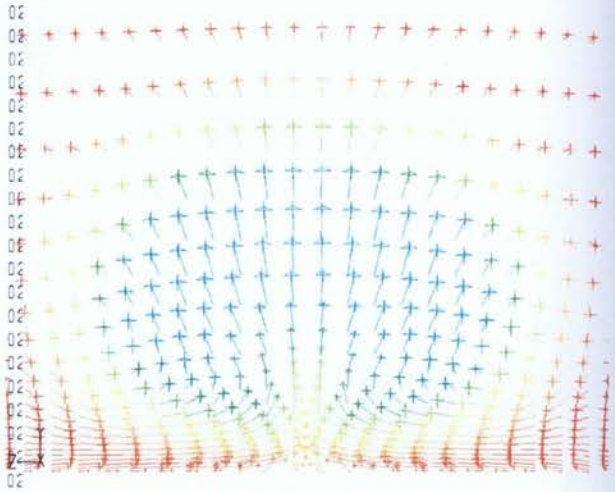

(b) x/D = 1

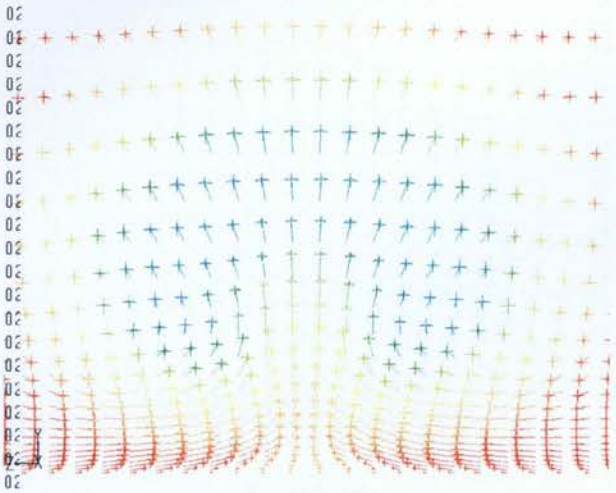

(c) x/D = 2

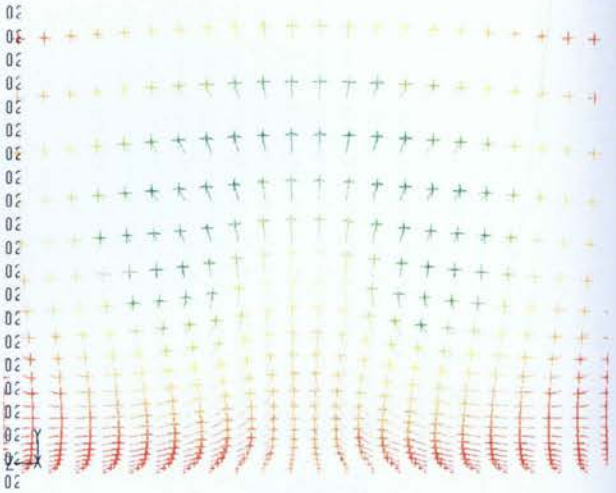

(d) x/D = 3

Figure 40: Flow Structure – Singe Hole (M=1.5)

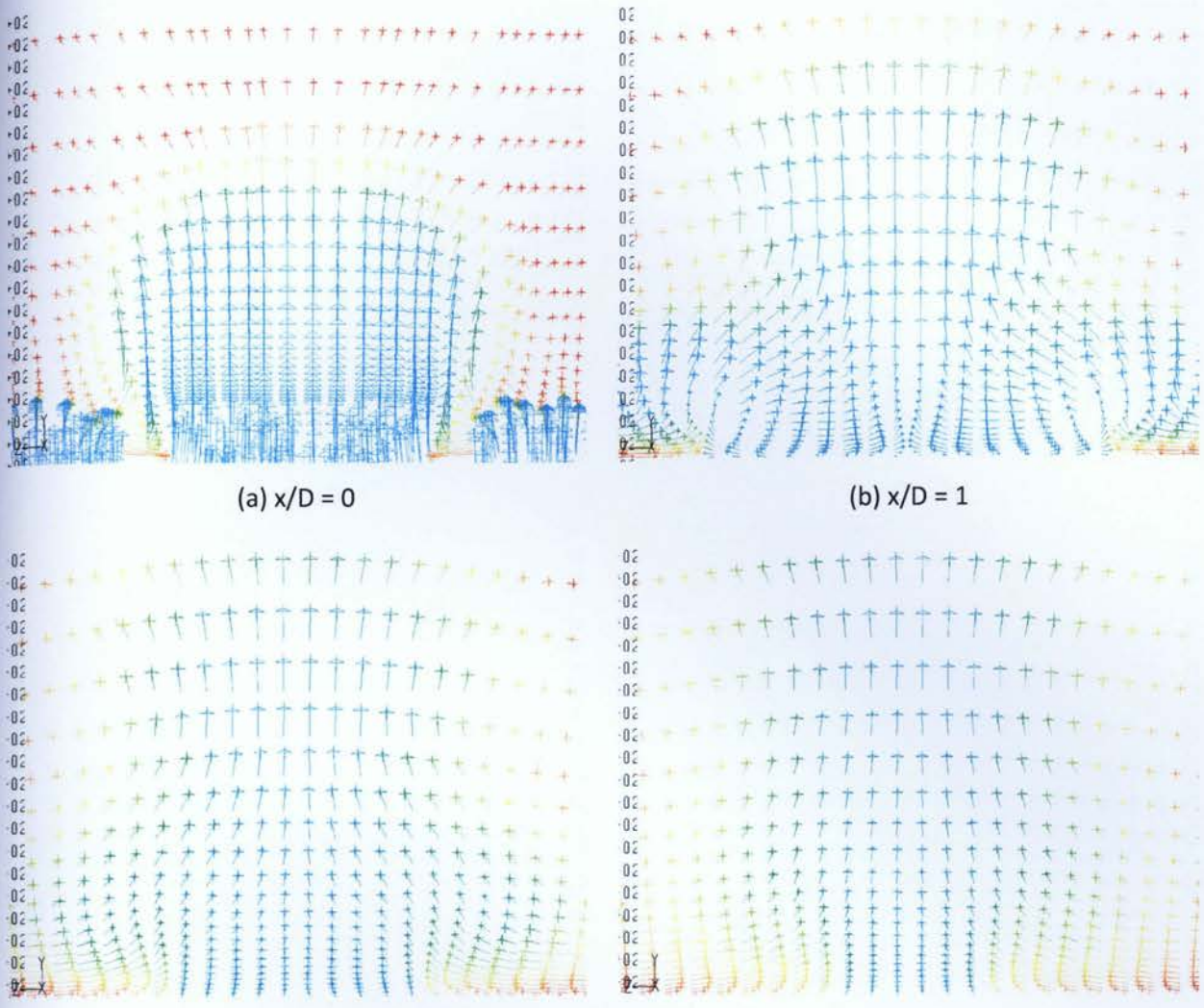

(a) x/D = 0

(b) x/D = 1

(c) x/D = 2

(d) x/D = 3

Figure 41: Flow Structure – Downstream Sister Holes (M=1.5)

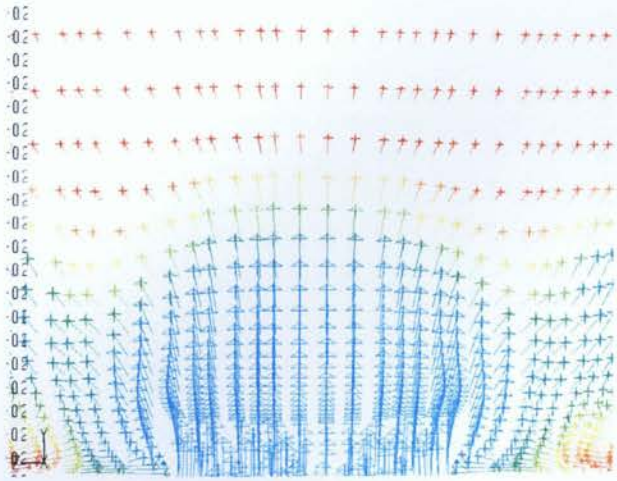

(a) x/D = 0

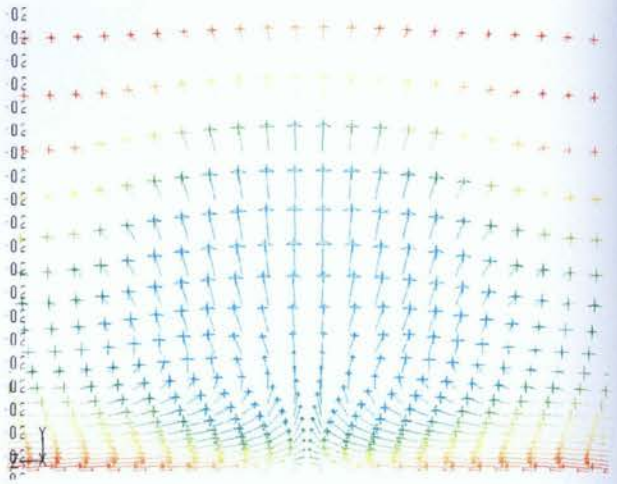

(a) x/D = 1

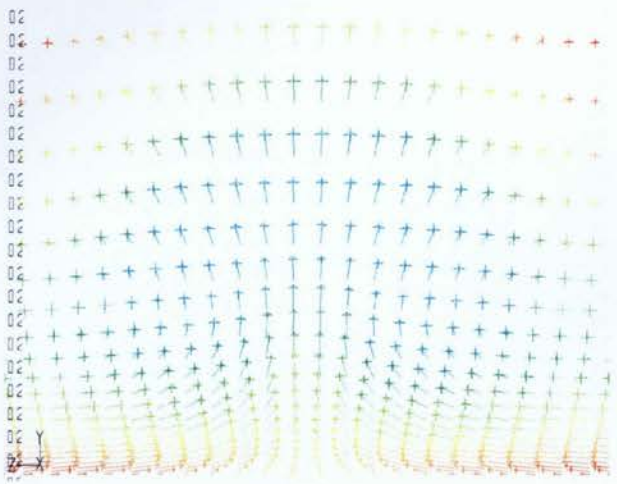

(b) x/D = 2

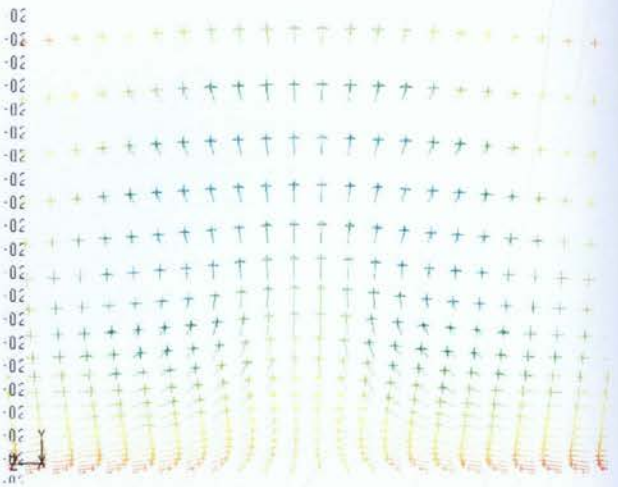

(c) x/D = 3

Figure 42: Flow Structure – Upstream Sister Holes (M=1.5)

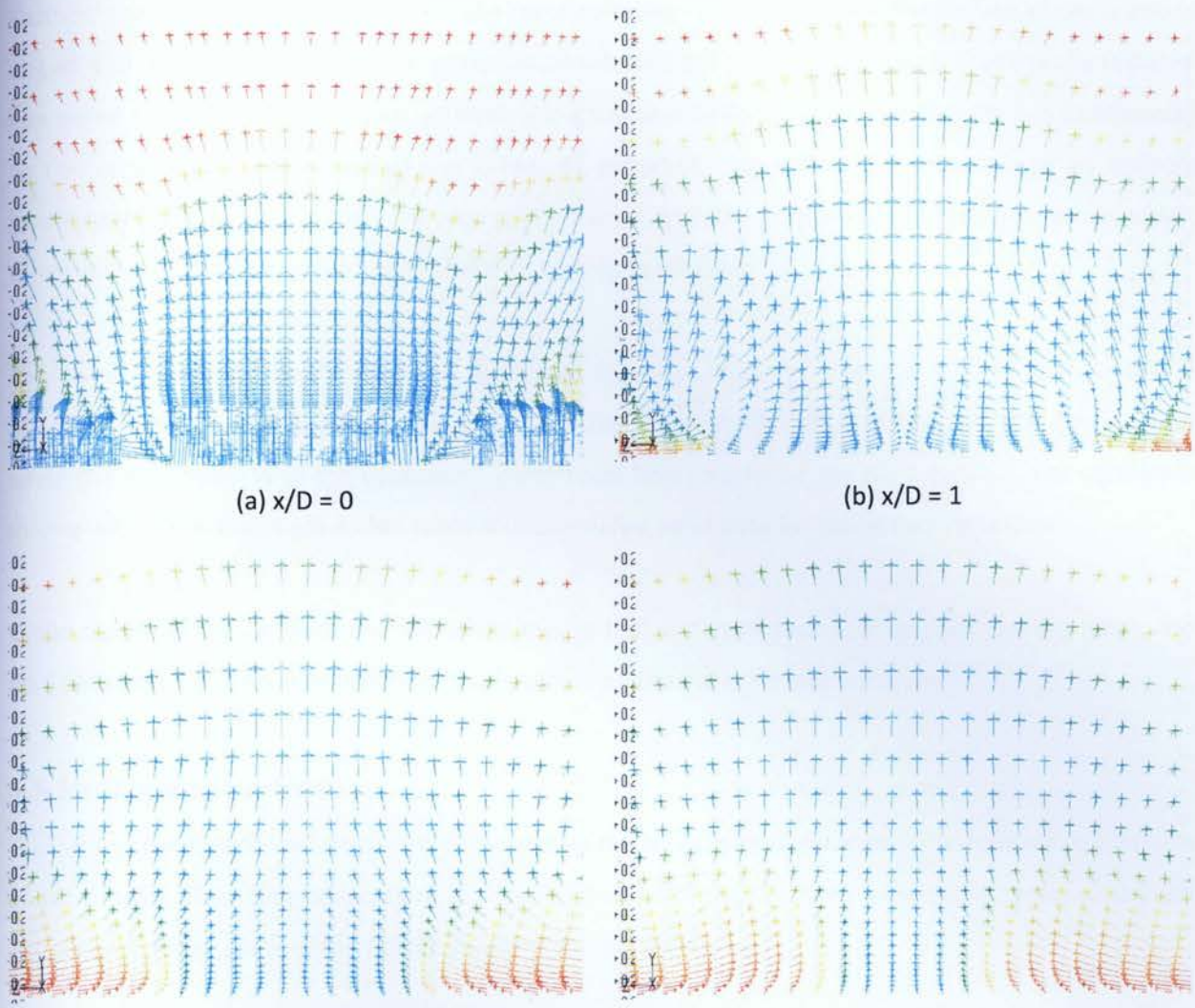

(a) x/D = 0

(b) x/D = 1

(c) x/D = 2

(d) x/D 3

Figure 43: Flow Structure – Upstream/Downstream Sister Holes (M=1.5)

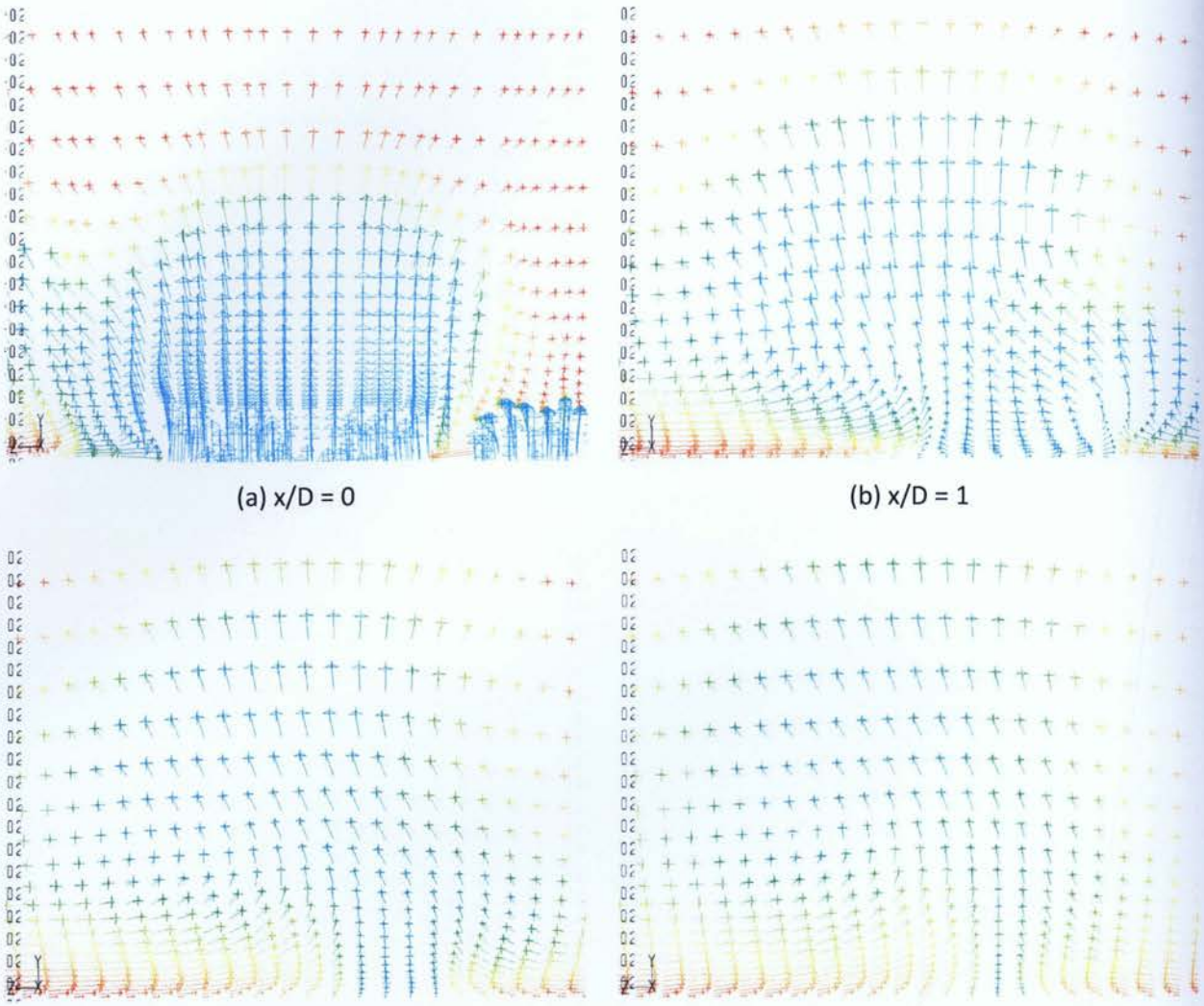

(a) x/D = 0

(b) x/D = 1

(c) x/D = 2

(d) x/D = 3

Figure 44: Flow Structure – Left/Right Sister Holes (M=1.5)

The trends remain consistent between these high blowing ratio cases, and, as discussed, become notably more pronounced. The counter-rotating vortex pair generated in the baseline study becomes increasingly powerful drawing the entire coolant stream off the surface of the blade, in turn, drawing the hot mainstream towards it. The downstream case, while improving the coolant condition, causes a significant amount of mixing, particularly at the extents of the domain, leading to flow that no longer remains attached to the plate and actually begins to counteract itself, drawing the primary coolant away from the surface.

Further, the upstream holes now offer the most cohesive results. Although the surface of the blade is not as well protected, the degree of entrainment into the hot mainstream flow is dramatically reduced compared to the downstream case, ultimately leading to a design which is significantly less detrimental to the aerodynamic properties of the blade. As expected, the left-right case produces an entirely incoherent flowfield with coolant that has mixed heavily with the mainstream to provide a solution that is neither cooled nor un-cooled, but rather, highly unpredictable.

The results in this section shed light on the results from this analysis. Here, it is better understood why the downstream holes are not necessarily the most optimal solution for sister hole film cooling, and while the effectiveness of the upstream/downstream holes might be the most optimal, the significant mixing with the mainstream makes them an unappealing candidate for actual cooling regimes.

While these figures illustrate the non-trivial mixing that occurs in such complex film cooling flows, the final section focuses on streamwise vorticity to further illustrate this phenomenon.

6.5 Streamwise Vorticity

Evaluating contours of streamwise vorticity enables the researcher to have one final look into the effects of sister holes of varying orientations on the flowfield. Although vorticity is not favourable, controlled vorticity may incur some of the most optimal blade cooling regimes.

The vorticity plots in the forthcoming analysis make use of the colour key given in Figure 45. This colour key remains constant over all long and short hole studies in this analysis. Further, the streamwise vorticity for the blowing ratios of M=0.2 and M=0.5 are shown in Figures 46 and 47.

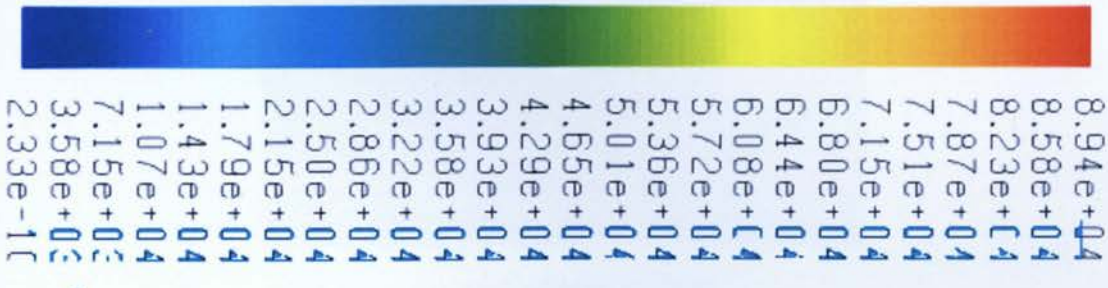

Figure 45: Vorticity Colour Key

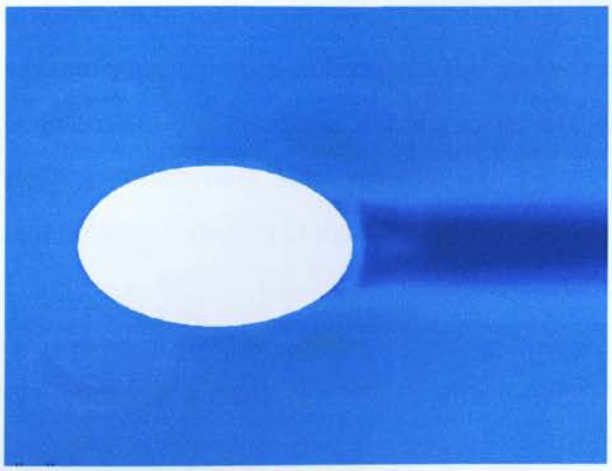

(a) Single Hole

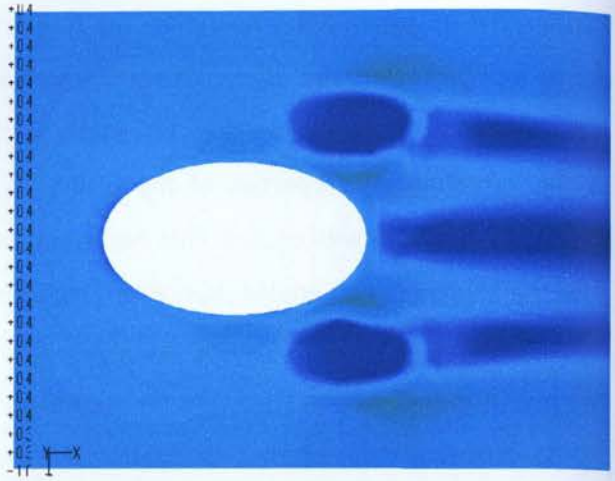

(b) Downstream Sister Holes

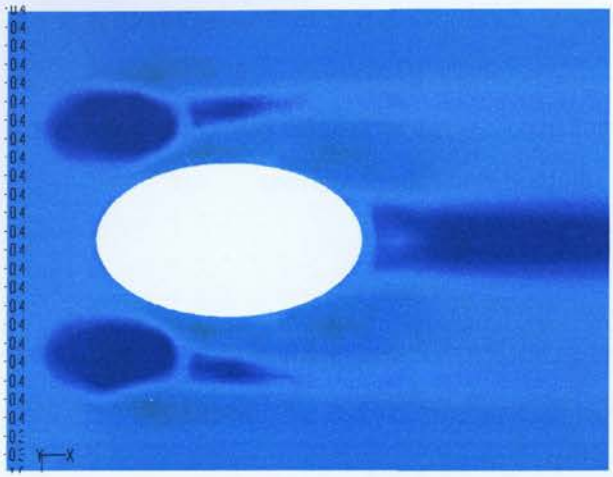

(c) Upstream Sister Holes

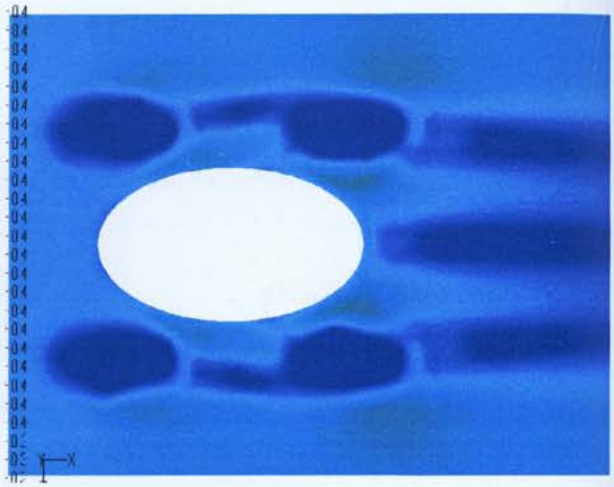

(d) Upstream/Downstream Sister Holes

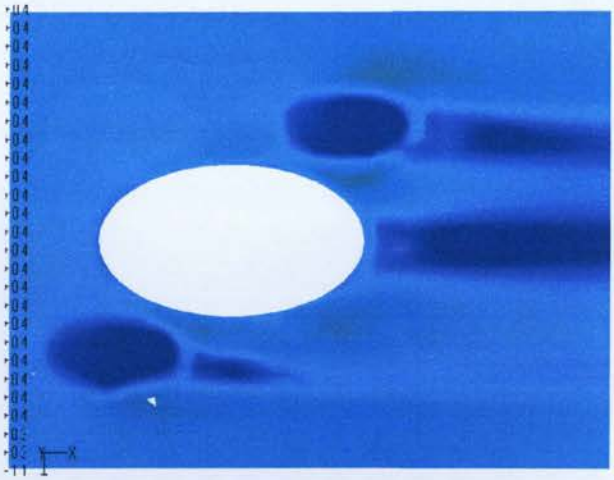

(e) Left/Right Sister Holes

Figure 46: Streamwise Vorticity – Long Hole (M=0.2)

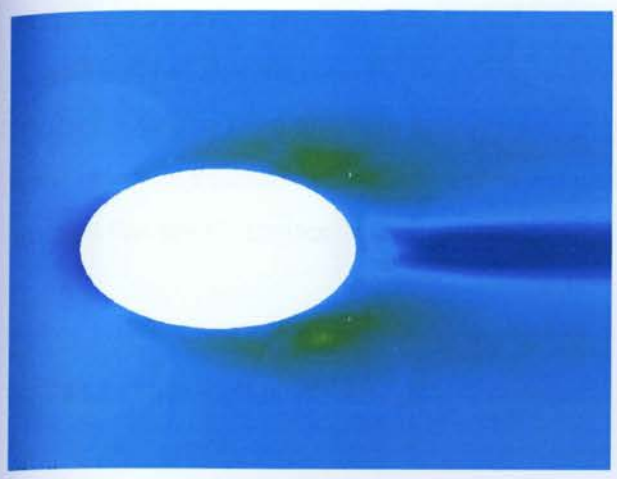

(a) Single Hole

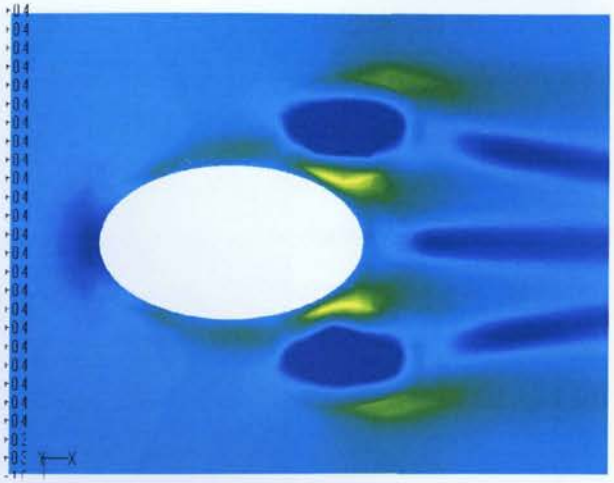

(b) Downstream Sister Holes

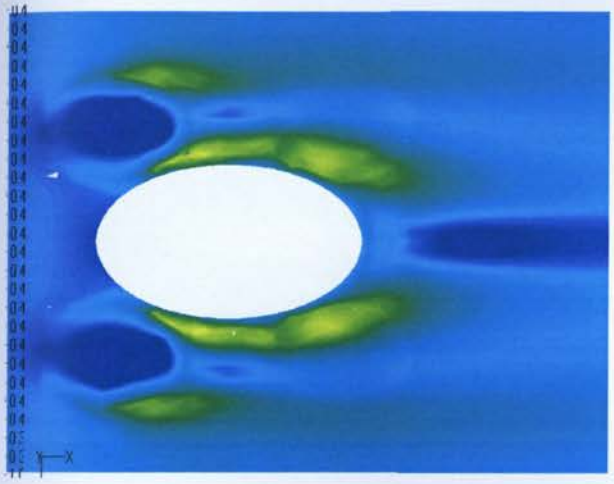

(c) Upstream Sister Holes

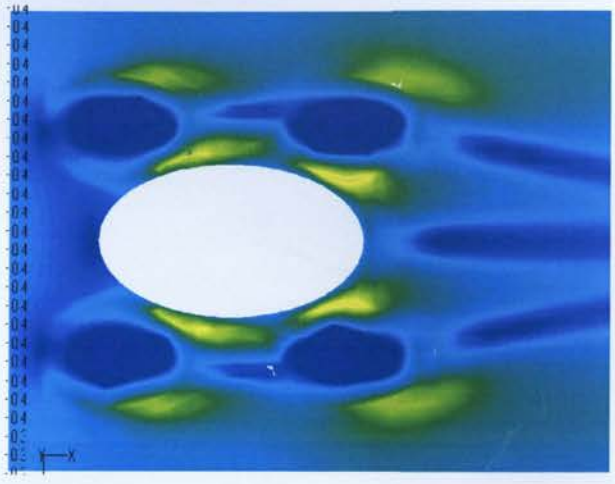

(d) Upstream/Downstream Sister Holes

(e) Left/Right Sister Holes

Figure 47: Streamwise Vorticity – Long Hole (M=0.5)

At the lowest blowing ratio of M=0.2, very little can be seen from a vorticity perspective. Increasing the blowing ratio to M=0.5, one can begin to see the formation of the vortex pairs causing swirling flow. A quick glance will be adequate to notice that the upstream-only holes offer the most cohesive vorticity field. It is neither erratic nor unexplainable. In contrast, any of the cases with downstream holes show that the vorticity downstream of the sister holes are small underdeveloped pockets. These will become amplified, as previous results dictate in the following analysis.

The high blowing ratio of M=1.0 and M=1.5 cases have their streamwise vorticity in Figures 48 and 49.

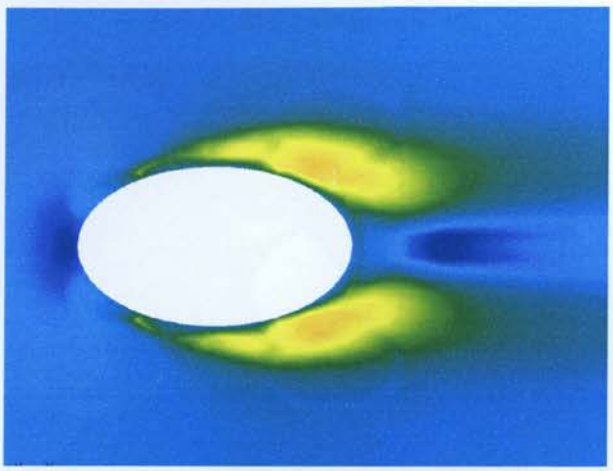

(a) Single Hole

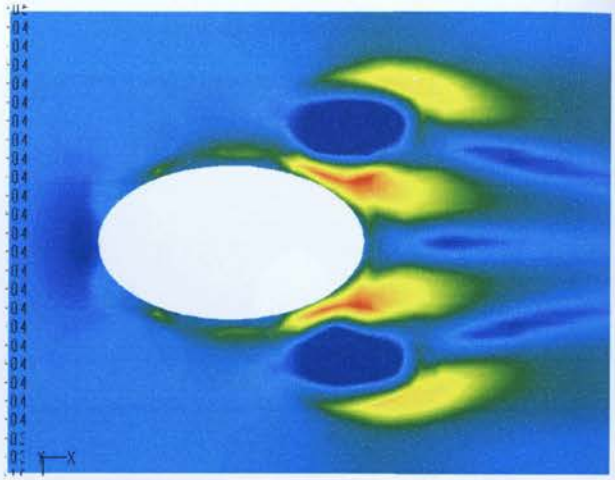

(b) Downstream Sister Holes

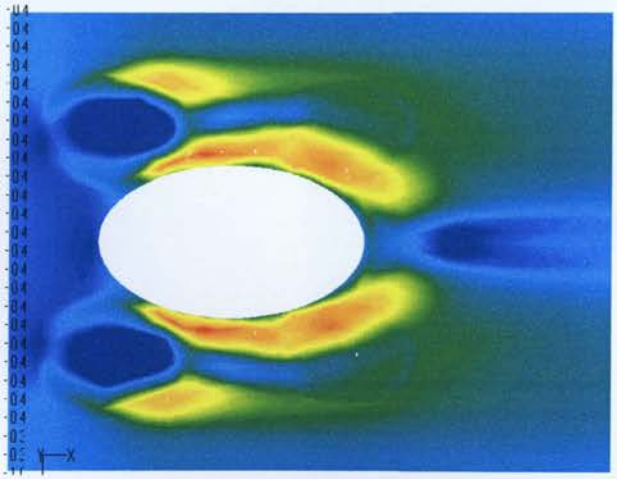

(c) Upstream Sister Holes

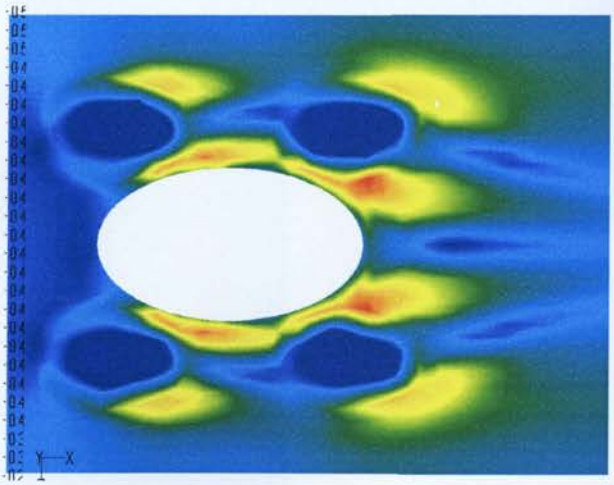

(d) Upstream/Downstream Sister Holes

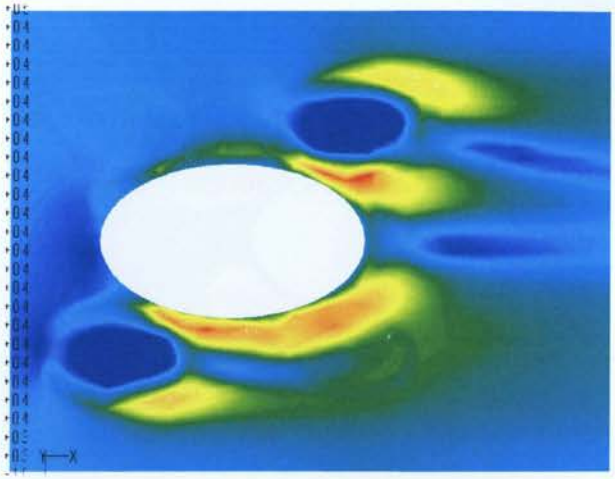

(e) Left/Right Sister Holes

Figure 48: Streamwise Vorticity – Long Hole (M=1.0)

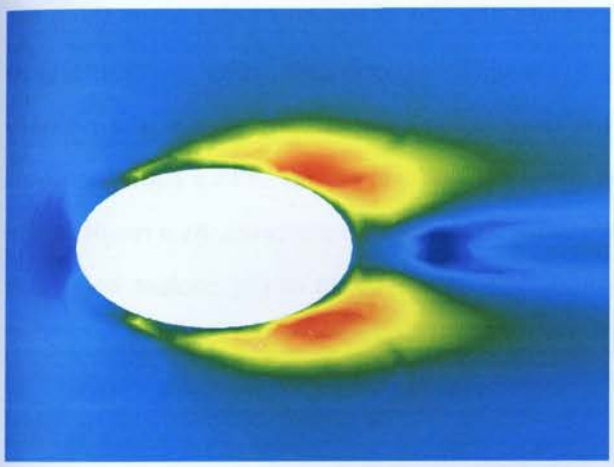

(a) Single Hole

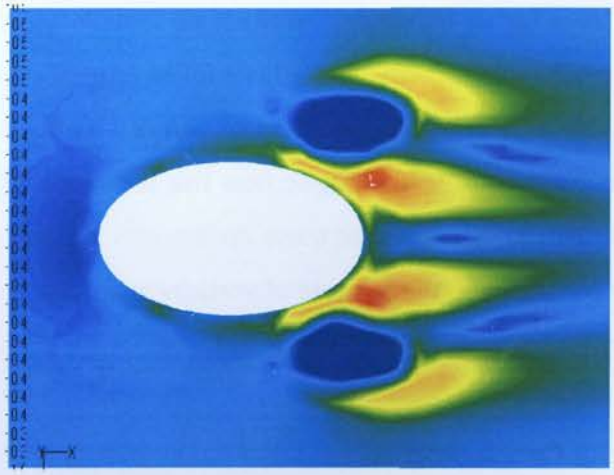

(b) Downstream Sister Holes

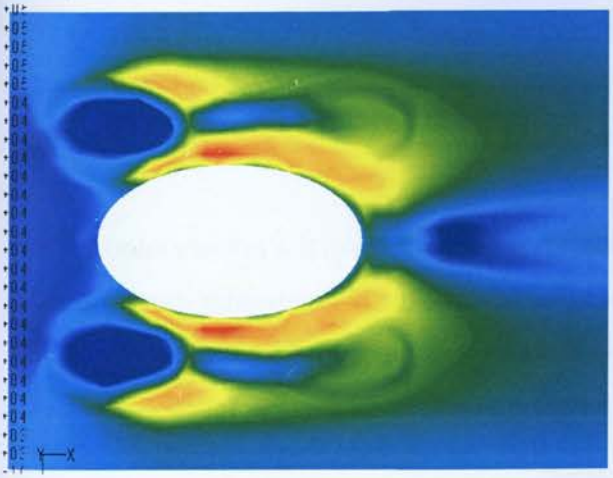

(c) Upstream Sister Holes

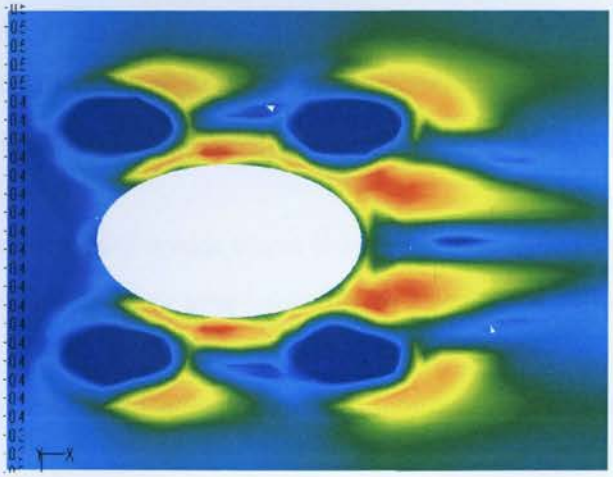

(d) Upstream/Downstream Sister Holes

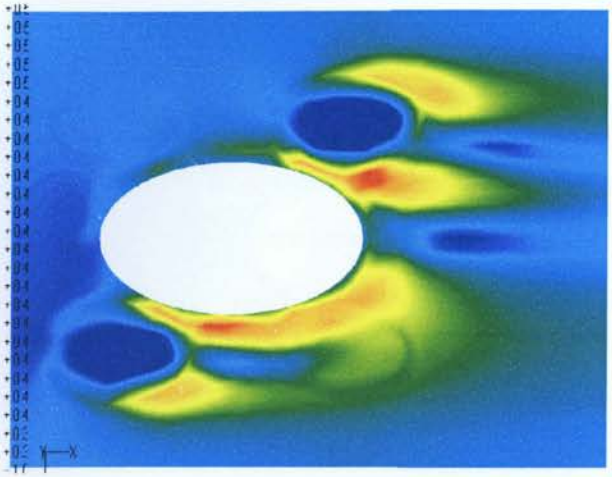

(e) Left/Right Sister Holes

Figure 49: Streamwise Vorticity – Long Hole (M=1.5)

These higher blowing ratios illustrate some interesting trends. The use of no sister holes offers the most predictable vorticity field. This is followed very closely by the upstream-only case. What is interesting to note here is that the pockets of vorticity hardly extend beyond the downstream edge of the primary coolant hole. This is largely how this technique offers the most uniform results with a high degree of effectiveness. Compare these results with those of any of the downstream hole cases. As a result of the hole position, the pockets of vorticity span considerably further downstream of the coolant holes and offer less structure in their design.

6.6 Conclusion

The results from the long-hole analysis provide consistent trends indicating that placing two sister holes upstream of the primary injection hole offers the most optimal design choice for this approach over the entire computational domain. The film cooling effectiveness from this design offers good results which are balanced by its small footprint into the mainstream flow.

Although at first glance it would appear that positioning holes downstream of the primary injection hole offer a better flowfield, the highly swirling nature of the flow makes it disadvantageous to cooling approaches. Similarly, the use of both upstream and downstream holes mixes too heavily with the mainstream without offering a significant performance improvement, making it impractical.

Finally, the use of the left/right cooling technique was studied as a means of combining the most optimal qualities of both upstream and downstream designs while minimizing the necessary mass flux. Unfortunately, the results did not indicate any improvement when the flowfield was evaluated, as the lack of flowfield cohesion caused the technique to be considered invalid.

This Page Intentionally Left Blank

7 Short Hole Models

To date, there has been limited research into the field of short hole film cooling; however, its practicality makes it an appealing research candidate. The current Section will evaluate the four sister hole geometries for the short hole case in a similar manner to the analysis for the long hole cases discussed previously. The analysis will be broken into one on adiabatic effectiveness, jet lift-off, flow structure, and streamwise vorticity, to study the domain in its entirety.

7.1 Sensitivity Analysis

Once again, to validate the computational grid, a sensitivity analysis was performed against the study of Hale [28]. As with the previous studies, the grids were generated by increasing the node count on each edge by 10% to arrive at four increasingly dense grids. To determine their validity, each grid was simulated using identical operating conditions to that of Hale [28]. Figure 50 contains the centreline and laterally averaged adiabatic effectiveness sensitivity analysis for the short hole case.

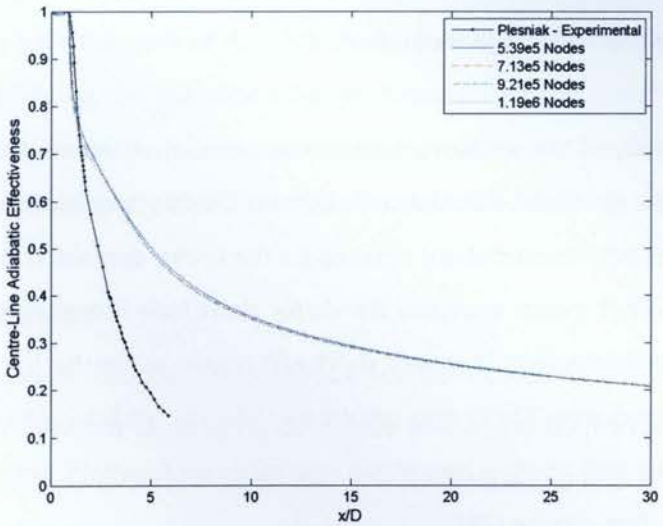

(a) Centreline Effectiveness

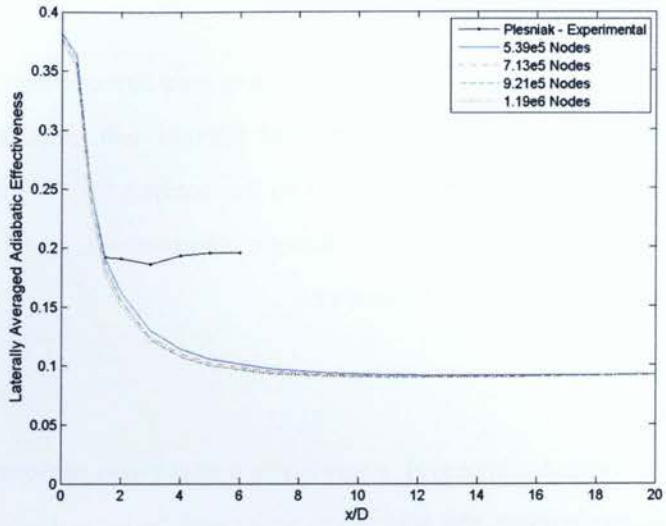

(b) Laterally Averaged Effectiveness

Figure 50: Sensitivity Analysis - Short Hole

It is quite clear that the grids do not replicate the data put forth by Hale [28] with any degree of accuracy. However, there is little doubt that the solution obtained by these grids is fully resolved and any of the grids can be considered grid independent.

With respect to the accuracy of the solution, it should be noted that the work of Hale [28] emphasized focus on an analysis of the flowfield, not the temperature distribution, meaning that the comparative results for the adiabatic effectiveness did not encompass the entire domain. It is interesting to note that the trends of Hale [28] do not match expected trends for short hole film cooling. The centreline results show a steep decline in effectiveness in a very short x/D region while the lateral results remain fairly consistent over the analyzed area. These two results partially contradict each other given the fact that Hale states that short hole film cooling provides a less cohesive flowfield, with lower effectiveness on the whole, than long hole film cooling [28].

To further validate the results, the study of Lutum et al. [24] was used as a secondary benchmarking tool. Although the geometry of the current study was similar to that of Lutum et al. [24], the operating parameters would have made the use of compressible flow regimes necessary and as such, the simulation was not performed with the current grid and solver. However, the more important outtake from this are the data trends, as they do not match that of Hale [28] but rather favour the results of the

current study. Figure 51 contains the centreline and laterally averaged effectiveness found in Lutum et al. [24]

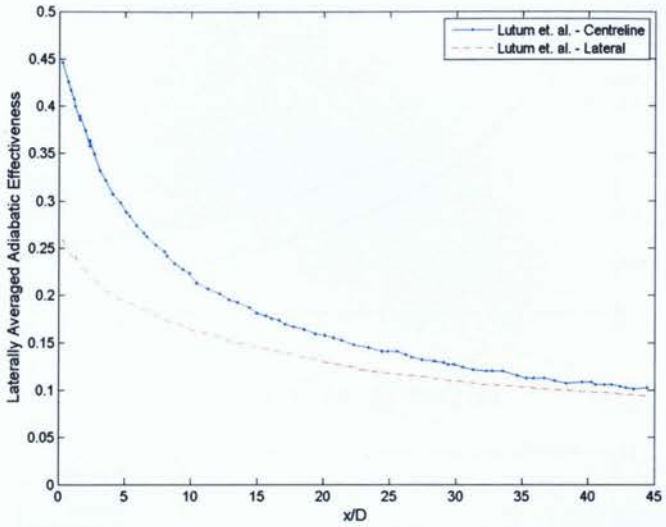

Figure 51: Short Hole Analysis - Lutum et al.

As a result, in evaluating both the work of Hale [28] and Lutum et al. [24], there was confidence in going forth with the current grids, as the evaluation herein focused more on sister hole improvement than precise data matching. Similarly, to reduce computational cost while optimizing the accuracy of the solution, the third most refined grid with 9.21×10^5 nodes was used for all further simulations.

7.2 Adiabatic Effectiveness

To remain consistent between studies, the adiabatic effectiveness results will be separated into low and high blowing ratios where the low blowing ratios include M=0.2 and M=0.5 and the high blowing ratios include M=1.0 and M=1.5. Figures 52 and 53 contain the centreline and laterally averaged effectiveness plots for the M=0.2 and M=0.5 blowing ratios, respectively.

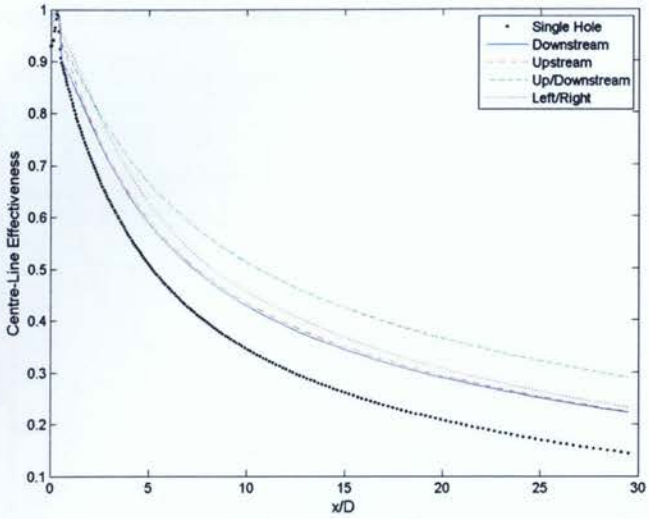

(a) Centreline Effectiveness

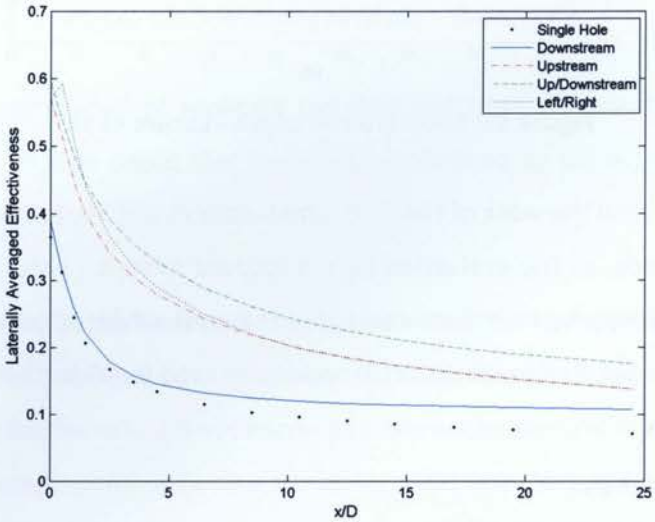

(b) Laterally Averaged Effectiveness

Figure 52: Adiabatic Effectiveness – Short Hole (M=0.2)

These results illustrate similar trends to those found in the long hole analysis. Most clearly, all sister hole cases offer improved performance over their single hole counterpart, particularly as the blowing ratio begins to increase. In a similar fashion to the results of Section 6, the near hole region seems to benefit most strongly from downstream sister holes while upstream sister holes dissipate less significantly causing greater lateral spread in the downstream direction. Note that at the moderately low blowing ratio of M=0.5, the centreline analysis shows significant performance improvements in the region of $5 \leq x/D \leq 10$ for cases with upstream holes, as a result of sister hole reattachment following their brief separation.

Figures 54 and 55 contain the centreline and laterally averaged effectiveness values for the high blowing ratios of M = 1.0 and M = 1.5.

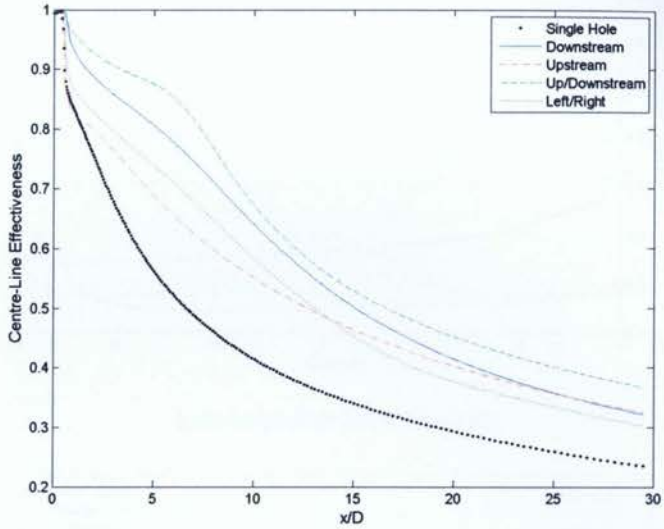

(a) Centreline Effectiveness

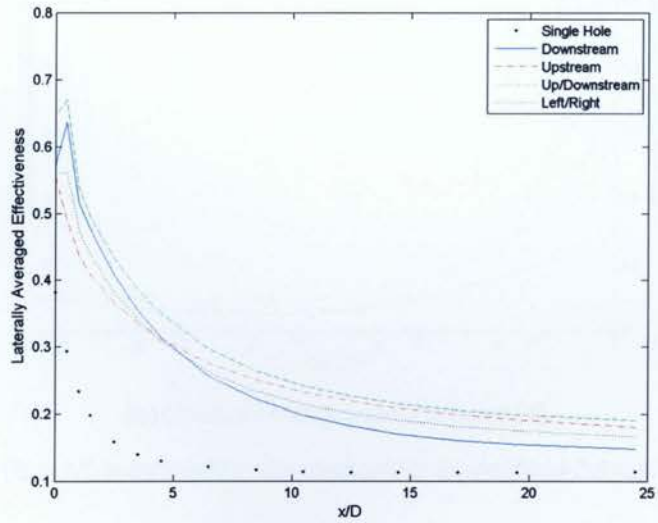

(b) Laterally Averaged Effectiveness

Figure 53: Adiabatic Effectiveness – Short Hole (M=0.5)

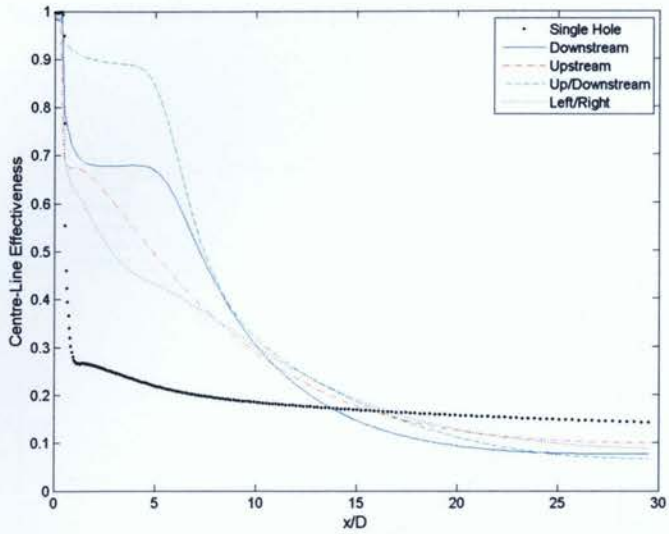

(a) Centreline Effectiveness

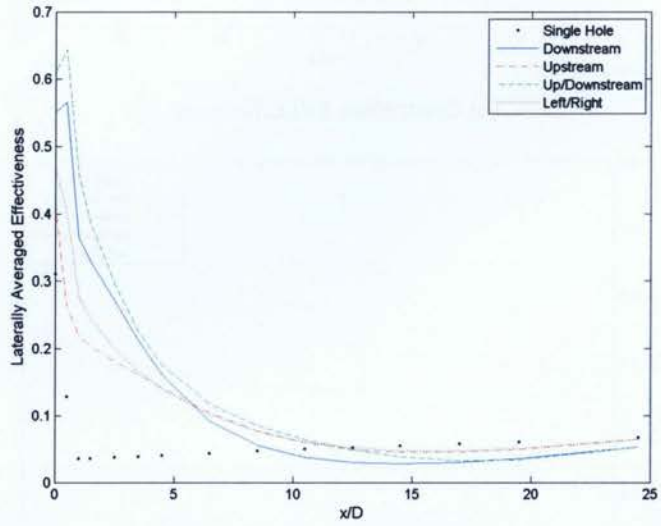

(b) Laterally Averaged Effectiveness

Figure 54: Adiabatic Effectiveness – Short Hole (M=1.0)

It is at these blowing ratios that the results become significantly more interesting. The first point of note is the near-hole improvements with the use of downstream sister holes. The centreline results illustrate that for both high blowing ratio cases, there is a plateau while the flow is fully attached to the surface before it begins to dissipate and mix with the mainstream flow. Obviously as a result of the four injection holes, the case with both up- and downstream holes offers the highest effectiveness in this region; however the necessity of such a large amount of coolant makes its applicability limited.

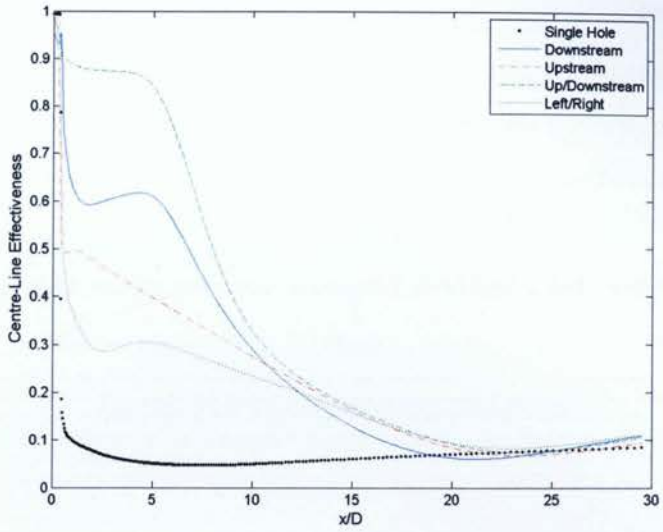

(a) Centreline Effectiveness

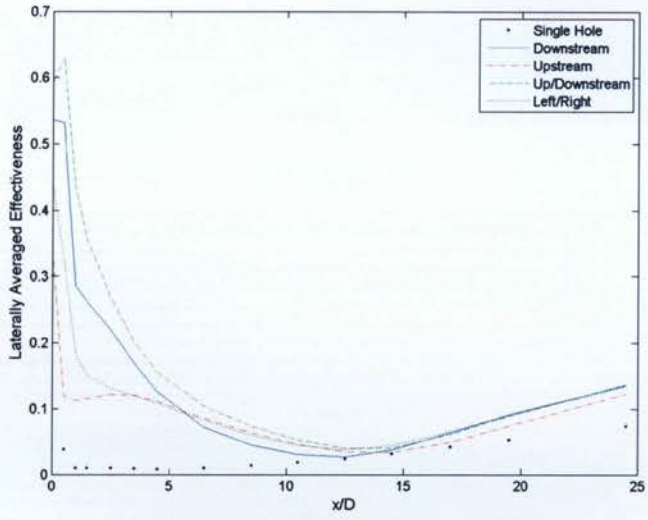

(b) Laterally Averaged Effectiveness

Figure 55: Adiabatic Effectiveness – Short Hole (M=1.5)

Unfortunately, the plateau trend, evident in the centreline analysis, does not hold true for the laterally averaged results; the laterally averaged effectiveness results maintain standard trends at all blowing ratios. It is interesting to note that the sister holes begin to match the laterally averaged effectiveness of the single hole case in the vicinity of $x/D \approx 12$. This trend is slightly different than that of the long hole cases as mainstream mixing is more dominant with short hole geometries.

To further expand upon this analysis, an evaluation of the primary jet lift-off follows.

7.3 Primary Jet Lift-Off

The long-hole study demonstrated that primary hole jet liftoff does not vary considerably as a result of the use of sister holes. However, it was noted that the temperature distribution (indicated by the colour of the velocity vectors) dramatically changes with the addition of sister holes.

Figures 56 and 57 contain the M=0.2 and M=0.5 blowing ratios for all simulated geometries.

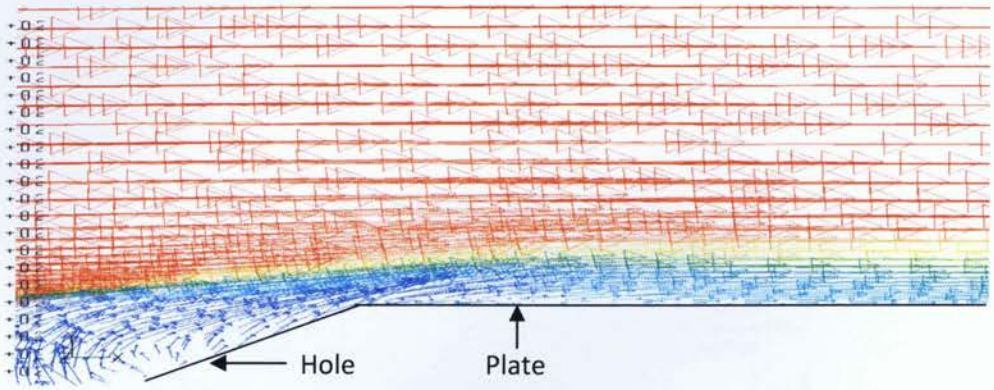

(a) Single Hole

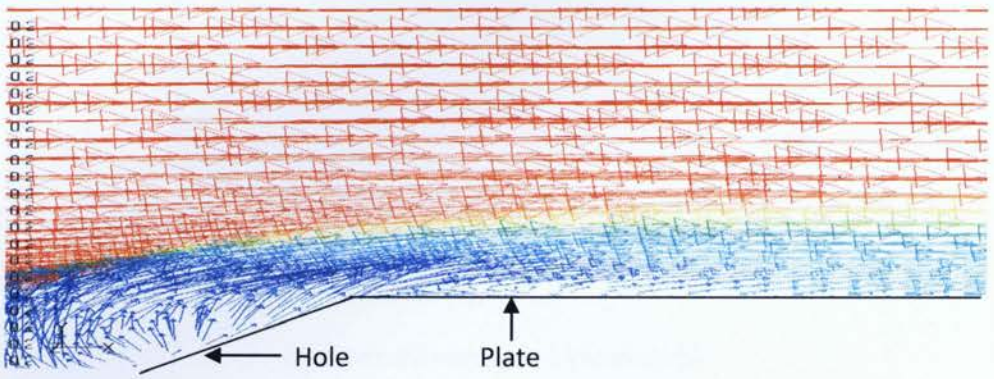

(b) Downstream Sister Holes

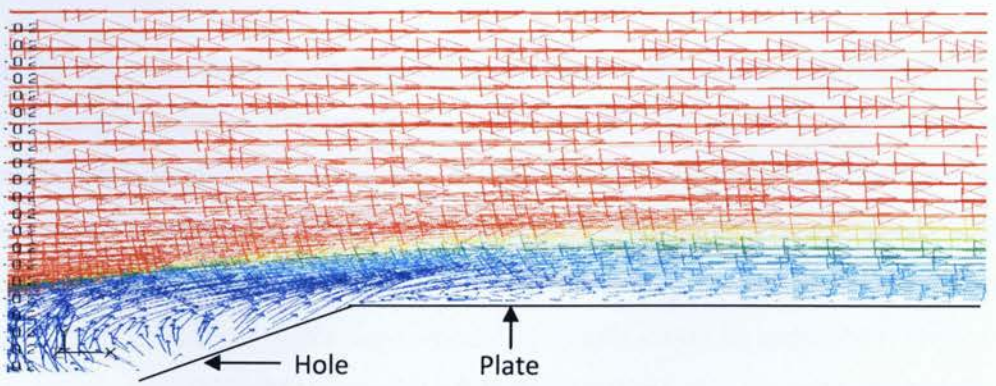

(c) Upstream Sister Holes

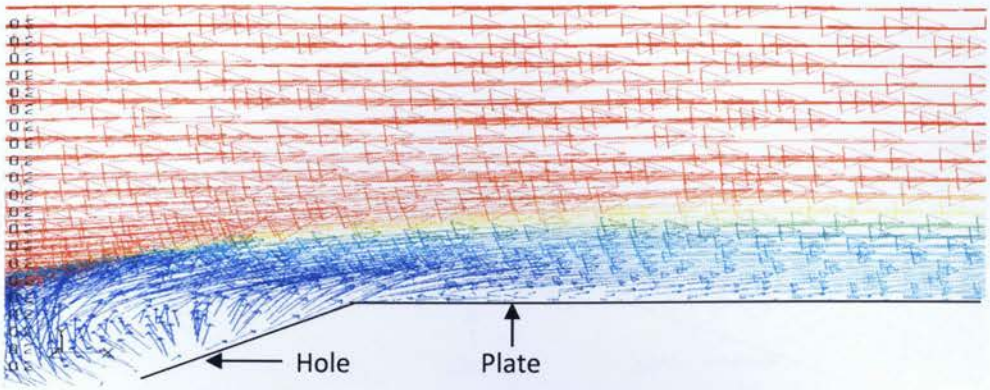

(d) Upstream/Downstream Sister Holes

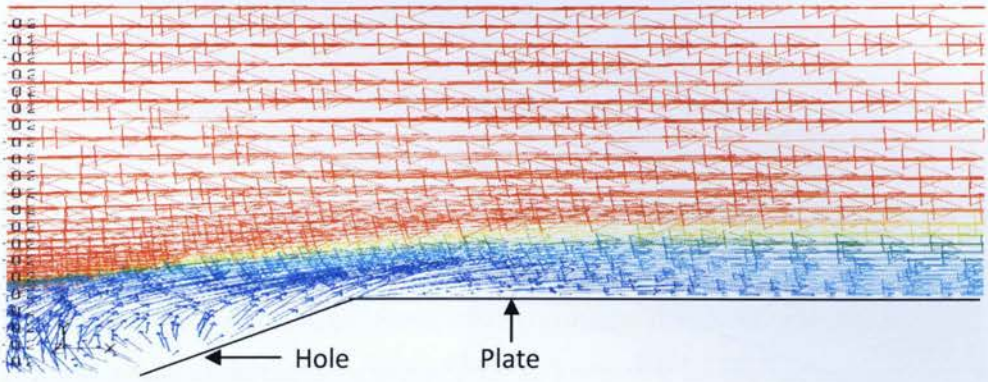

(e) Left/Right Sister Holes

Figure 56: Jet Lift-Off – Short Hole (M=0.2)

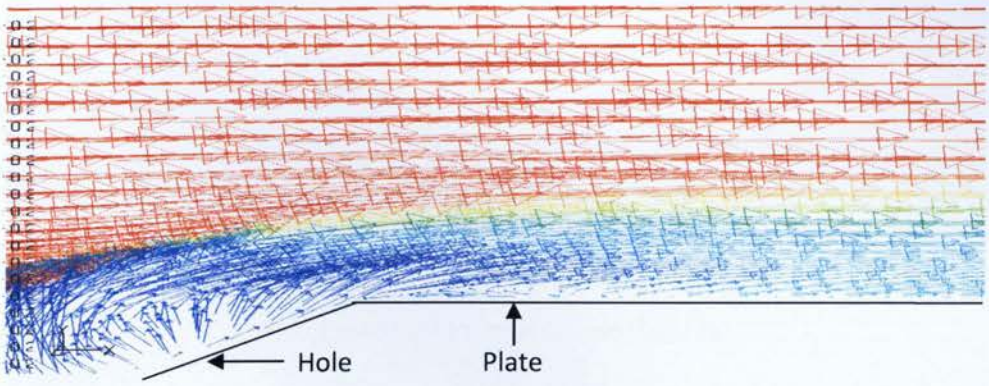

(a) Single Hole

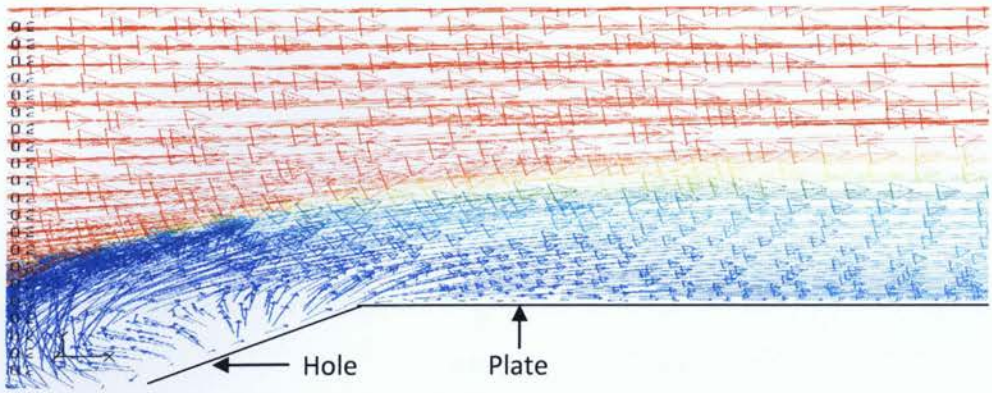

(b) Downstream Sister Holes

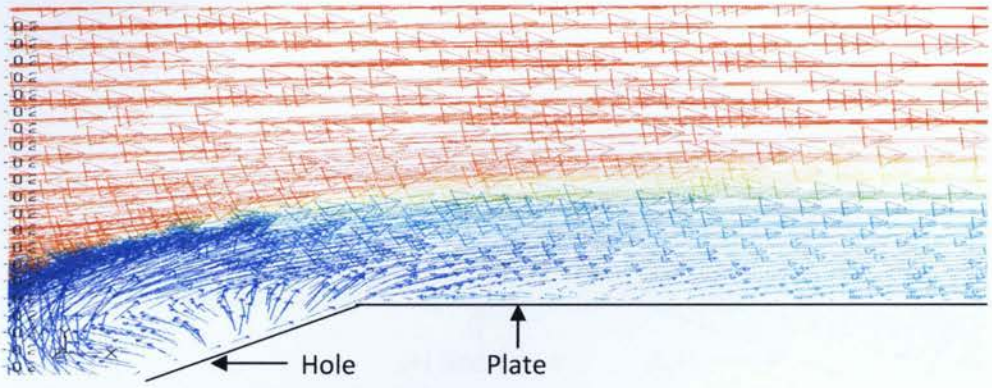

(c) Upstream Sister Holes

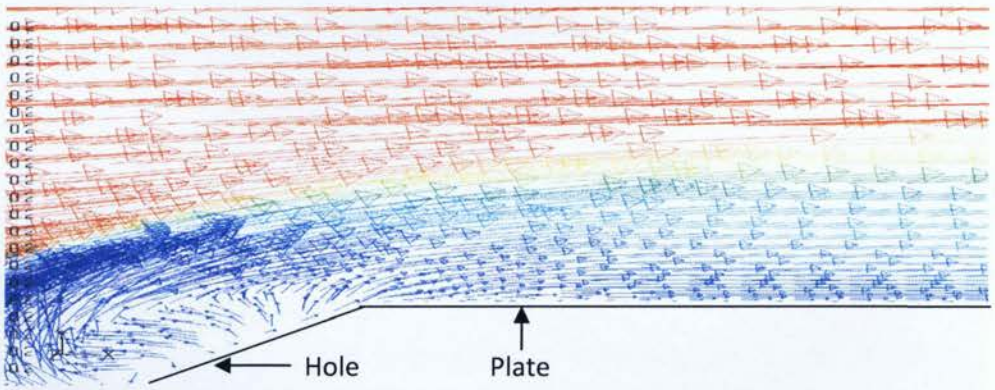

(d) Upstream/Downstream Sister Holes

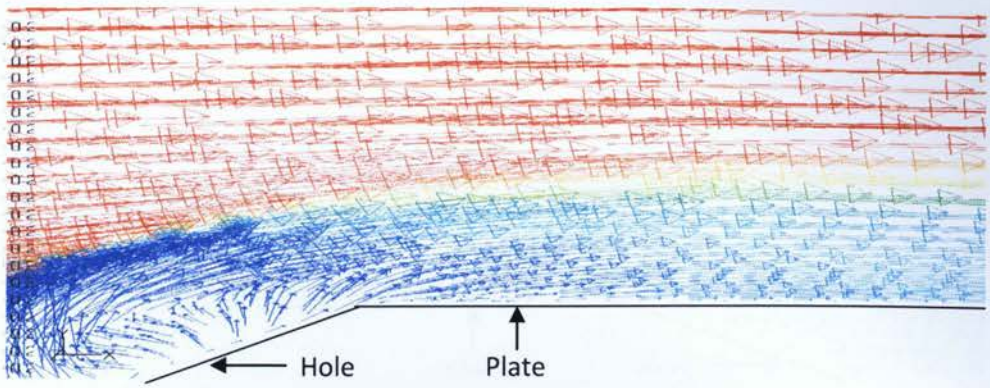

(e) Left/Right Sister Holes

Figure 57: Jet Lift-Off – Short Hole (M=0.5)

Similar to the long-hole study, at such low blowing ratios, there is very little separation and the flow is largely attached to the wall as it proceeds downstream. However, there are a couple of interesting points to note with this analysis. Firstly, the nature of the flow emanating from the hole is dramatically different from that of the long-hole study. The long-hole case demonstrated highly cohesive flow with very little back-flow within the hole itself. Here, there is considerable swirling within the hole as the flow has not been given ample opportunity to settle, prior to entraining on the hot mainstream. Further, the upstream-only holes at a blowing ratio of M=0.5 demonstrate the least cohesive temperature field, as noted by the temperature distribution.

The higher blowing ratios of M=1.0 and M=1.5 are contained in Figures 58 and 59.

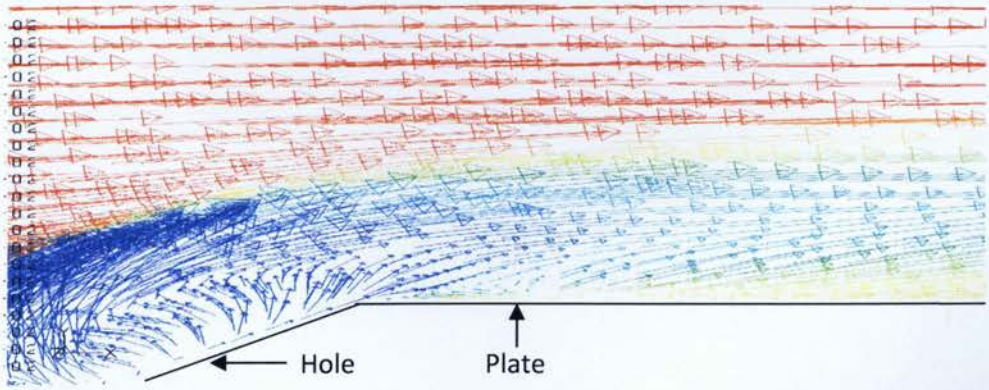

(a) Single Hole

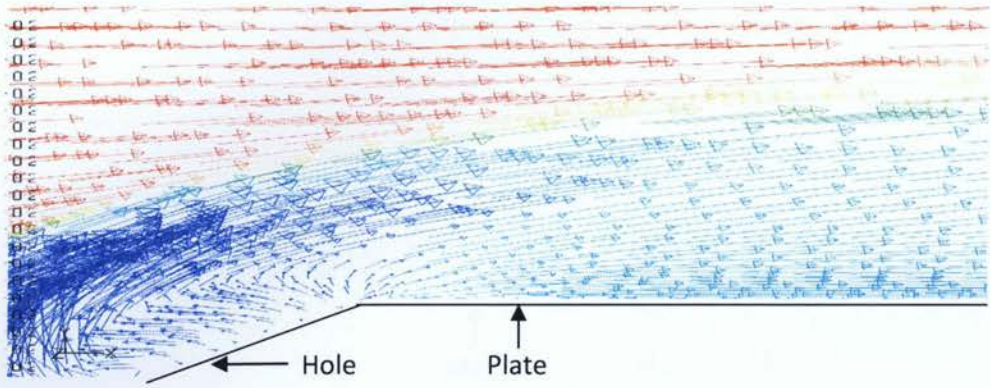

(b) Downstream Sister Holes

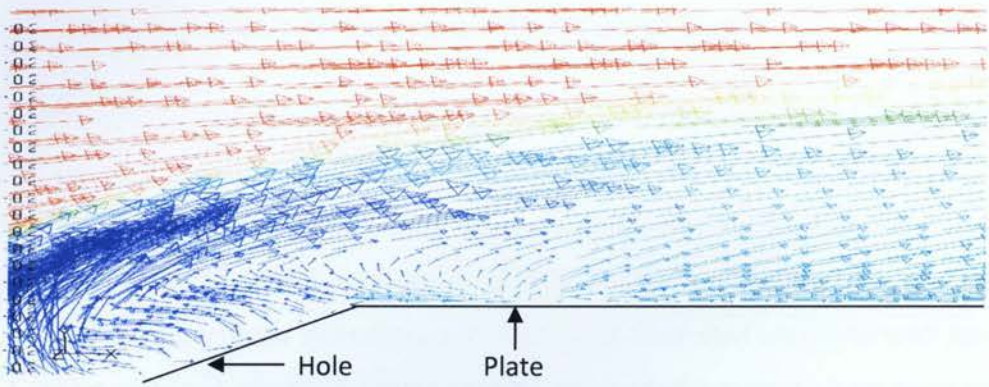

(c) Upstream Sister Holes

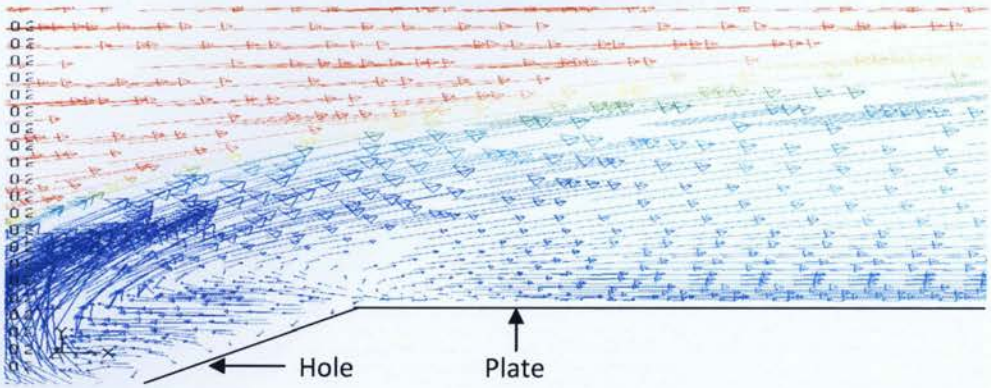

(d) Upstream/Downstream Sister Holes

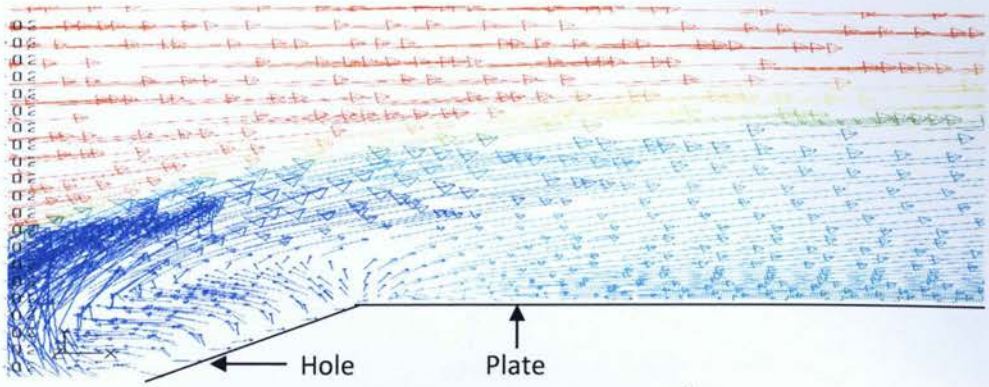

(e) Left/Right Sister Holes

Figure 58: Jet Lift-Off – Short Hole (M=1.0)

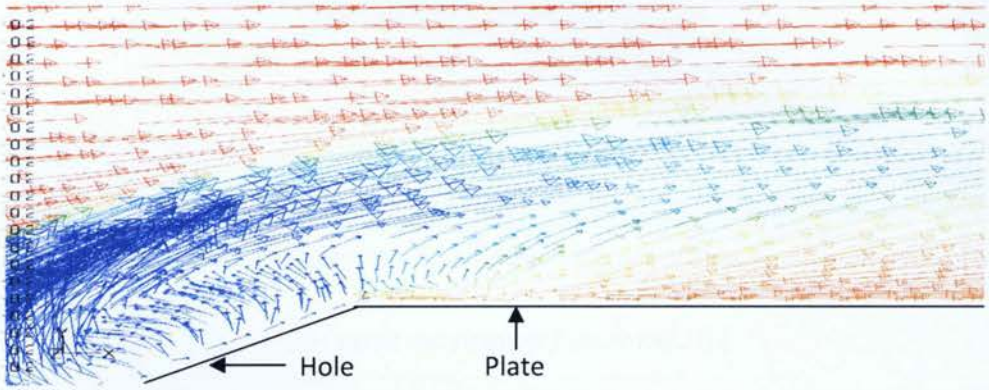

(a) Single Hole

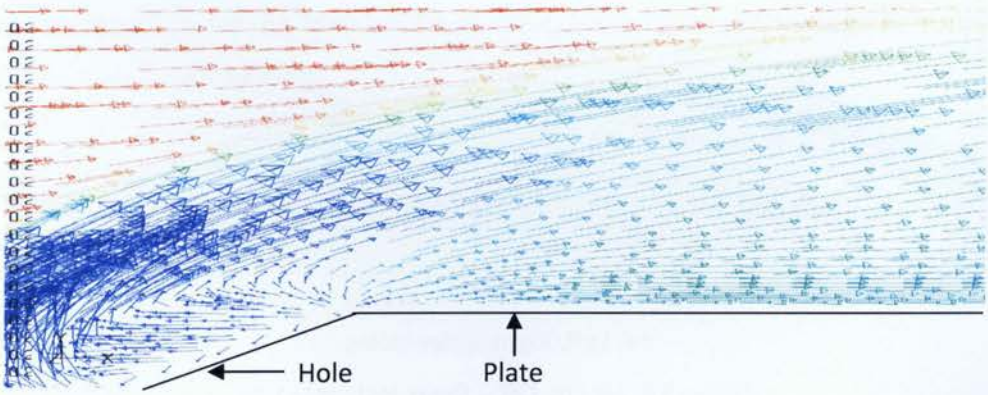

(b) Downstream Sister Holes

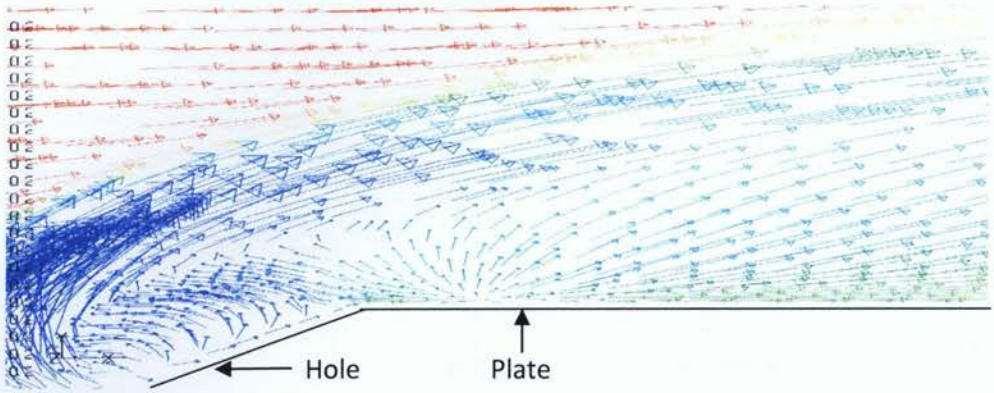

(c) Upstream Sister Holes

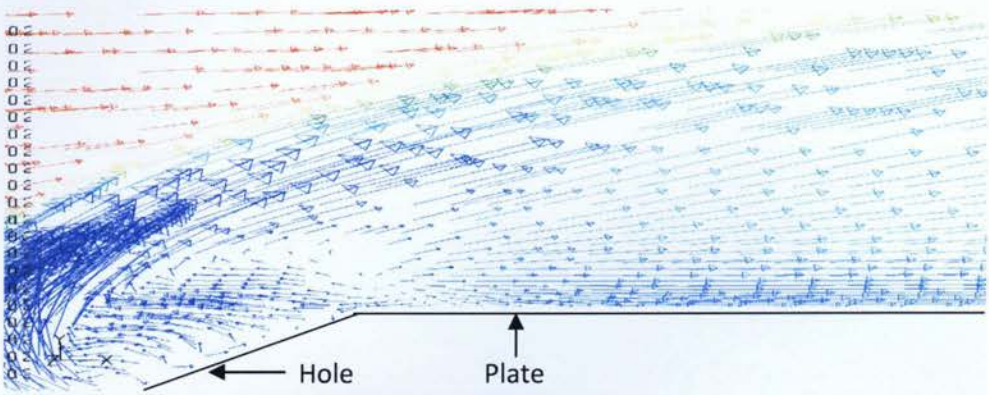

(d) Upstream/Downstream Sister Holes

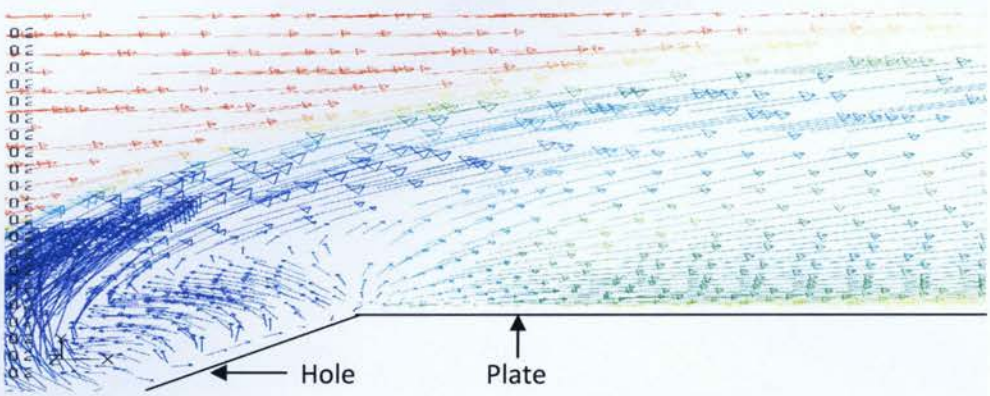

(e) Left/Right Sister Holes

Figure 59: Jet Lift-Off – Short Hole (M=1.5)

At these higher blowing ratios, the flowfield becomes significantly more complex. Once again, the flow reversal within the hole is quite dramatic and should not be neglected in this analysis. At the exit of the hole, the case with only upstream holes, once again, demonstrates its lack of applicability as the flow continues to separate. Notice that at higher blowing ratios in particular, the addition of sister holes to

the solution causes the entire coolant flow to penetrate further into the mainstream causing potential aerodynamic losses that could be detrimental to turbine performance.

Here, the case with only downstream holes once again offers the most optimal performance and is a good compromise of amount of coolant to flow cohesion. The left/right case, as expected from the long-hole study, offers no notable improvements over the other cases, becoming one of the poorest performing designs.

Although the jet-liftoff of the short-hole study provided more insight into the flowfield than the long-hole study, further evaluation of the flowfield, by studying the flow at varying x/D locations, was of interest.

7.4 Primary Flow Structure

The research of Hale [28] clearly notes that the primary kidney-shaped vortex structure dominates the flowfield and by not adequately controlling it, an otherwise applicable technique can offer very poor results.

Each blowing ratio is evaluated at four x/D locations, x/D = 0, 1, 2, and 3. Figures 60 through 64 contain the primary flow structure for the M=0.2 blowing ratio, while Figures 65 through 69 contain the flow structure for the M=0.5 blowing ratio.

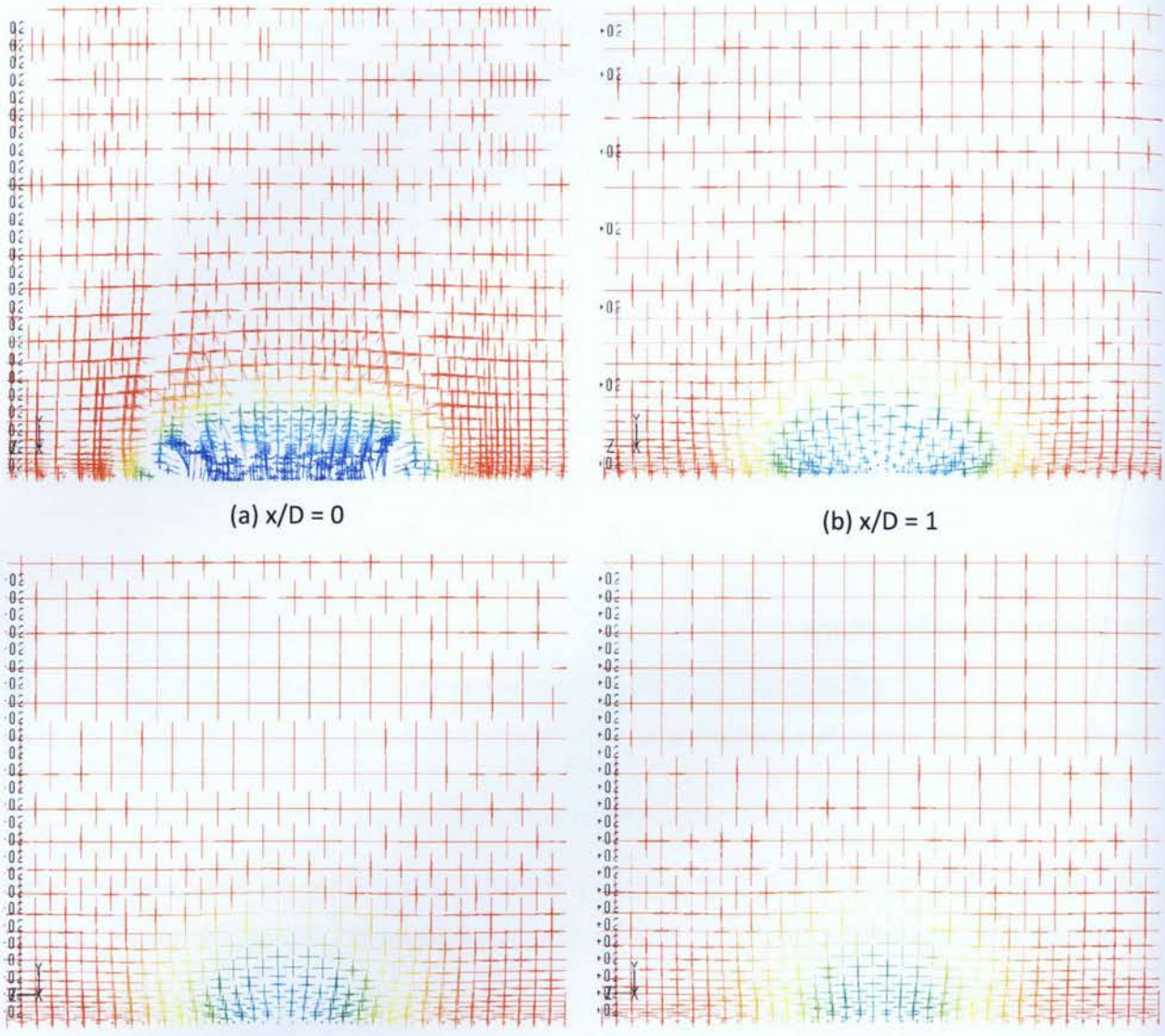

(a) x/D = 0

(b) x/D = 1

(c) x/D = 2

(d) x/D = 3

Figure 60: Flow Structure – Single Hole (M=0.2)

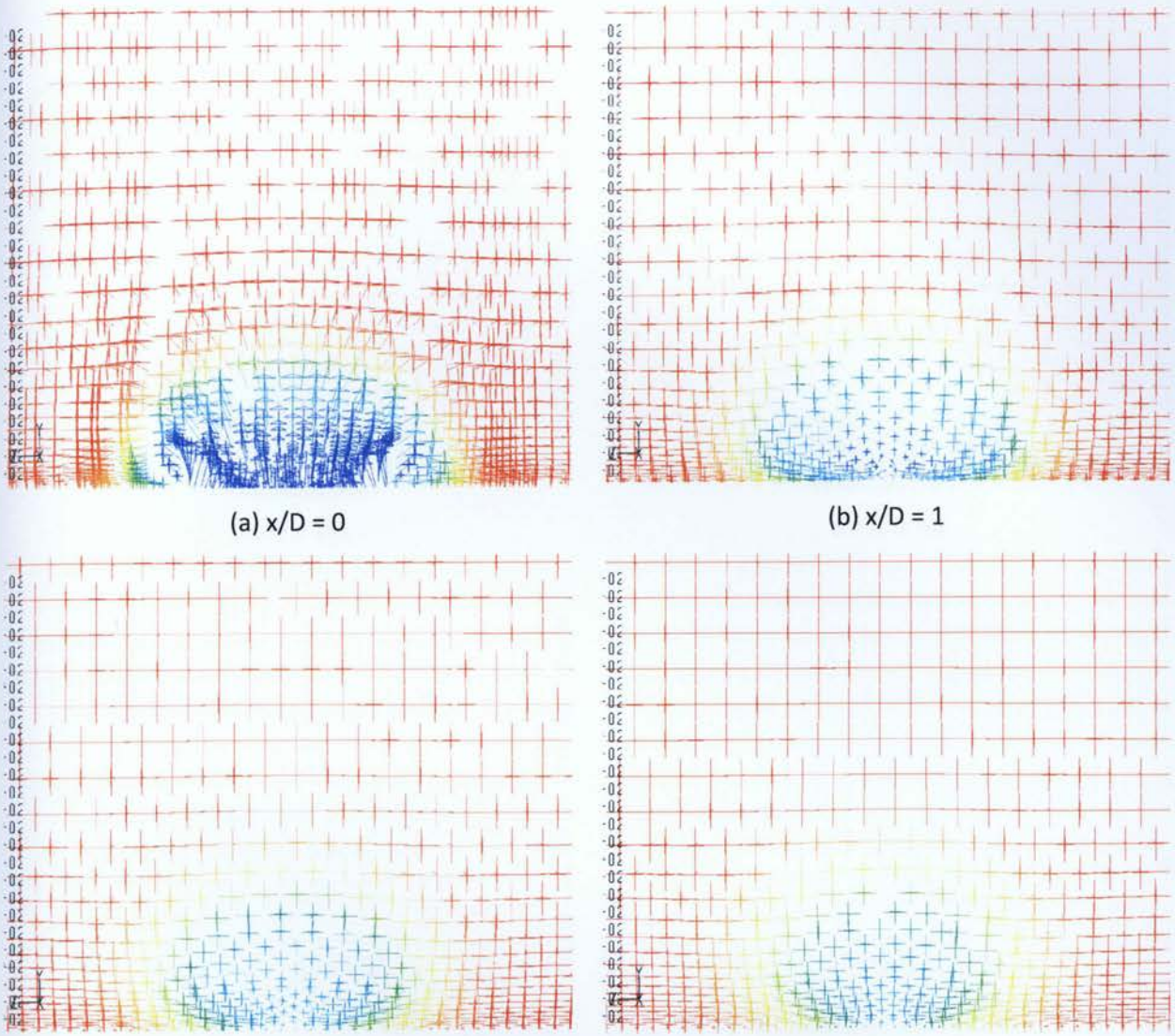

(a) x/D = 0

(b) x/D = 1

(c) x/D = 2

(d) x/D = 3

Figure 61: Flow Structure – Downstream Sister Holes (M=0.2)

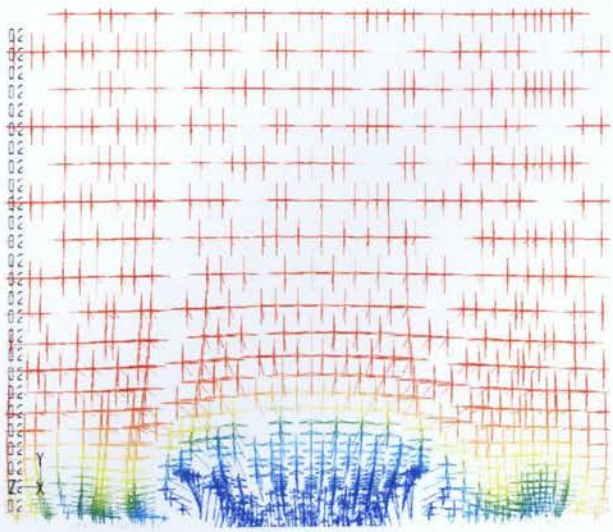

(a) x/D = 0

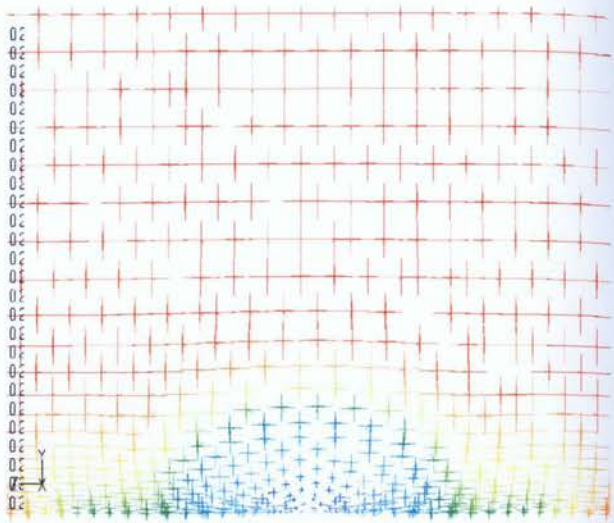

(b) x/D = 1

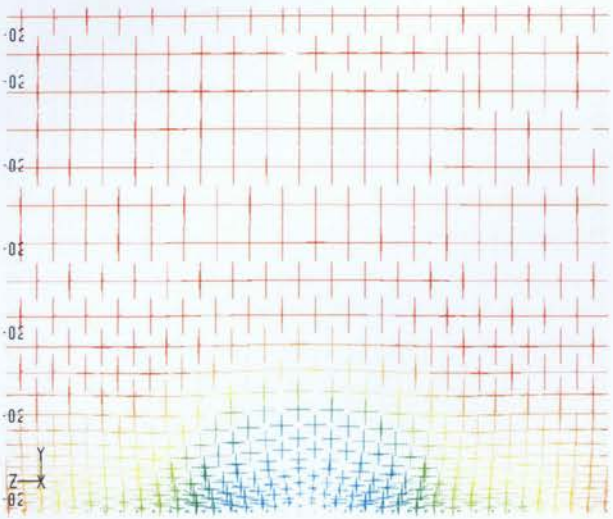

(c) x/D = 2

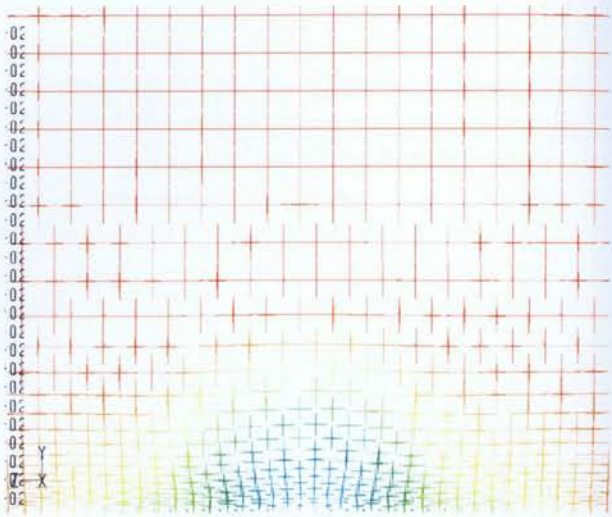

(d) x/D = 3

Figure 62: Flow Structure – Upstream Sister Holes (M=0.2)

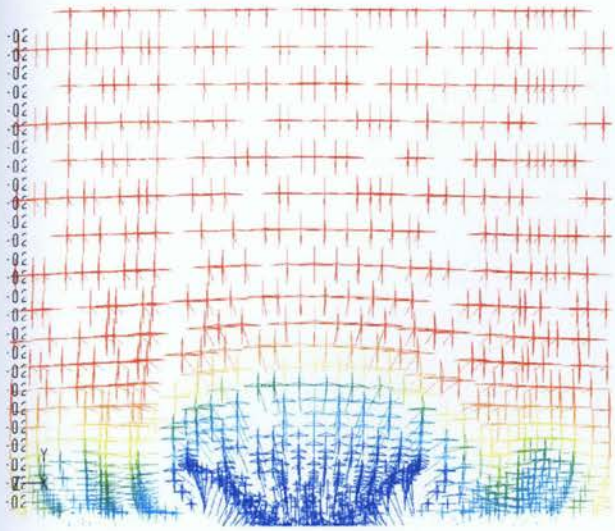

(a) x/D = 0

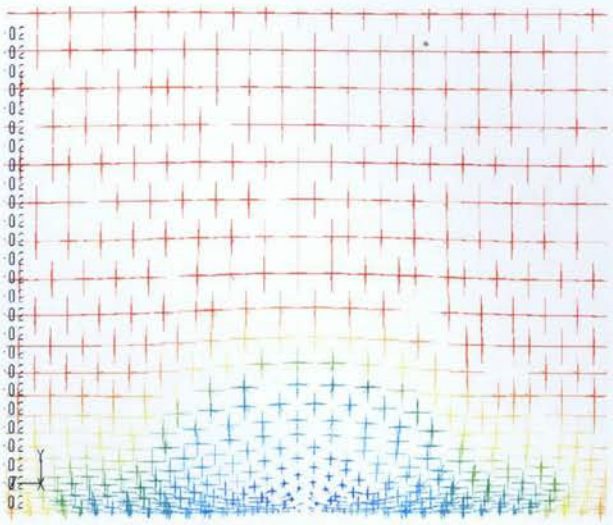

(b) x/D = 1

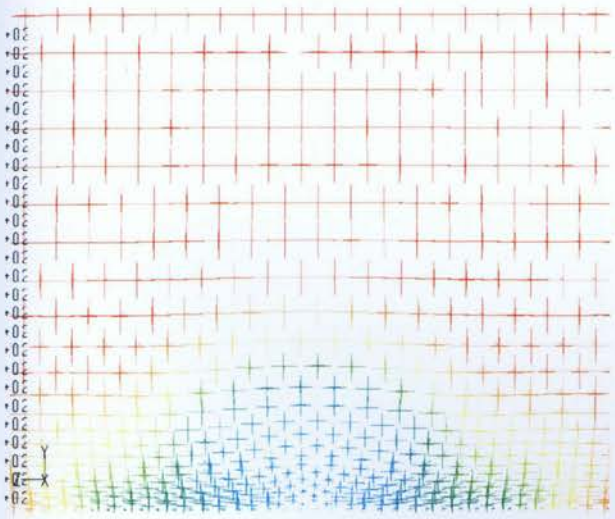

(c) x/D = 2

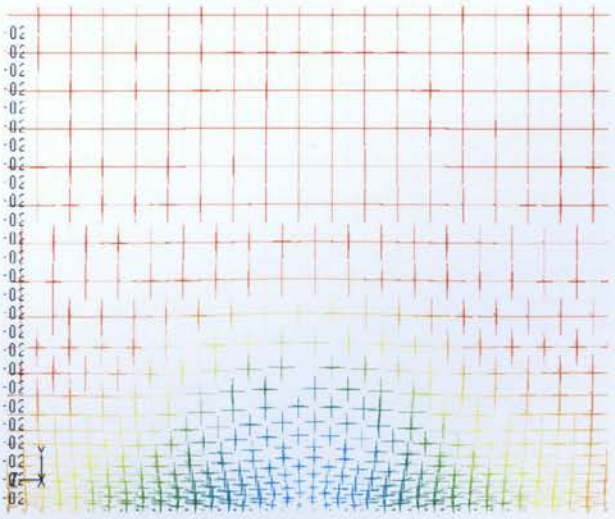

(d) x/D = 3

Figure 63: Flow Structure – Upstream/Downstream Sister Holes (M=0.2)

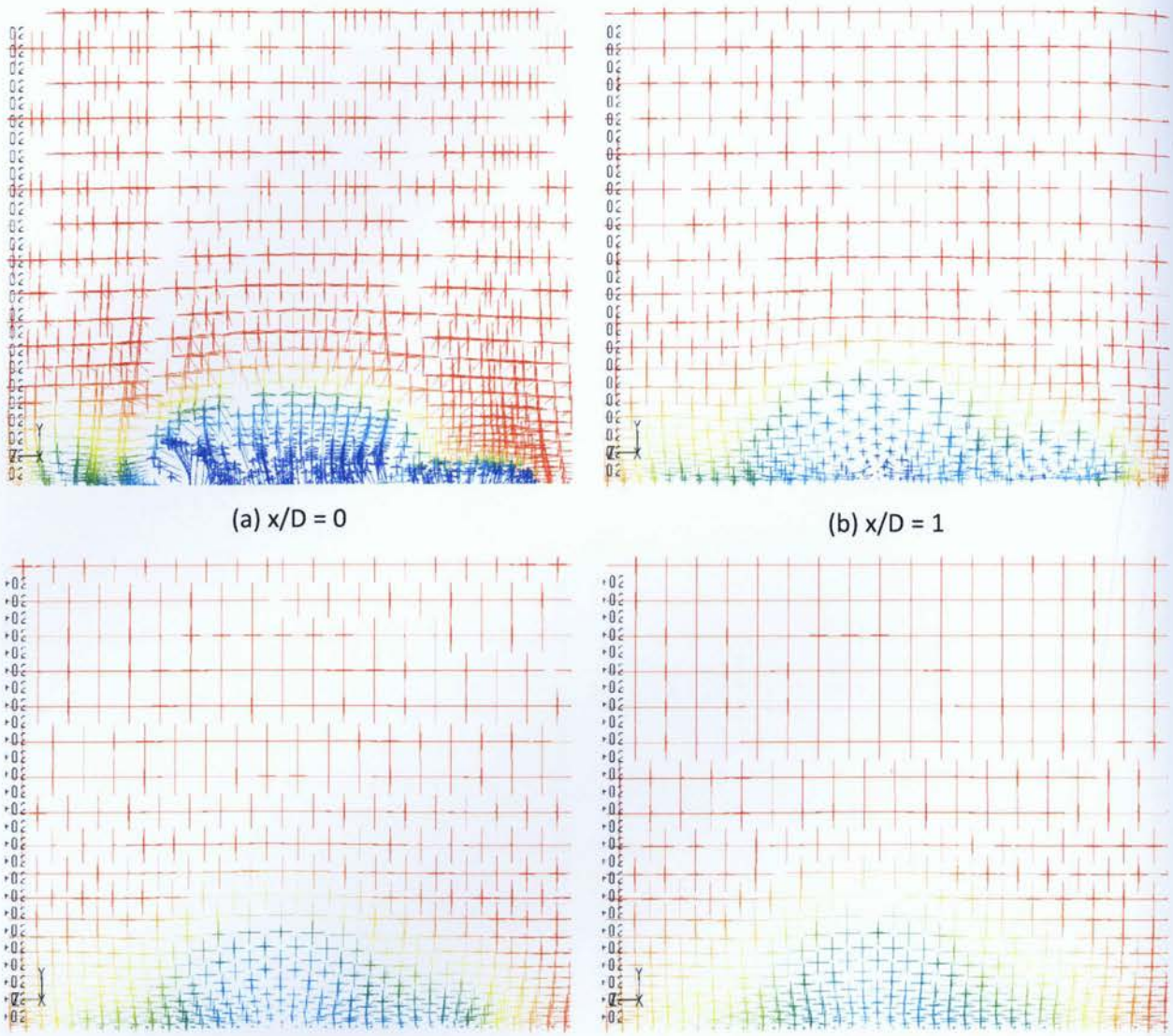

(a) x/D = 0

(b) x/D = 1

(c) x/D = 2

(d) x/D = 3

Figure 64: Flow Structure – Left/Right Sister Holes (M=0.2)

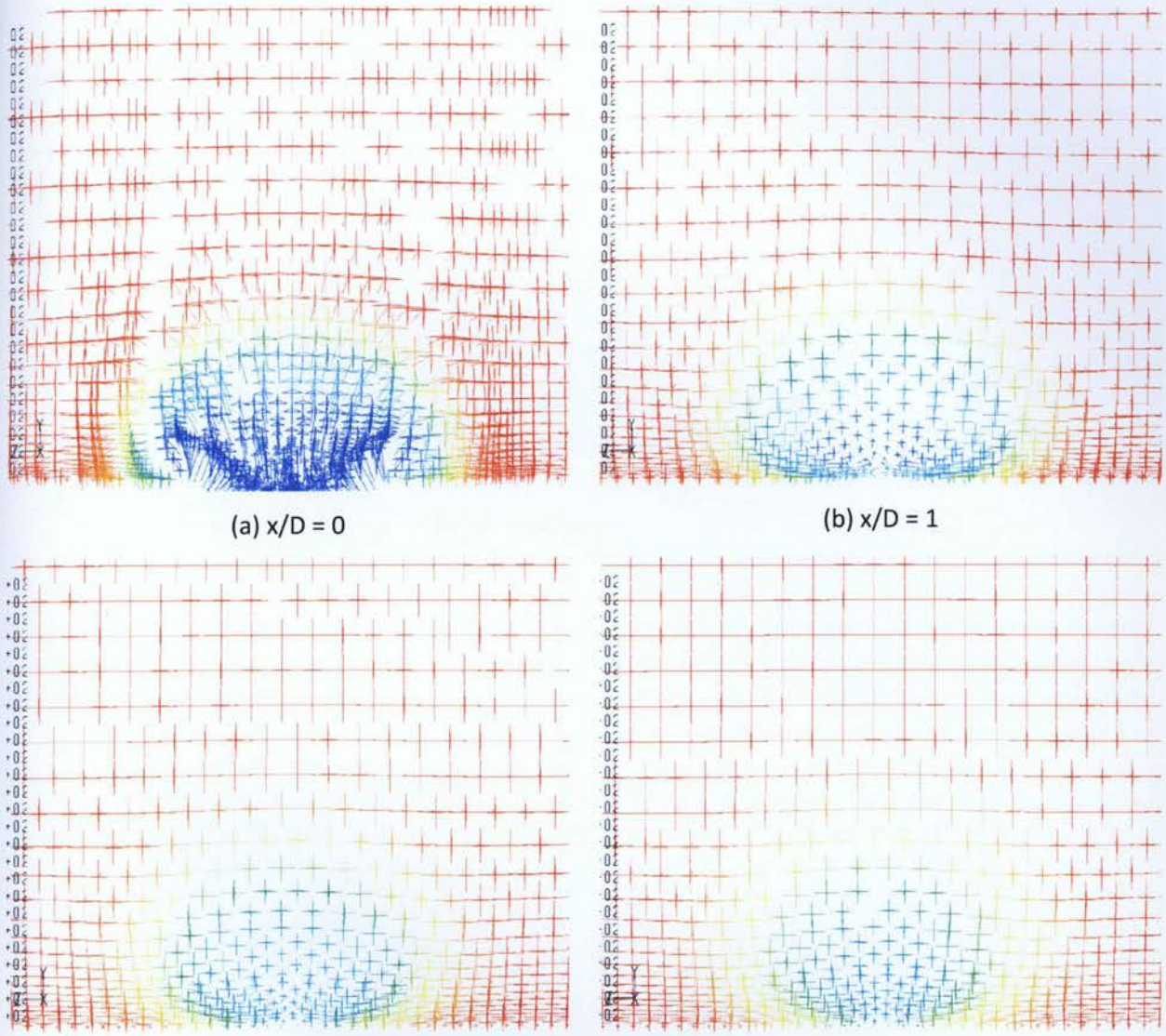

(a) x/D = 0

(b) x/D = 1

(c) x/D = 2

(d) x/D = 3

Figure 65: Flow Structure – Single Hole (M=0.5)

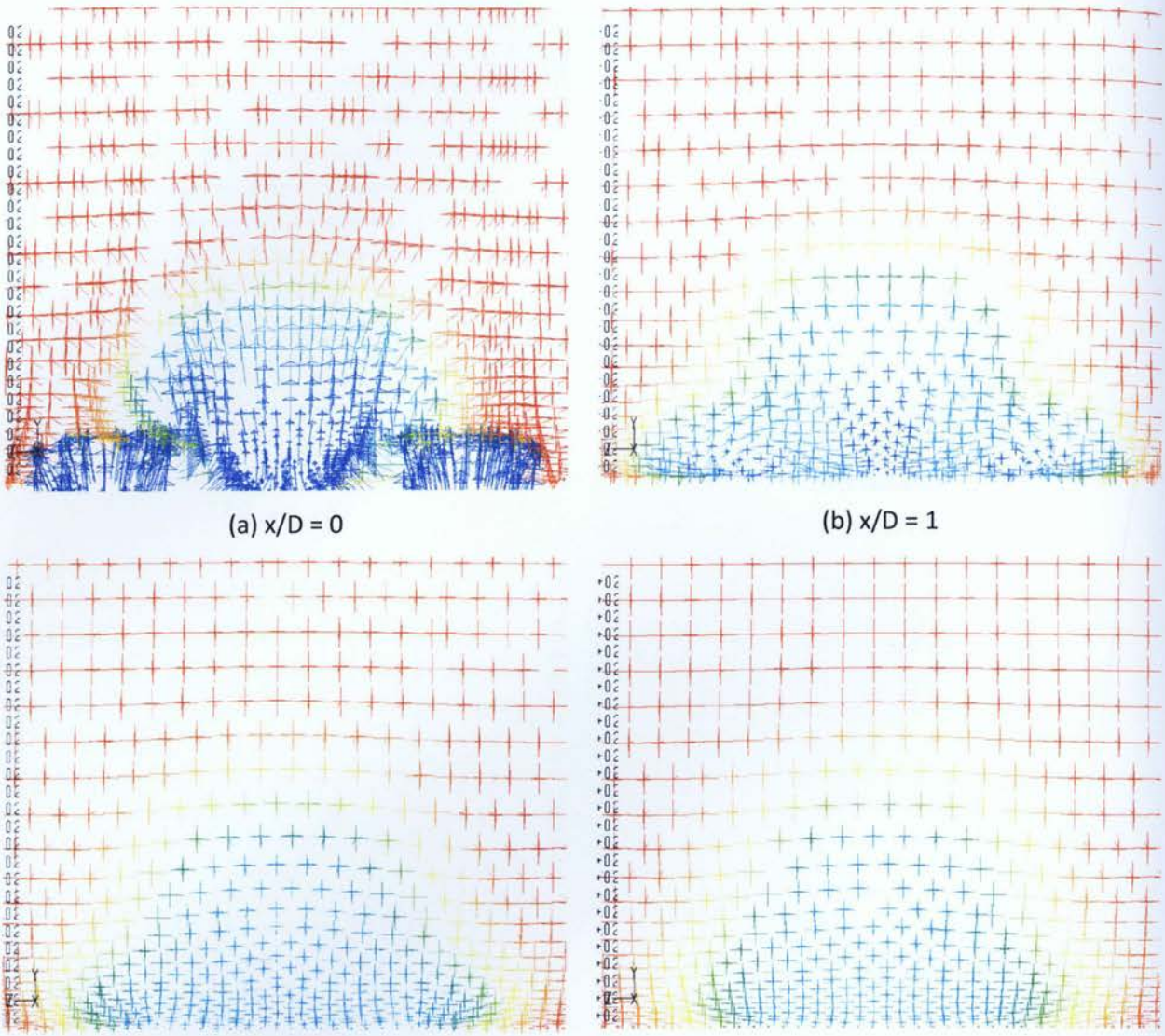

(a) x/D = 0

(b) x/D = 1

(c) x/D = 2

(d) x/D = 3

Figure 66: Flow Structure – Downstream Sister Holes (M=0.5)

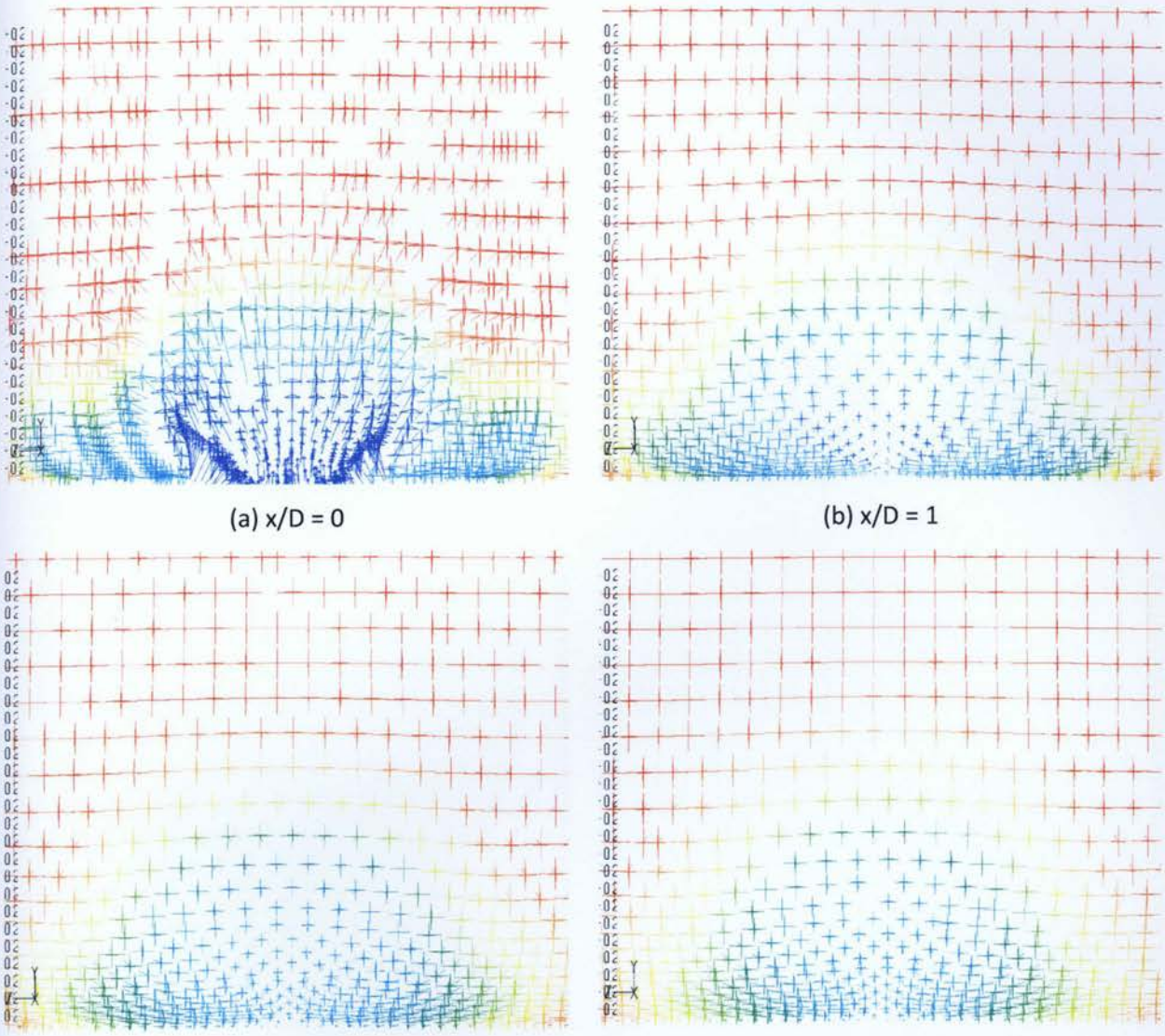

(a) x/D = 0

(b) x/D = 1

(c) x/D = 2

(d) x/D = 3

Figure 67: Flow Structure – Upstream Sister Holes (M=0.5)

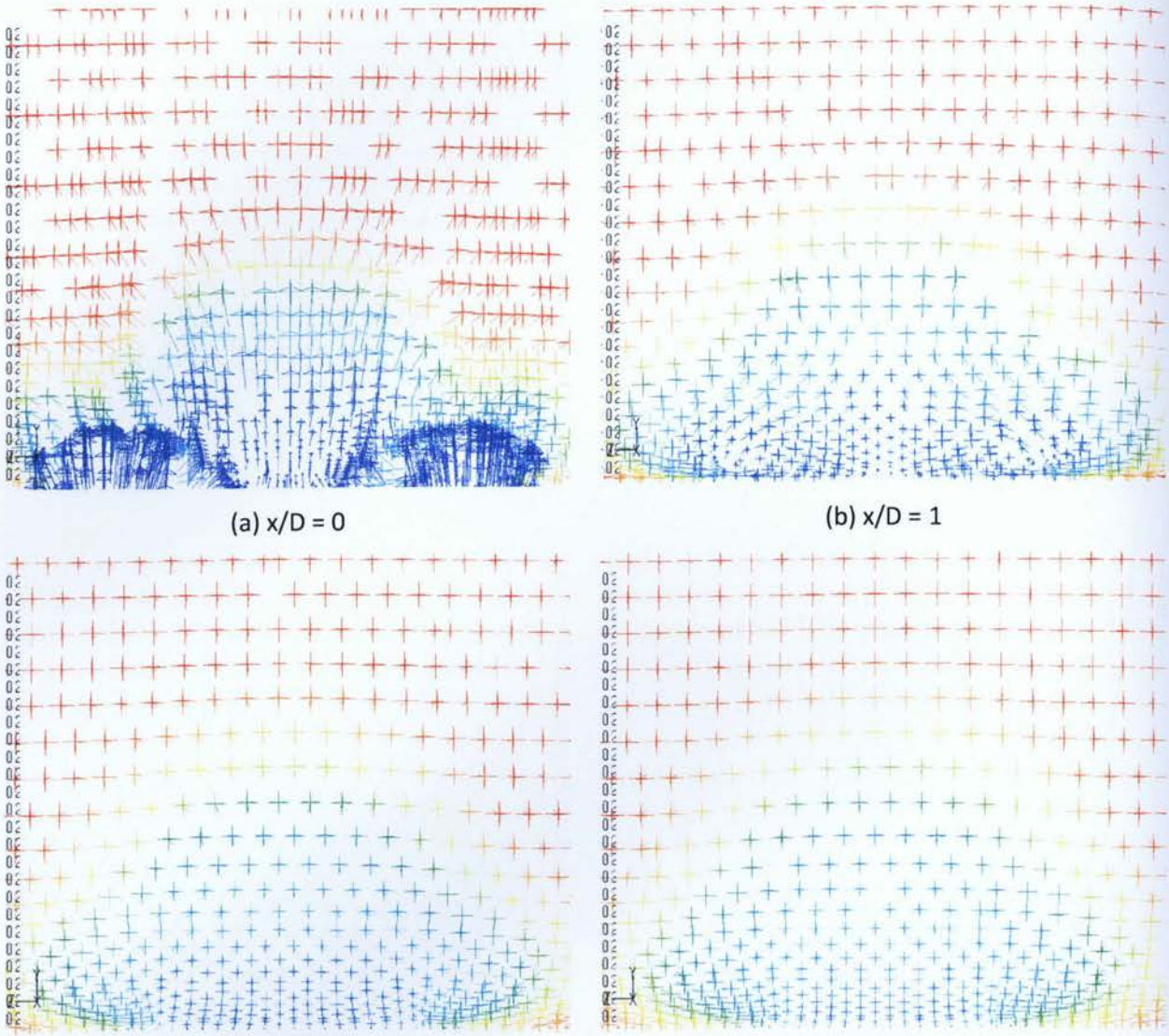

(a) x/D = 0

(b) x/D = 1

(c) x/D = 2

(d) x/D = 3

Figure 68: Flow Structure – Upstream/Downstream Sister Holes (M=0.5)

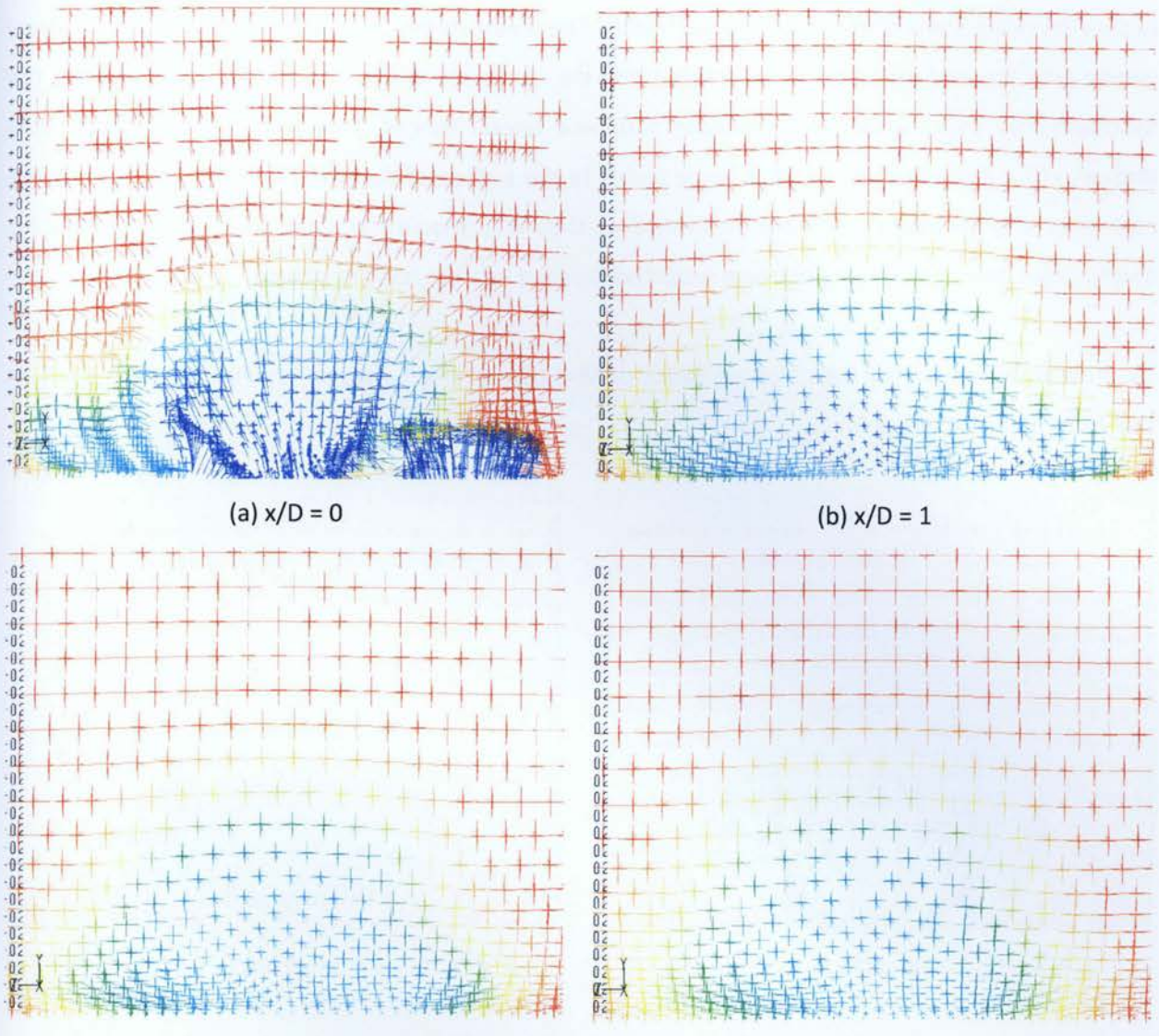

(a) x/D = 0

(b) x/D = 1

(c) x/D = 2

(d) x/D = 3

Figure 69: Flow Structure – Left/Right Sister Holes (M=0.5)

Already discussed to its extent, the lowest blowing ratio of M=0.2 does not illustrate any characteristics of concern. The flow is too slow to separate, and the vortex pairs do not develop to any notable degree. The coolant is concentrated along the centreline and, on the whole, lateral spread is minor, even for the sister hole cases.

As the blowing ratio was increased to M=0.5, a more defined vortex pair became apparent. Although the flow was not fully developed, the swirling flow became apparent for both single and sister hole regimes. The most notable cases of interest are the upstream-only and downstream-only sister hole geometries

as they illustrate some of the most unique trends. The downstream case demonstrates a strong lateral spread with forward-facing velocity vectors along the centreline of the injection hole. In contrast, the upstream-only case, while demonstrating sufficient lateral spread, illustrates highly swirling flow through x/D = 3 where the coolant is being pulled to the surface of the plate. However, this is only the case since the upstream holes are positioned as they are; should the same swirling be evident for downstream holes, the hot mainstream would be dragged into the coolant stream.

The flow structure for the high blowing ratios of M=1.0 and M=1.5 are given in Figures 70 through 74 and 75 through 79, respectively.

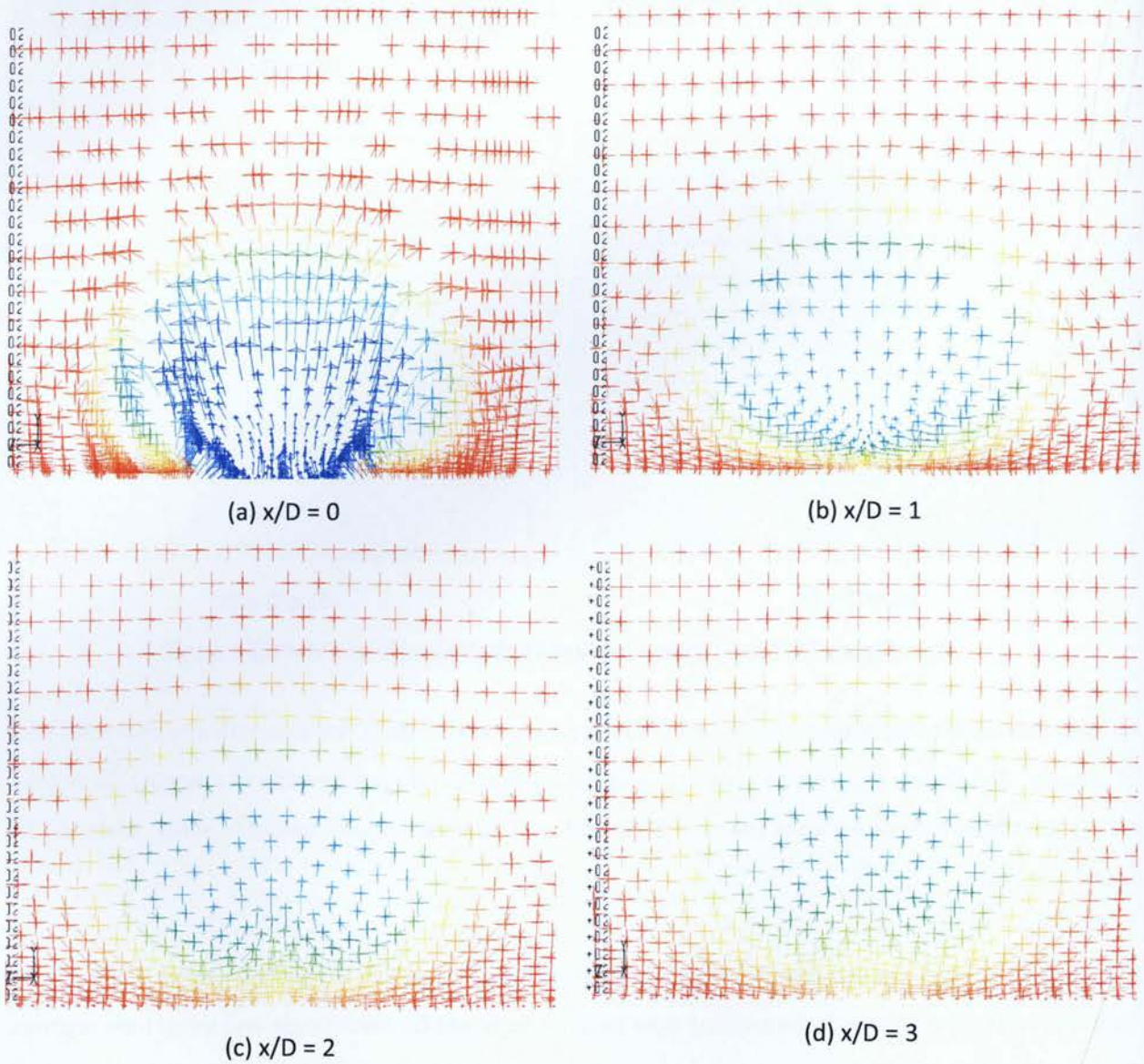

(a) x/D = 0

(b) x/D = 1

(c) x/D = 2

(d) x/D = 3

Figure 70: Flow Structure – Single Hole (M=1.0)

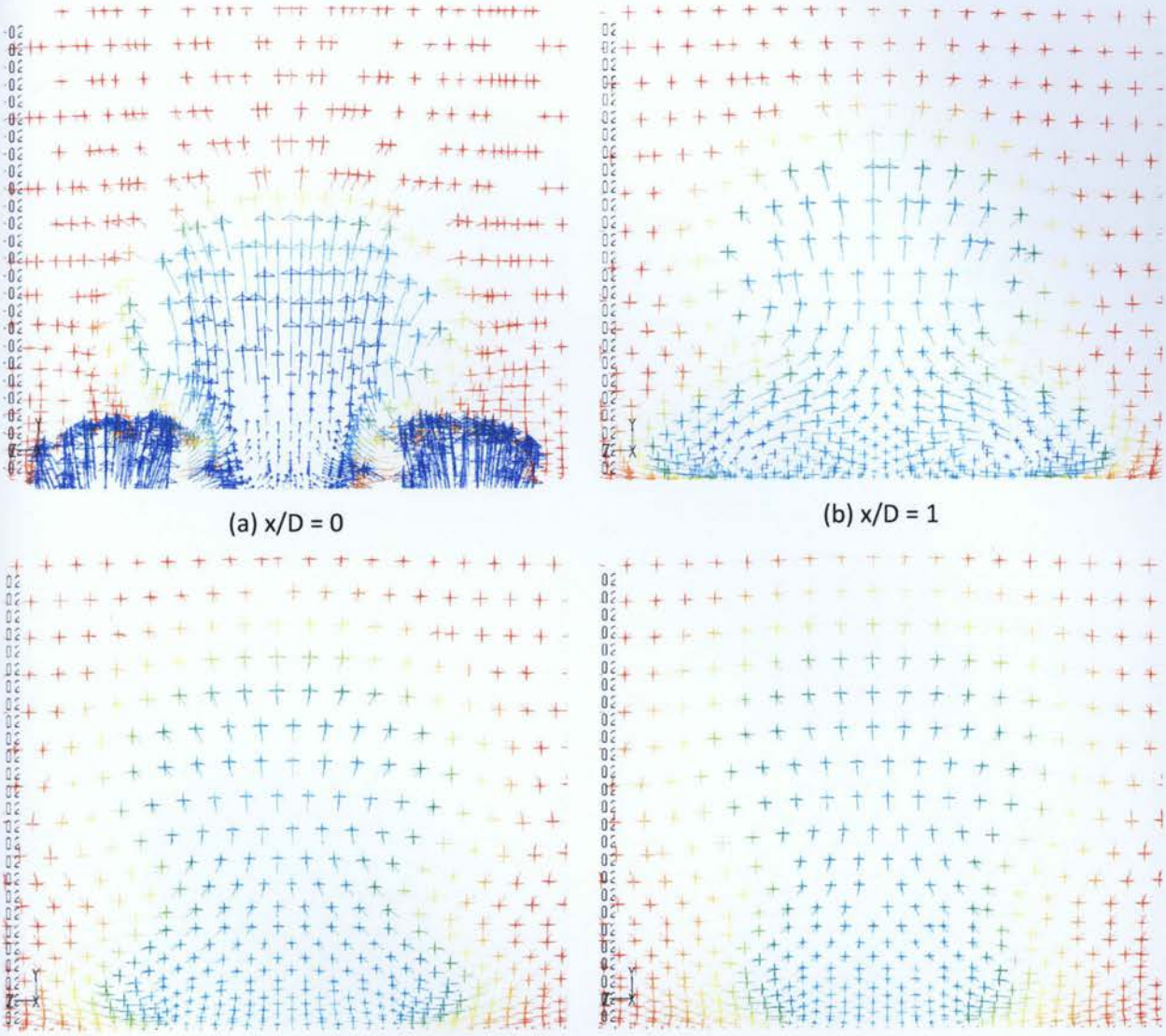

(a) x/D = 0

(b) x/D = 1

(c) x/D = 2

(d) x/D = 3

Figure 71: Flow Structure – Downstream Sister Holes (M=1.0)

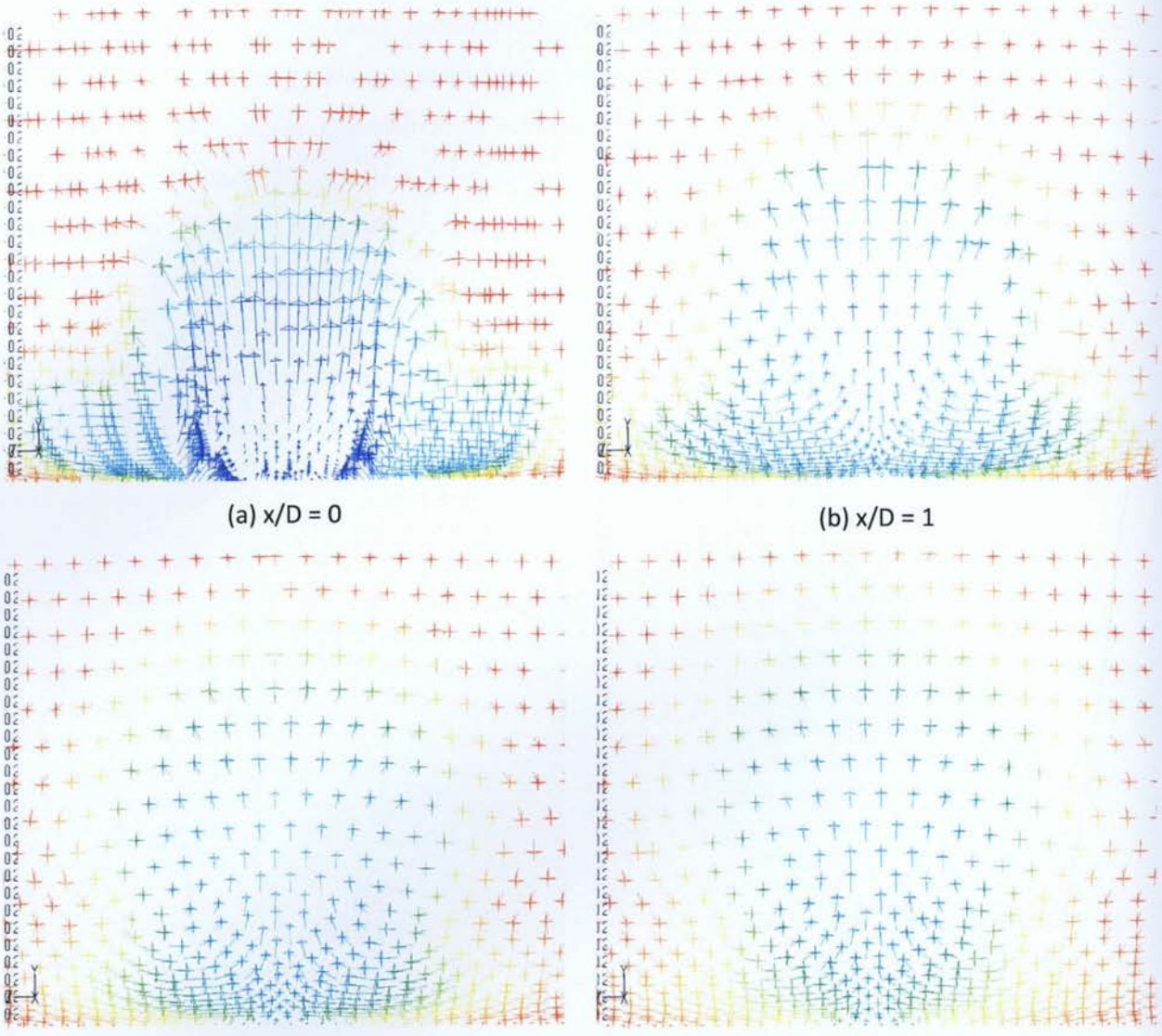

(a) x/D = 0

(b) x/D = 1

(c) x/D = 2

(d) x/D = 3

Figure 72: Flow Structure – Upstream Sister Holes (M=1.0)

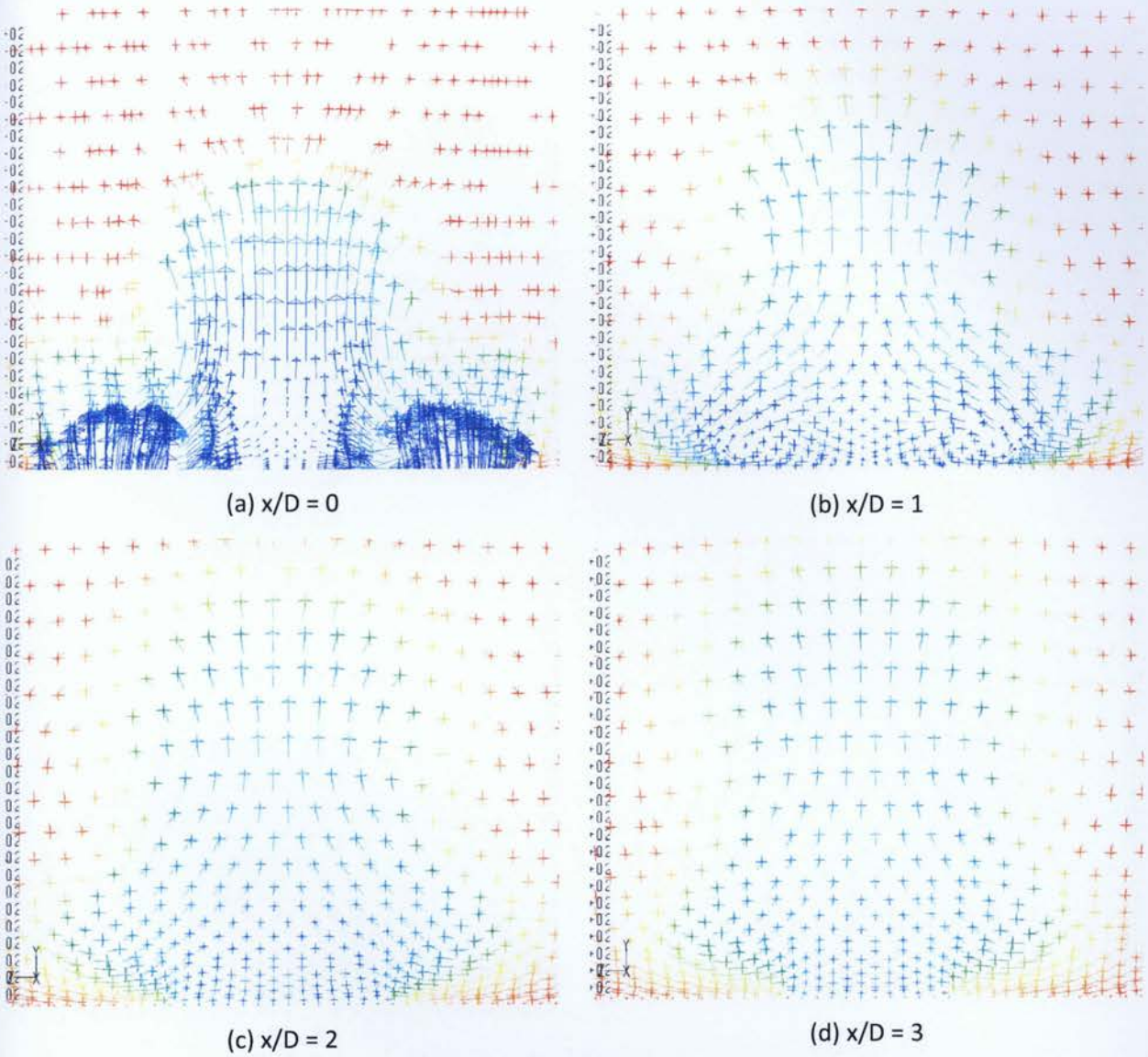

(a) x/D = 0

(b) x/D = 1

(c) x/D = 2

(d) x/D = 3

Figure 73: Flow Structure – Upstream/Downstream Sister Holes (M=1.0)

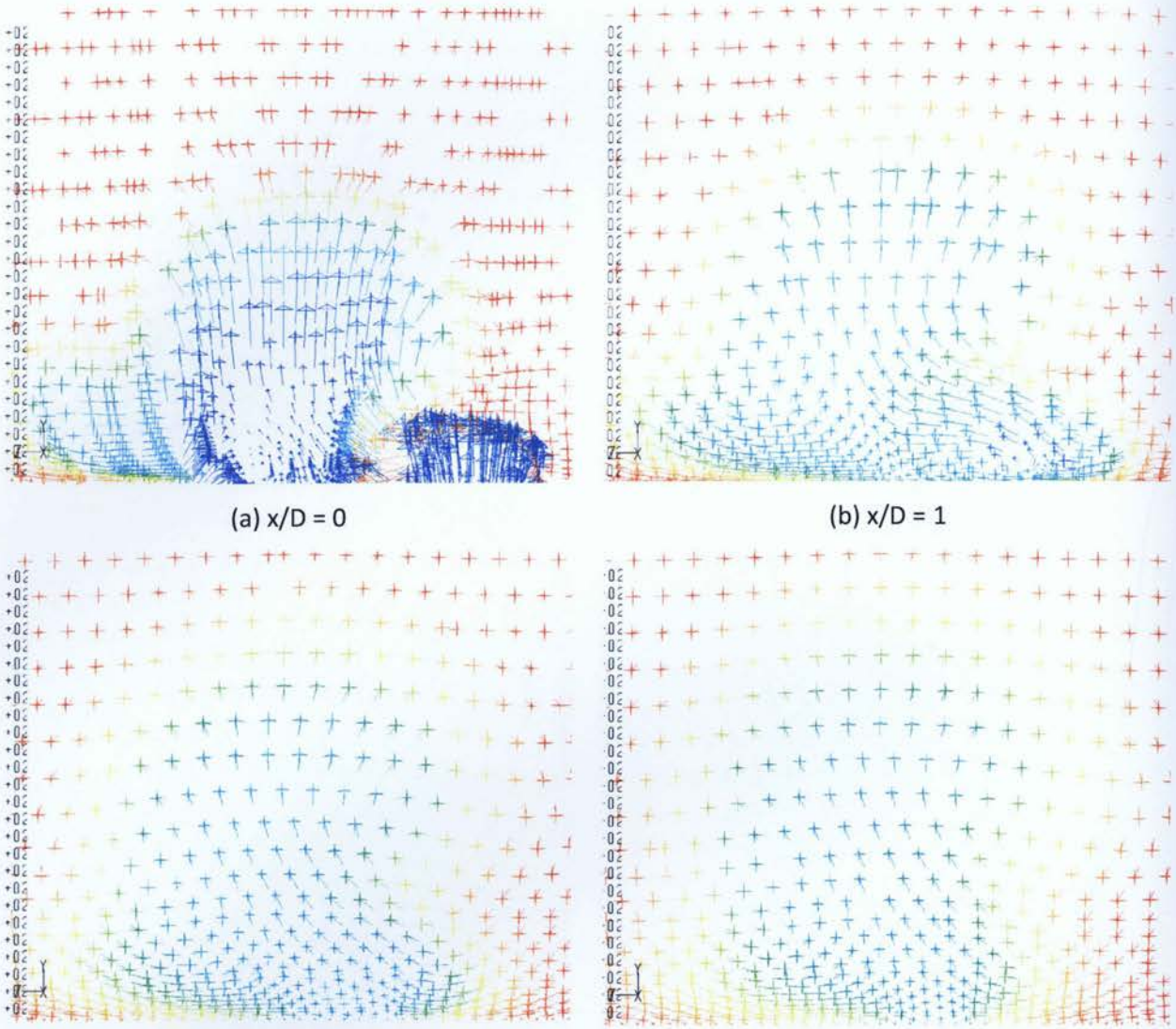

(a) x/D = 0

(b) x/D = 1

(c) x/D = 2

(d) x/D = 3

Figure 74: Flow Structure – Left/Right Sister Holes (M=1.0)

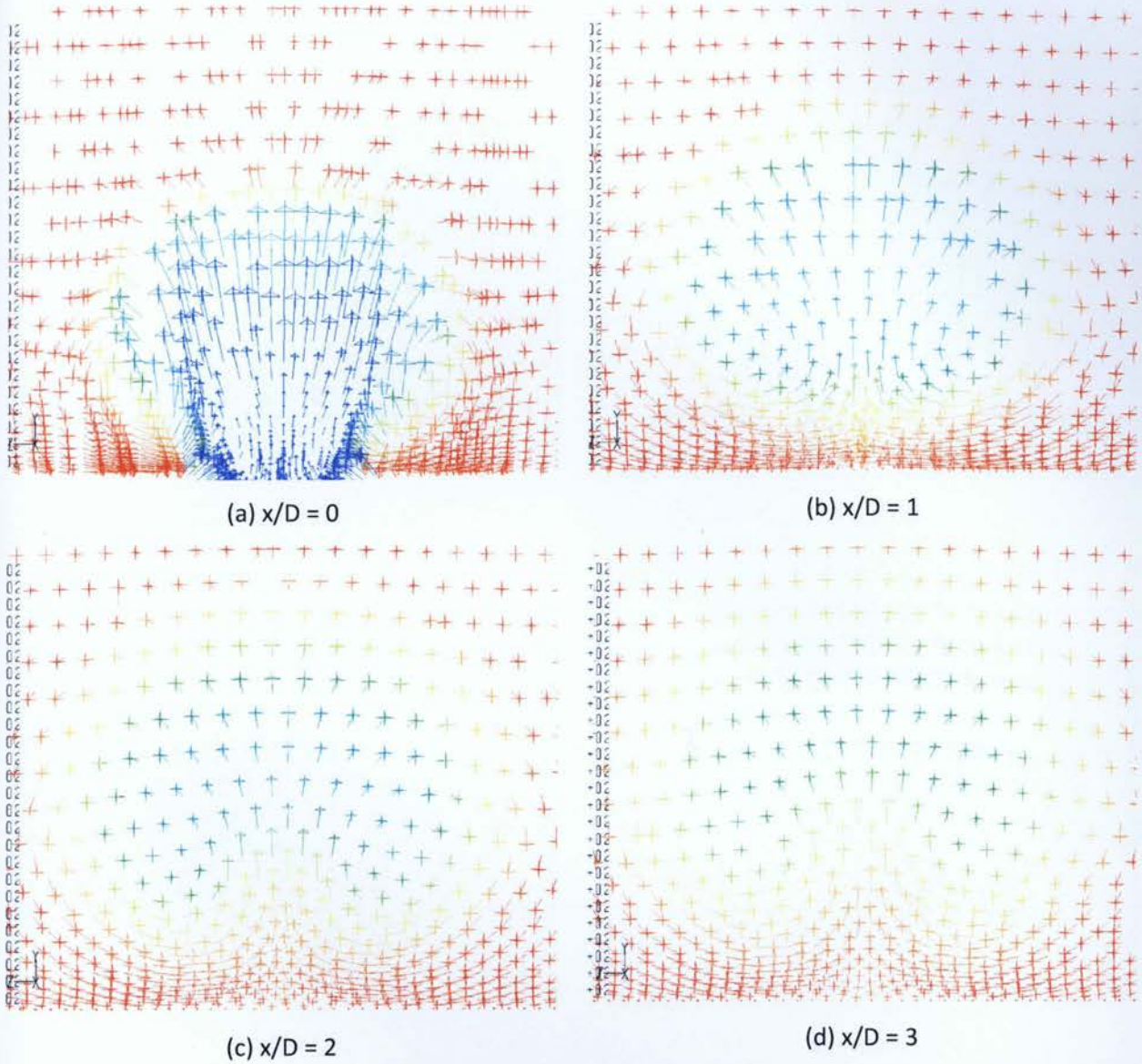

(a) x/D = 0

(b) x/D = 1

(c) x/D = 2

(d) x/D = 3

Figure 75: Flow Structure – Single Hole (M=1.5)

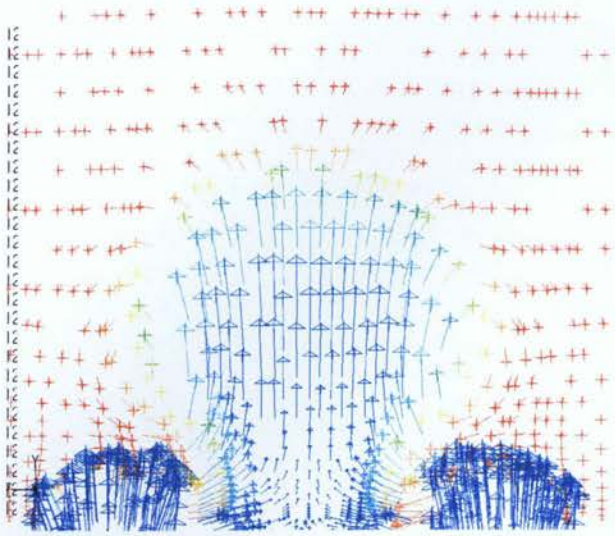

(a) x/D = 0

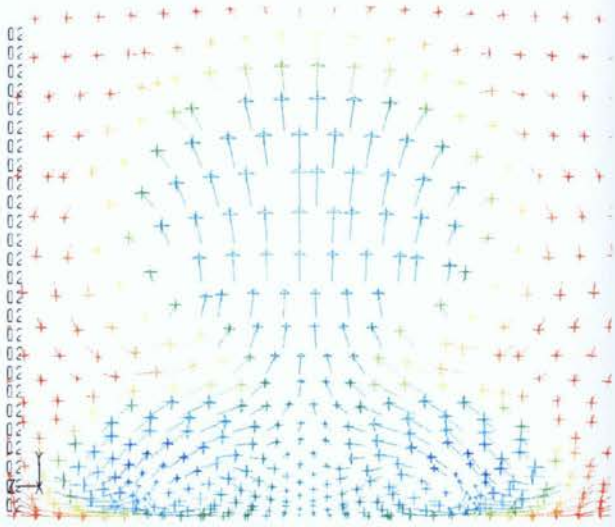

(b) x/D = 1

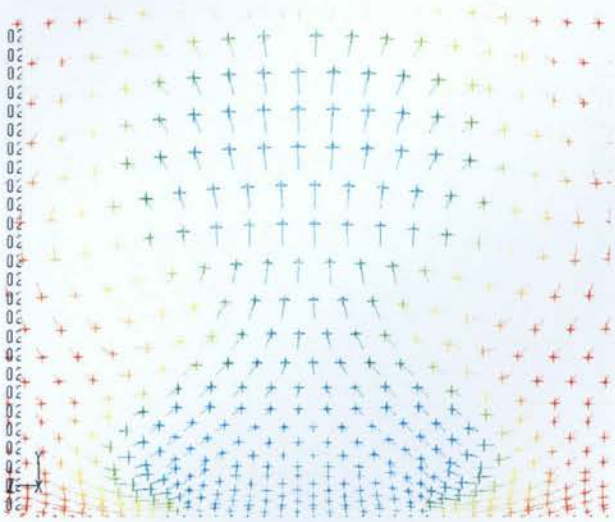

(c) x/D = 2

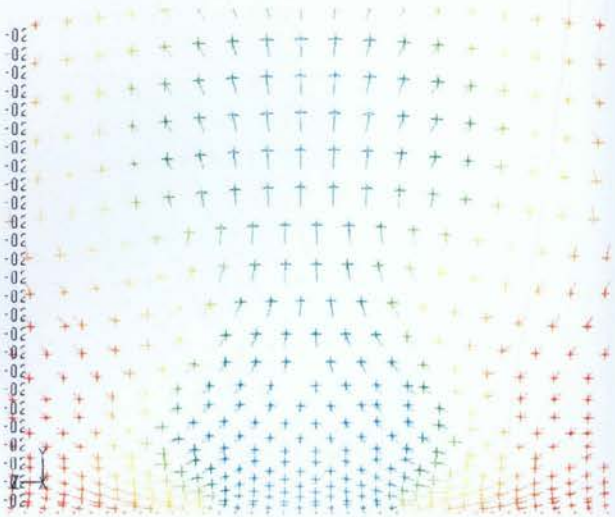

(c) x/D = 3

Figure 76: Flow Structure – Downstream Sister Holes (M=1.5)

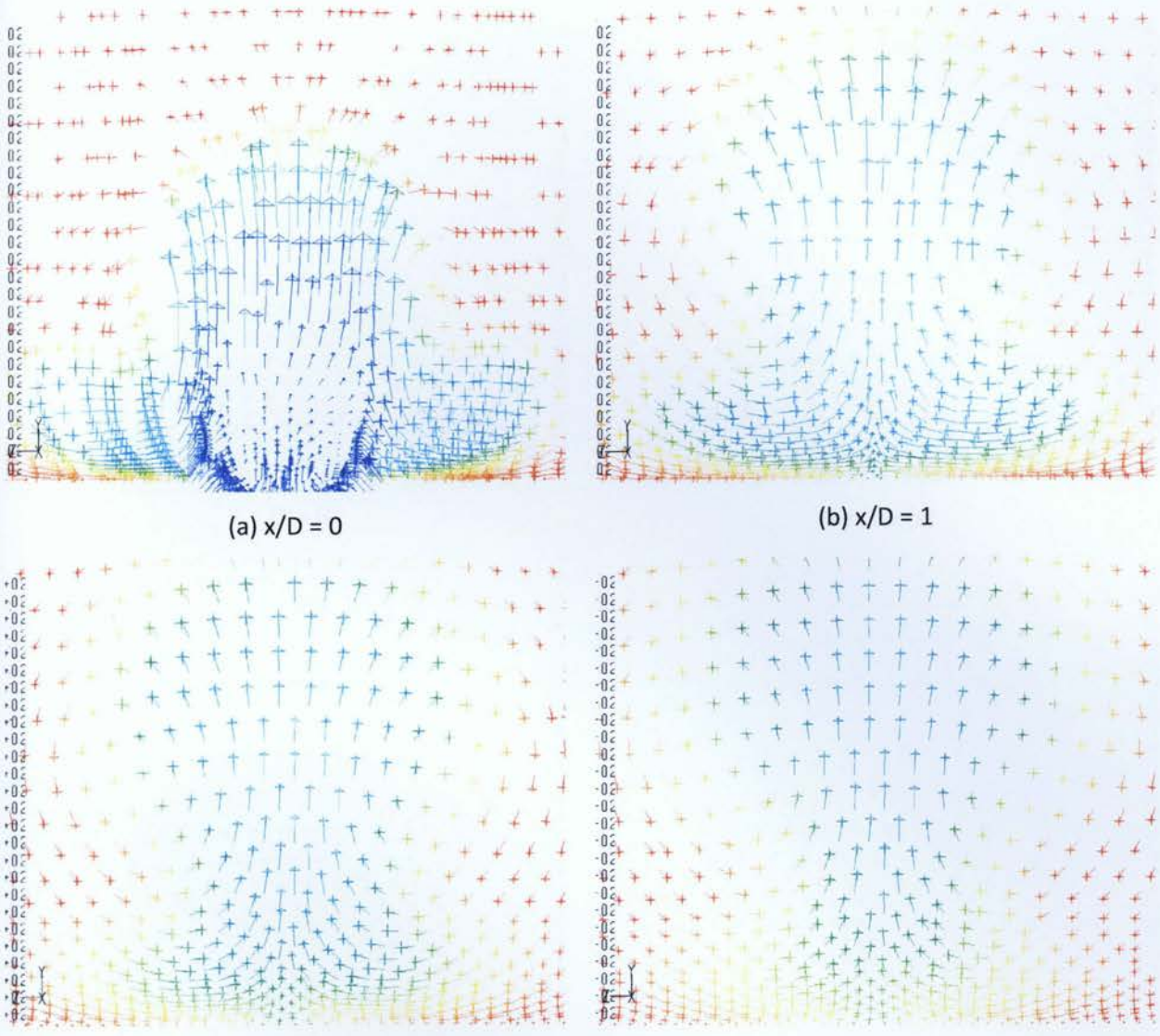

(a) x/D = 0

(b) x/D = 1

(c) x/D = 2

(d) x/D = 3

Figure 77: Flow Structure – Upstream Sister Holes (M=1.5)

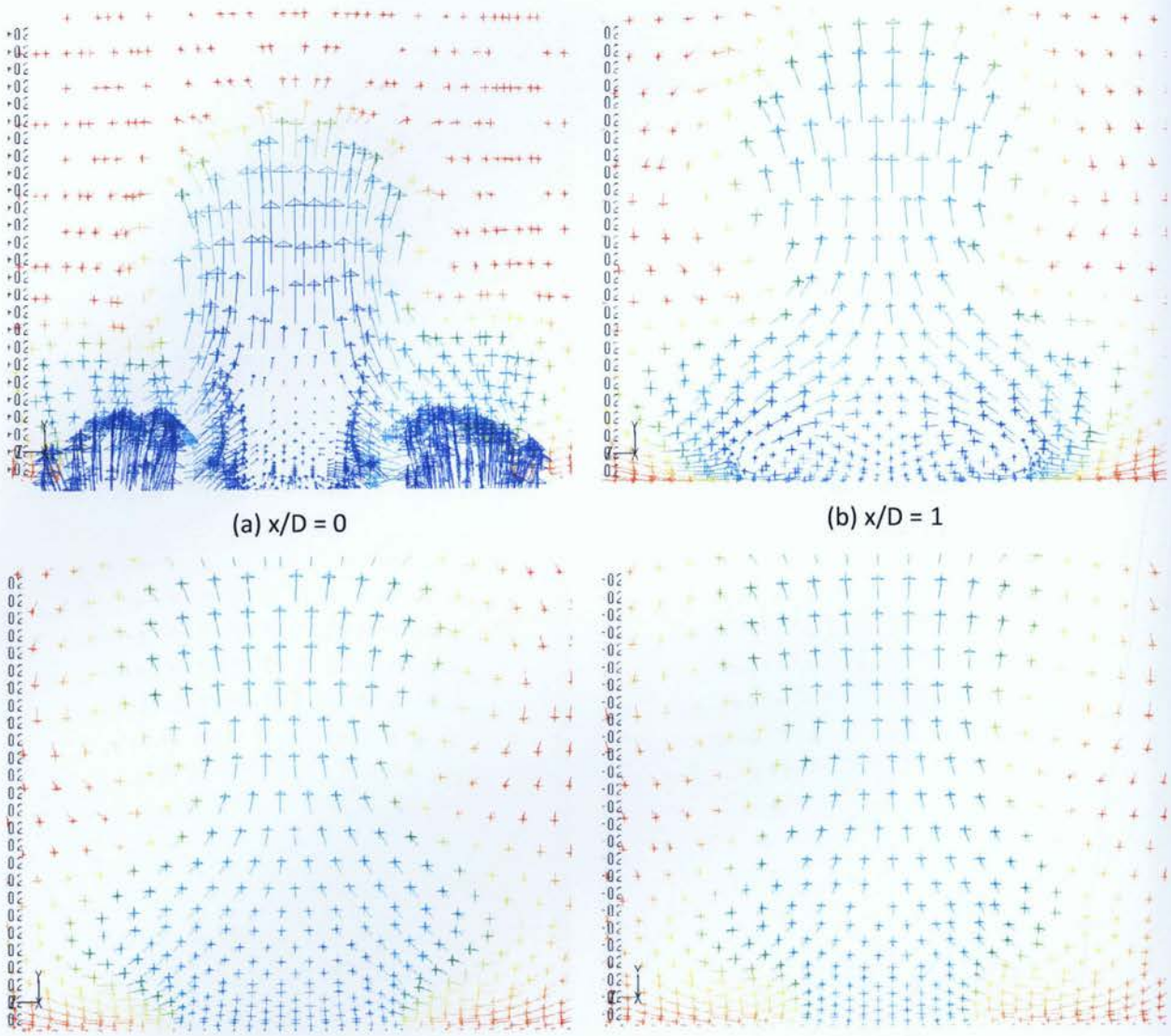

(a) x/D = 0

(b) x/D = 1

(c) x/D = 2

(d) x/D = 3

Figure 78: Flow Structure – Upstream/Downstream Sister Holes (M=1.5)

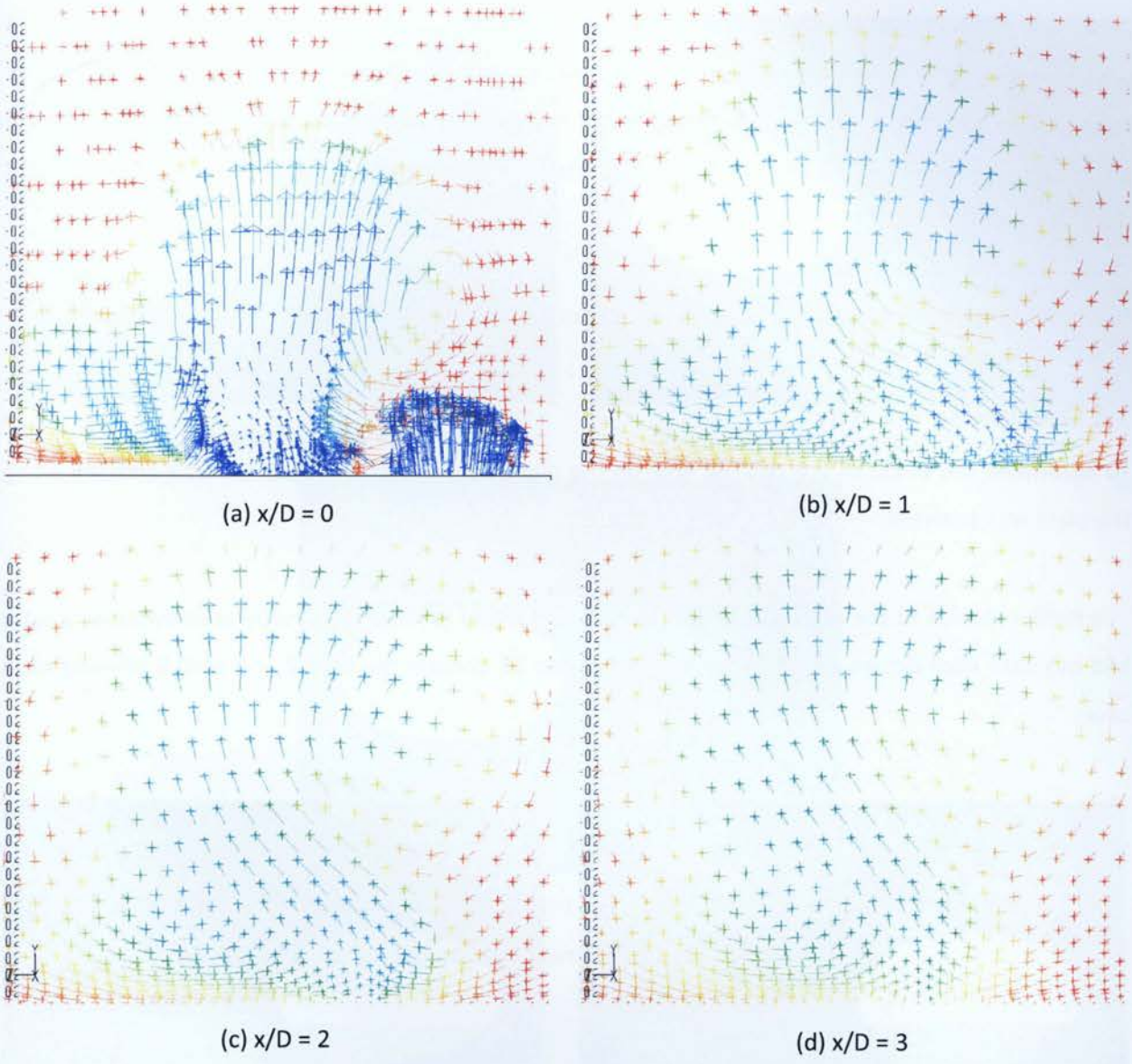

(a) x/D = 0

(b) x/D = 1

(c) x/D = 2

(d) x/D = 3

Figure 79: Flow Structure – Left/Right Sister Holes (M=1.5)

Here, the first point to note is the significant separation of the single hole case. There is virtually no coolant coverage downstream of the hole, causing detrimental effects to this film cooling regime. Similarly, the left-right case shows very little flow adhesion at these high blowing ratios, and, as with the long-hole case, shows a highly erratic flowfield with a significant degree of jet penetration into the mainstream.

At these higher blowing ratios, the downstream-only case is shown to be the optimal design candidate as it offers the best combination of coolant use and aerodynamic performance. All design candidates

penetrate deep into the mainstream at such high blowing ratios, but the downstream-only and upstream-downstream cases are the only geometries to maintain flow adhesion as far downstream as x/D = 3. The upstream holes begin to draw the hot mainstream under the coolant stream as a result of the rotation of the reformed CRVPs while the downstream holes continue to push the coolant towards the surface of the plate.

To complete the analysis, a brief discussion on streamwise vorticity will ensue.

7.5 Streamwise Vorticity

To determine the effect of the swirling flow on the plate, an analysis of the streamwise vorticity along the plate was analyzed.

In a similar fashion to the results of the jet liftoff study, these results will be separated by blowing ratio and evaluate each design side-by-side. Figures 80 and 81 contain the M=0.2 and M=0.5 blowing ratio cases.

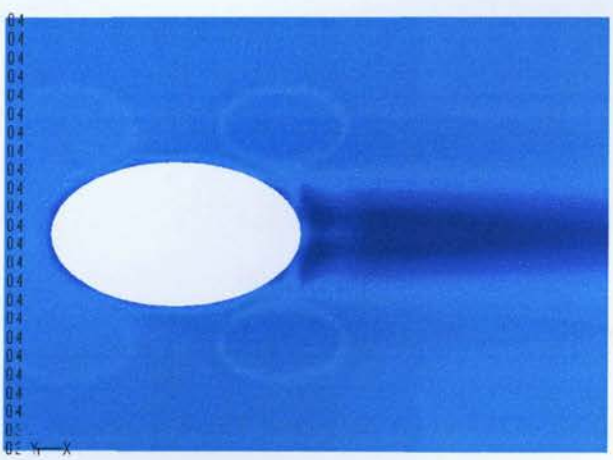

(a) Single Hole

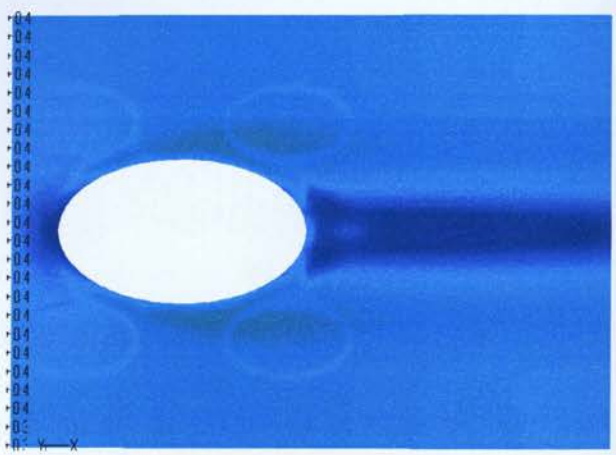

(b) Downstream Sister Holes

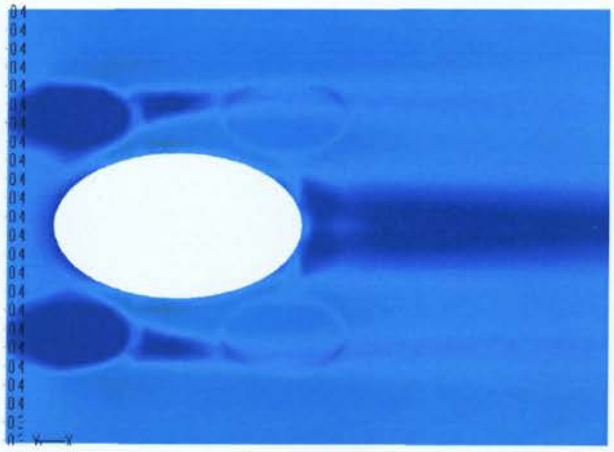

(c) Upstream Sister Holes

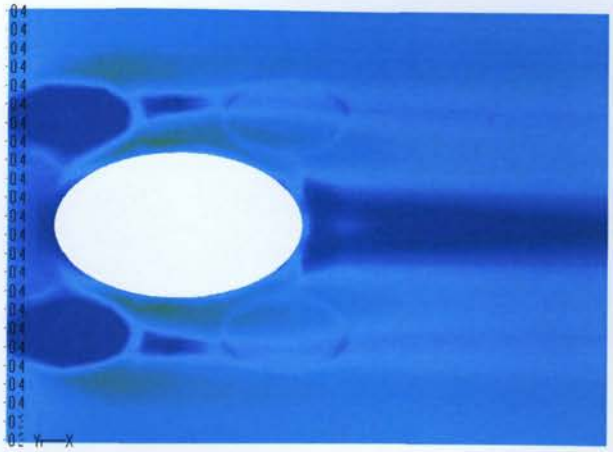

(d) Upstream/Downstream Sister Holes

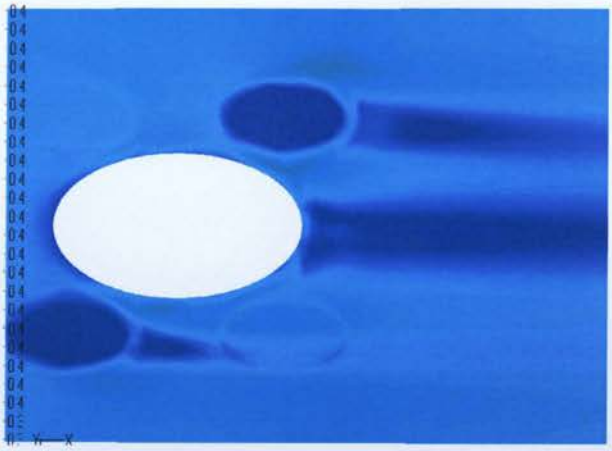

(e) Left/Right Sister Holes

Figure 80: Streamwise Vorticity – Short Hole (M=0.2)

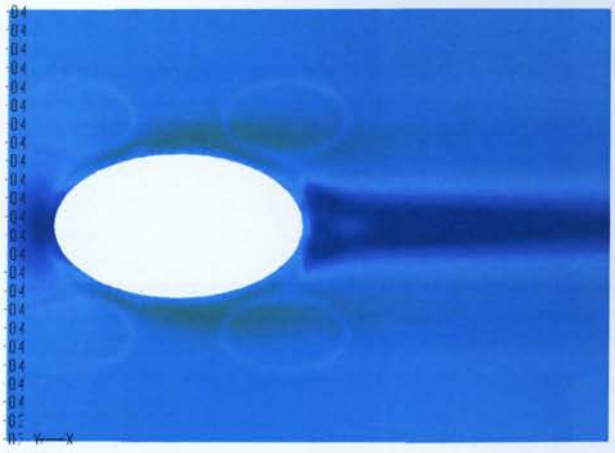

(a) Single Hole

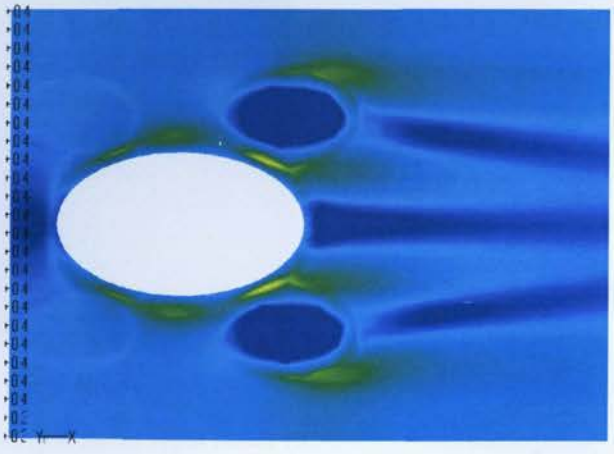

(b) Downstream Sister Holes

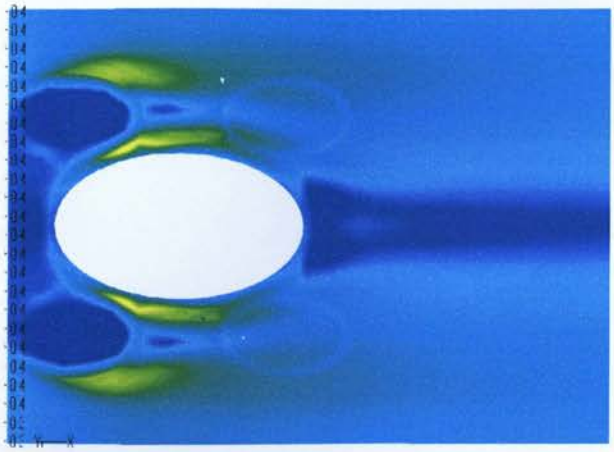

(c) Upstream Sister Holes

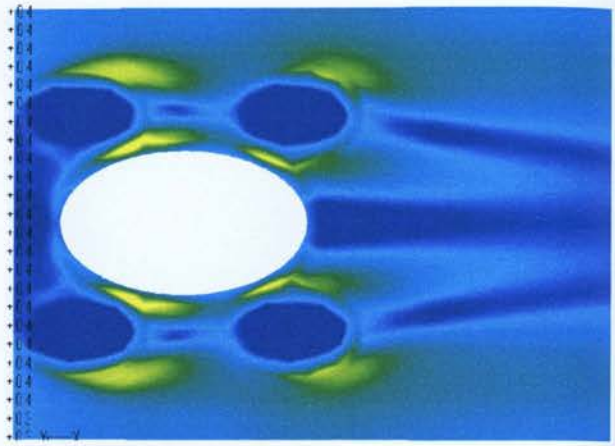

(d) Upstream/Downstream Sister Holes

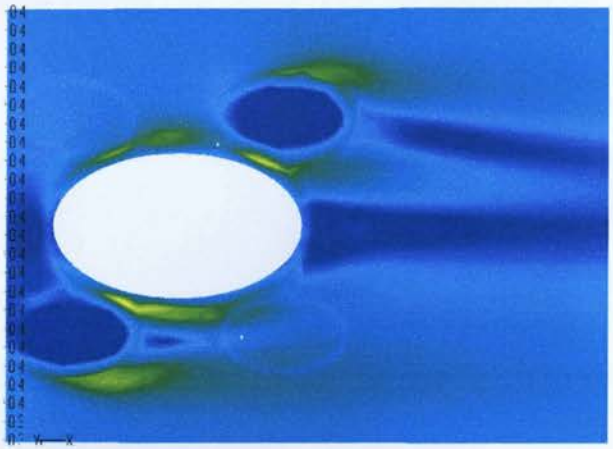

(e) Left/Right Sister Holes

Figure 81: Streamwise Vorticity – Short Hole (M=0.5)

The M=0.5 blowing ratio illustrates the first useful trends; however, it still leaves much to be desired. The magnitude of vorticity emanating from each hole is relatively similar between geometries and there is little interaction between holes. Note that in contrast to the long hole study, geometries with downstream holes offer the most uniform flowfield.

Figures 82 and 83 contain the streamwise vorticity analysis for the M=1.0 and M=1.5 blowing ratios.

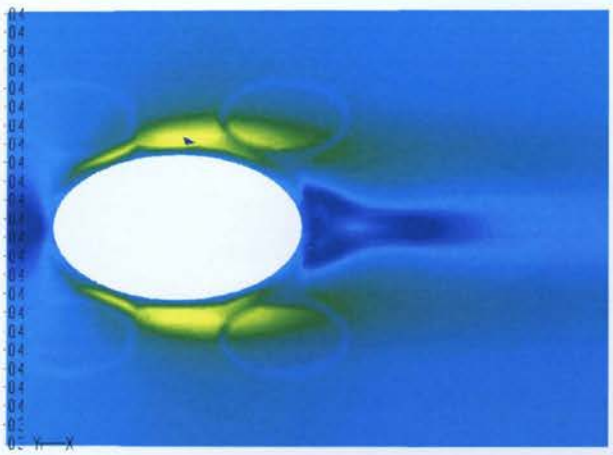

(a) Single Hole

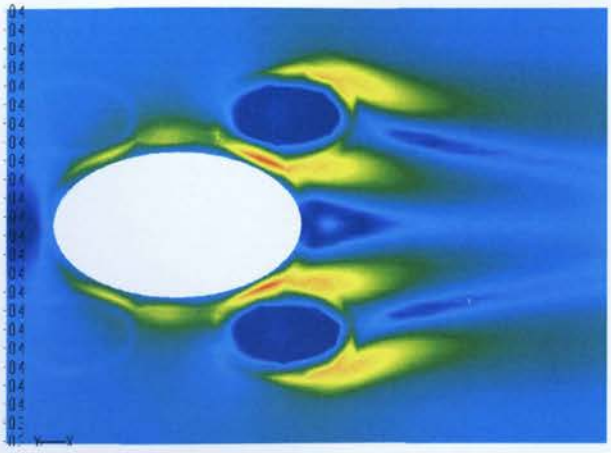

(b) Downstream Sister Holes

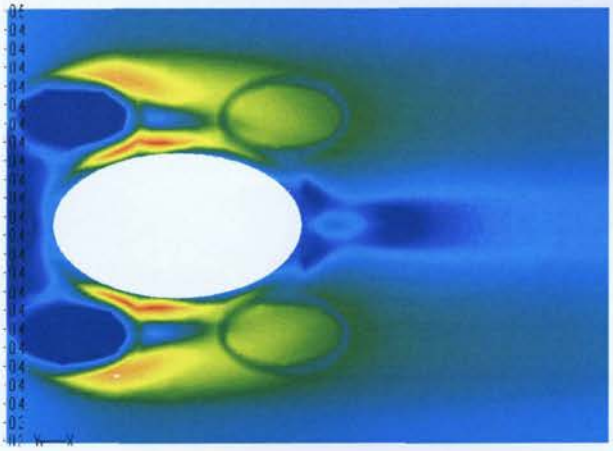

(c) Upstream Sister Holes

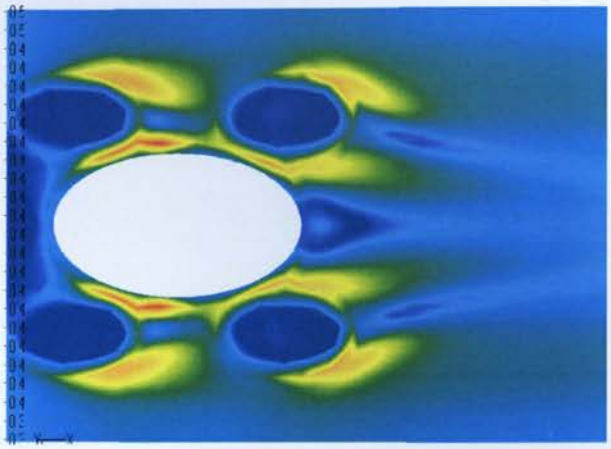

(d) Upstream/Downstream Sister Holes

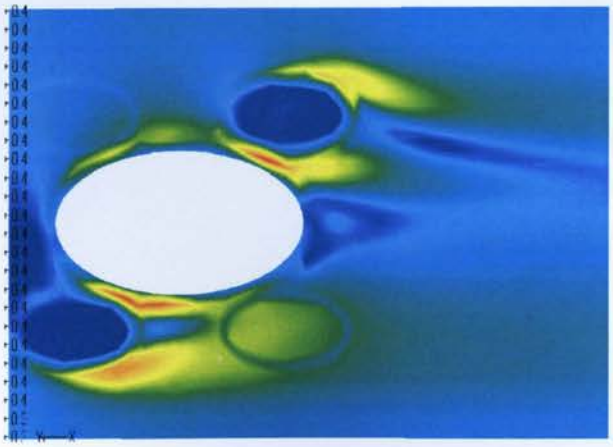

(e) Left/Right Sister Holes

Figure 82: Streamwise Vorticity – Short Hole (M=1.0)

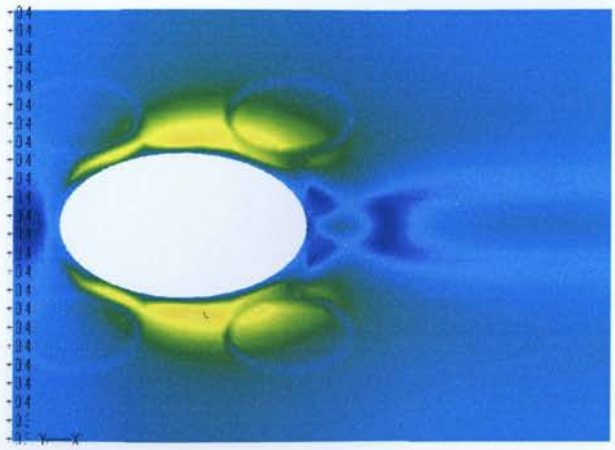

(a) Single Hole

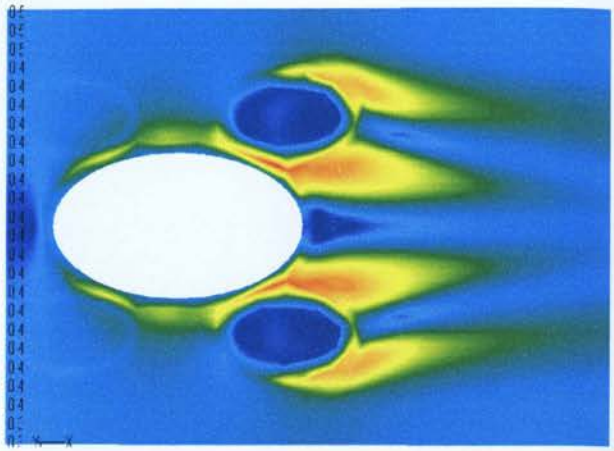

(b) Downstream Sister Holes

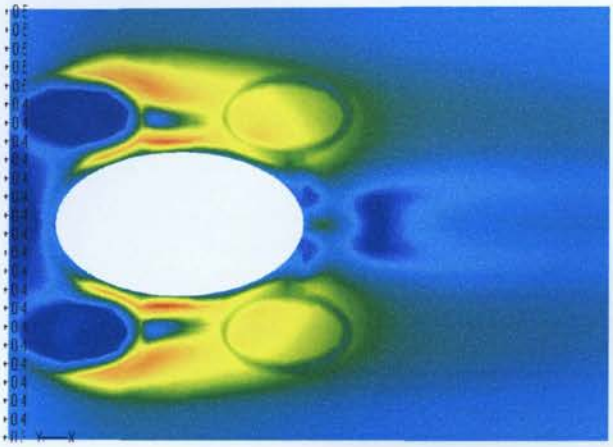

(c) Upstream Sister Holes

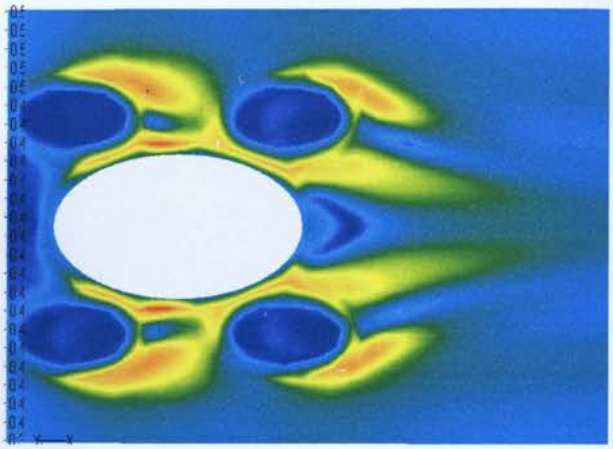

(d) Upstream/Downstream Sister Holes

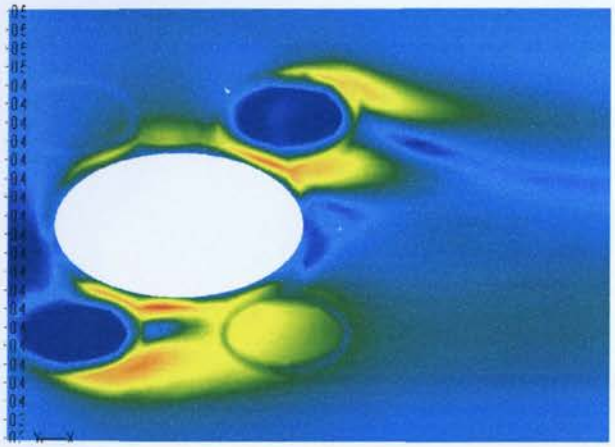

(e) Left/Right Sister Holes

Figure 83: Streamwise Vorticity – Short Hole (M=1.5)

These higher blowing ratios shed further light onto the discussion of design applicability. It is interesting to note the vortex interaction of the upstream holes with the CRVP of the primary injection hole.

It is evident that there is negligible vorticity downstream of the primary injection hole in studies with only upstream holes, as a result of the upstream holes almost entirely nullifying vorticity along the plate. Meanwhile, the cases with downstream holes continue to provide uniform flowfield with pockets of zero vorticity. It is important to note that the rationale behind the improved performance of the downstream holes is largely based upon the flow's attachment to the plate, and although this drives the magnitude of vorticity up, this technique provides a better cooling solution.

7.6 Long Hole vs. Short Hole Results

Although the primary focus of the research held within focused on analyzing the most optimal sister hole position for each independent L/D ratio, there is relevance in discussing the variations in results as a function of L/D ratio.

As has been discussed in detail, the flowfield emanating from long and short holes differ significantly from one another. This is clearly noted in the analysis of Sections 6 and 7, particularly in an evaluation of the primary vortex structures and adiabatic effectiveness. While both studies indicate that in the near-hole region, downstream holes improve performance while further downstream, the use of upstream holes improves performance, the physics behind the rationales differ. Long hole studies provide flow that is well developed, causing the CRVPs to interact most thoroughly. The less defined flow structure in the short hole cases permits the coolant streams to interact to a certain extent but also rely on the interaction of each individual hole with the mainstream to produce the results observed.

At low blowing ratios, due to the short hole flow not having sufficient development length to form, one notes that the long hole counter rotating vortex pairs are considerably more defined than that of the short hole research. As such, the sister holes amply interact with the CRVP from the primary hole in the long hole study, but can offer little performance gains for the short hole case as a result of there being no well defined vortex to counter. The downstream holes offer improved performance largely due to their immediate impact under the separated flow of the primary jet.

At higher blowing ratios, the CRVP becomes more defined, but one must note the degree of separation and entrainment into the mainstream flow of the short holes. In contrast, the long holes still maintain more cohesion leading to similar flow characteristics as the low blowing ratio cases.

These results are further validated in evaluating the streamwise vorticity of each case. It is of particular interest to notice the cohesion of the contours of the long hole study whereby the short hole flow is significantly less refined, resulting in a more erratic solution. The long hole case has the added benefit of a large plenum to settle the flow, before entering the long holes in which it can fully develop its structure, prior to interacting with the mainstream flow. In contrast, the short holes are limited by their narrow plenum which forces the flow to make a sharp turn to enter the mainstream flow in which there is barely enough room for the flow to recover from the turn, let alone develop its primary structures.

7.7 Conclusion

The results from the short-hole analysis produce similar trends to those noted in the long-hole analysis. Notably, downstream sister holes provide better near-hole coverage than upstream holes while the opposite is true further downstream. The justification is of a similar nature to that of the long-hole study, in that the upstream holes separate and reattach downstream, improving performance in this region.

Of particular interest, here, are the plateaus evident in the effectiveness study. These are a direct result of the CRVP interaction and lead to a more uniformly cooled blade, as a result of the underdeveloped flow emanating from these short holes. However, due to the erratic nature of the flowfield, it is difficult to discern the effect of aerodynamic mixing, evident as significant recirculation regions are noted within the hole, detracting from the efficiency of the cooling technique.

8 Conclusions and Recommendations for Future Work

The analysis of the current study evaluated the use and applicability of sister holes to improve film cooling through active flow control. An evaluation of simple half-plane models allowed for the determination of an optimal injection angle and to determine the basic applicability of this technique. This was followed by a detailed analysis of long and short hole film cooling with the use of sister holes to determine its applicability in more realistic cooling regimes.

The results obtained from this analysis were highly desirable, indicating that, as one would expect, the use of shallow angle injection holes offered more favourable film cooling effectiveness than large angle injection holes, but both were vastly improved with the use of downstream sister holes. Further analysis determined the optimal configuration of the holes.

The studies on long and short sister hole film cooling provided a plethora of useful and interesting results, further validating the use of such cooling configurations. Four unique geometries were studied: two downstream holes, two upstream holes, two upstream and two downstream holes, and one upstream and one downstream hole. Both led to the same general conclusion that placing holes downstream of the primary injection hole offer improved effectiveness in the near field while the upstream holes improve performance further downstream. An evaluation of the flow structure indicates that the primary CRVP is countered by the secondary vortex structures of the sister holes leading to better overall effectiveness. Of note is the penetration of each technique into the freestream, as the case with upstream holes penetrates more significantly, reducing aerodynamic effectiveness.

The case with one hole upstream and one hole downstream was found to produce a highly erratic flowfield with both long and short holes and was deemed undesirable, while the case with both upstream and downstream coolant holes did not offer performance gains to warrant the necessary increase in coolant mass flux.

Further, the long and short hole studies differ primarily between the flow structure emanating from their holes. The short hole flow is significantly underdeveloped, and the turning incurred by the low E/D ratio of 1 incurs significant swirling to the flow. As a result, the flow emanating from the coolant hole was of a highly swirling nature resulting in a significantly less cohesive flow structure.

On the whole, the sister hole cooling technique was found to be effective. The selection of upstream or downstream coolant holes depends largely on the structure of the remaining jets on the blade. Should multiple rows of holes be used, it is likely that downstream holes are the most optimal candidate as they protect the field well, up until x/D = 10, while should only a single row be operable, upstream holes protect the plate more uniformly.

Future research into this technique should evaluate this prospect experimentally. Although the concept was proven thoroughly by comparing sister hole results against single hole results computationally, previous studies have indicated that the use of the realizable k-ε turbulence model does not entirely predict the structure of the flow, ultimately affecting the solution. Further, variations in hole orientation and short hole plenum geometry can have dramatic effects on the film cooling flow physics and would provide interesting research candidates.

Appendix A - MATLAB Algorithms

The following section contains the algorithms used to convert raw thermal data into the adiabatic effectiveness results analyzed in the present study. Section A.1 contains the algorithm used to evaluate the performance of each grid while Section A.2 focuses on the film cooling effectiveness of each of the geometries evaluated.

A.1 Sensitivity Analysis

```
function [lat_err, cl_err] = full_geom_sensitivity()

% Define Static Variables
D = .0127;

% Go to Data Directory
cd ('C:\Users\Marc\Documents\Graduate Studies\Research\Results');

% Loop for long and short hole studies
for angle = 1:2
   x_cl_exp = [];
   y_cl_exp = [];
   x_lat_exp = [];
   y_lat_exp = [];

   switch angle
      case 1
         cd ('..\Hale');
      case 2
         cd ('..\..\Long_Hole\Sinha');
      otherwise
         disp('Error!!!');
   end

   % Set input parameters
   if angle == 1
      T_cold_comp = 317.8;
      T_hot_comp = 298.0;
      exp_cl_data = fopen('Hale-CL.txt');
      exp_lat_data = fopen('Hale-LAT.txt');
   else
      T_cold_comp = 249.8;
      T_hot_comp = 300.2;
      exp_cl_data = fopen('Sinha-CL.txt');
      exp_lat_data = fopen('Sinha-LAT.txt');
   end

   % Read experimental centreline data
```

```
exp_cl = fscanf(exp_cl_data, '%f');
fclose(exp_cl_data);
x_cl_exp(1,:) = exp_cl(1:2:end);
y_cl_exp(1,:) = exp_cl(2:2:end);

% Read experimental lateral data
exp_lat = fscanf(exp_lat_data, '%f');
fclose(exp_lat_data);
x_lat_exp(1,:) = exp_lat(1:2:end);
y_lat_exp(1,:) = exp_lat(2:2:end);

% Loop through four grids used in sensitivity analysis
for grid=1:4
   non_garbage_lat =[];
   non_garbage_cl = [];
   garbage_cl = [];
   garbage_lat = [];
   cl_input = [];
   a = 1;
   b = 1;
   cl = 0;
   lat = 0;
   dummy_cl = 0;
   dummy_lat = 0;

   % Set input file names for sensitivity analysis
   if angle == 1
      cl_id = ['CL-SH', int2str(grid), '-Hale.txt'];
   else
      cl_id = ['CL-LH', int2str(grid-2), '-Sinha.txt'];
   end

   % Read centreline input data
   start = 12*(angle-1) + grid + 2*(grid-1);
   cl_data = fopen(cl_id);
   garbage_cl = textscan(cl_data, '%s %s %s %s', 3);
   non_garbage_cl = textscan(cl_data, '%f %f');
   fclose(cl_data);
   cl_input(:,1) = ((non_garbage_cl{1,1})/D);
   cl_input(:,2) = non_garbage_cl{1,2};

   % Organize and process centreline data
   for ct = 1:length(cl_input)
      if cl_input(ct) >= 0 && dummy_cl == 0
         dummy_cl = 1;
         cl_start(grid, angle) = ct;
         break;
      end
   end
   cl_end(grid, angle) = length(cl_input);
   cl_dat(1:length(cl_input), start) = cl_input(:,1)-5.5;
```

```
    cl_dat(1:length(cl_input), start+1) = cl_input(:,2);
    cl_dat(1:length(cl_input), start+2) = (T_hot_comp - cl_dat(1:length(cl_input), start+1))/(T_hot_comp –
T_cold_comp);
    lat_loc = [1,2,3,4,4.5, 5,5.5,6,6.5,7,8,9,10,12,14,16,18,20,22.5,25,30];
    count = 0;

    % Read, organize, and process laterally averaged data
    while (count < length(lat_loc))
      lat_dat = [];
      count = count +1;
      if angle == 1
        lat_id = ['SH', int2str(grid), '-Hale-D', num2str(lat_loc(count)), '.txt'];
      else
        lat_id = ['LH', int2str(grid-2), '-Sinha-D', num2str(lat_loc(count)), '.txt'];
      end
      lat_data = fopen(lat_id);
      garbage_lat = textscan(lat_data, '%s %s %s %s', 3);
      non_garbage_lat = textscan(cl_data, '%f %f');
      fclose(lat_data);

      lat_dat(:,1) = ((non_garbage_lat{1,1})/D);
      lat_dat(:,2) = non_garbage_lat{1,2};
      lat_dat(:, 3) = (T_hot_comp - lat_dat(:, 2))/(T_hot_comp-T_cold_comp);
      lat_avg(count, start) = lat_loc(count)-5.5;
      lat_avg(count, start + 1) = trapz(lat_dat(:,1), lat_dat(:,3))/(3);
    end
    lat_start(grid, angle) = 6;
    lat_end(grid, angle) = 21;

    % Determine deviation between numerical and experimental centreline
    % adiabatic effectiveness
    for (y = 1:cl_end(grid, angle))
      for (cycle = 1:(length(x_cl_exp)-1))
        if cl_dat(y,start) == x_cl_exp(cycle)
          cl = cl + abs(cl_dat(y, start +2) - y_cl_exp(cycle))/y_cl_exp(cycle);
          a = a+1;
        else
          if cl_dat(y, start) > x_cl_exp(cycle) && cl_dat(y, start) < x_cl_exp(cycle+1)
            interp = y_cl_exp(cycle+1) - (y_cl_exp(cycle+1)-y_cl_exp(cycle))*(x_cl_exp(cycle+1)-
cl_dat(y,start))/(x_cl_exp(cycle+1)-x_cl_exp(cycle));
            cl = cl + abs(interp-cl_dat(y,start+2))/y_cl_exp(cycle);
            a = a+1;
          end
        end
      end
    end
    cl_err(grid, angle) = cl/a;

    % Determine deviation between numerical and experimental centreline
    % adiabatic effectiveness
    for (y = 1:lat_end(grid, angle))
```

```
        for (cycle = 1:(length(x_lat_exp)-1))
          if lat_avg(y,start) == x_lat_exp(cycle)
            lat = lat + abs(lat_avg(y, start +1) - y_lat_exp(cycle))/y_lat_exp(cycle);
            b = b+1;
          else
            if lat_avg(y, start) > x_lat_exp(cycle) && lat_avg(y, start) < x_lat_exp(cycle+1)
              interp = y_lat_exp(cycle+1) - (y_lat_exp(cycle+1)-y_lat_exp(cycle))*(x_lat_exp(cycle+1)-
lat_avg(y,start))/(x_lat_exp(cycle+1)-x_lat_exp(cycle));
              lat = lat + abs(interp - lat_avg(y, start+1))/y_lat_exp(cycle);
              b = b+1;
            end
          end
        end
      end
      lat_err(grid, angle) = lat/b;
    end

    % Plot centreline effectiveness against experimental results
    figure
    plot(x_cl_exp, y_cl_exp, '.-k');
    hold on;
    plot(cl_dat(cl_start(1,angle):cl_end(1,angle), start-9), cl_dat(cl_start(1,angle):cl_end(1,angle), start-7), '-b');
    plot(cl_dat(cl_start(2,angle):cl_end(2,angle), start-6), cl_dat(cl_start(2,angle):cl_end(2,angle), start-4), '-.r');
    plot(cl_dat(cl_start(3,angle):cl_end(3,angle), start-3), cl_dat(cl_start(3,angle):cl_end(3,angle), start-1), '--g');
    plot(cl_dat(cl_start(4,angle):cl_end(4,angle), start), cl_dat(cl_start(4,angle):cl_end(4,angle), start+2), ':k');
    xlabel('x/D', 'FontSize', 12); ylabel('Centre-Line Adiabatic Effectiveness', 'FontSize', 12);
    if angle == 1
      legend('Hale - Experimental', '5.39e5 Nodes', '7.13e5 Nodes', '9.21e5 Nodes' , '1.19e6 Nodes');
      save_cl = 'CL-Hale.png';
    else
      legend('Sinha - Experimental', '8.24e5 Nodes', '1.09e6 Nodes', '1.43e6 Nodes' , '1.86e6 Nodes');
      save_cl = 'CL-Sinha.png';
    end
    axis([0,30, 0, 1]);
    saveas(gcf, save_cl);
    close

    % Plot laterally averaged effectiveness against experimental results
    figure;
    plot(x_lat_exp, y_lat_exp, '.-k');
    hold on;
    plot(lat_avg(lat_start(1,angle):lat_end(1, angle), start-9), lat_avg(lat_start(1,angle):lat_end(1, angle), start-8), '-
b');
    plot(lat_avg(lat_start(2,angle):lat_end(2, angle), start-6), lat_avg(lat_start(2,angle):lat_end(2, angle), start-5), '-
.r');
    plot(lat_avg(lat_start(3,angle):lat_end(3, angle), start-3), lat_avg(lat_start(3,angle):lat_end(3, angle), start-2), '--
g');
    plot(lat_avg(lat_start(4,angle):lat_end(4, angle), start), lat_avg(lat_start(4,angle):lat_end(4, angle), start+1), ':k');
    xlabel('x/D', 'FontSize', 12); ylabel('Laterally Averaged Adiabatic Effectiveness', 'FontSize', 12);
    if angle == 1
      legend('Hale - Experimental', '5.39e5 Nodes', '7.13e5 Nodes', '9.21e5 Nodes' , '1.19e6 Nodes');
      save_lat = 'LAT-Hale.png';
```

```
    else
        legend('Sinha - Experimental', '5.00e5 Nodes', '6.46e5 Nodes', '8.24e5 Nodes' , '1.03e6 Nodes');
        save_lat = 'LAT-Sinha.png';
    end
    axis([0,20, 0, 0.4]);
    saveas(gcf, save_lat);
    close
end

% Return to root directory
cd C:\
cd('.\Users\Marc\Documents\Graduate Studies\Research\MATLAB Code');
```

A.2 Adiabatic Effectiveness

```
function [cl_dat, lat_avg] = angle_adi_eff()

% Define Static Variables
D = .0127;
T_h= 353.18;
T_c = 293.12;
runs = [20, 50, 100, 150];
lat_loc = [1,2,3,4,4.5, 5,5.5,6,6.5,7,8,9,10,12,14,16,18,20,22.5,25,30];

% Go to Data Directory
cd('c:\Users\Marc\Documents\Graduate Studies\Research\Results');

% Loop through all geometries
for hole_size = 1:10

    switch hole_size
        case 1
            cd('.\Short_Hole\Base\data');
        case 2
            cd('..\..\Down\data');
        case 3
            cd('..\..\Up\data');
        case 4
            cd('..\..\Up_Down\data');
        case 5
            cd('..\..\Left_Right\data');
        case 6
            cd('..\Long_Hole\Base\data');
        case 7
            cd('..\..\Down\data');
        case 8
            cd('..\..\Up\data');
        case 9
            cd('..\..\Up_Down\data');
        case 10
```

```
    cd('..\..\Left_Right\data');
  otherwise
    disp('ERROR!!!');
end

% Evaluate all blowing ratios M=0.2, 0.5, 1.0, 1.5
for idx = 1:4

  % Define variables
  dummy = zeros(2,1);
  count = 0;
  non_garbage_lat =[];
  non_garbage_cl = [];
  garbage_cl = [];
  garbage_lat = [];
  cl_input = [];
  dummy_cl = 0;

  if idx < 3
    br = 'M_0';
  else
    br = 'M_';
  end

  % Read centreline input data
  cl_id = ['CL-', br, num2str(runs(idx)) '.txt'];
  start = 12*(hole_size-1) + idx + 2*(idx-1);
  cl_data = fopen(cl_id);
  garbage_cl = textscan(cl_data, '%s %s %s %s', 3);
  non_garbage_cl = textscan(cl_data, '%f %f');
  fclose(cl_data);
  cl_input(:,1) = ((non_garbage_cl{1,1})/D)-5.5;
  cl_input(:,2) = non_garbage_cl{1,2};

  % Organize and process centreline data
  for ct = 1:length(cl_input)
    if cl_input(ct,1) >= 0 && dummy_cl == 0
      dummy_cl = 1;
      cl_start(idx, hole_size) = ct;
      break;
    end
  end
  cl_end(idx, hole_size) = length(cl_input);
  cl_dat(1:length(cl_input), start) = cl_input(:,1);
  cl_dat(1:length(cl_input), start+1) = cl_input(:,2);
  cl_dat(1:length(cl_input), start+2) = (T_h - cl_dat(1:length(cl_input), start+1))/(T_h - T_c);

  % Read, organize, and process lateral data
  while (count < length(lat_loc))
    lat_dat = [];
    count = count +1;
```

```
        lat_id = [br, num2str(runs(idx)) '-D', num2str(lat_loc(count)), '.txt'];
        lat_data = fopen(lat_id);
        garbage_lat = textscan(lat_data, '%s %s %s %s', 3);
        non_garbage_lat = textscan(cl_data, '%f %f');
        fclose(lat_data);

        lat_dat(:,1) = ((non_garbage_lat{1,1})/D);
        lat_dat(:,2) = non_garbage_lat{1,2};
        lat_dat(:, 3) = (T_h - lat_dat(:, 2))/(T_h-T_c);
        lat_avg(count, start) = lat_loc(count)-5.5;
        lat_avg(count, start + 1) = trapz(lat_dat(:,1), lat_dat(:,3))/(3);
    end
    lat_start(idx, hole_size) = 6;
    lat_end(idx, hole_size) = 21;
end

% Plot long and short hole results
if hole_size == 5 || hole_size == 10
    cd('..\..');

    % Separate long and short hole studies
    if hole_size == 5
        offset = 0;
        index = 0;
        hole_type = 'SH';
    else
        offset = 60;
        index = 5;
        hole_type = 'LH';
    end

    % Plot M=0.2 Centreline Effectiveness
    figure;
    plot(cl_dat(cl_start(1,1+index):cl_end(1,1+index), 1+offset), cl_dat(cl_start(1,1+index):cl_end(1,1+index),
3+offset), '.k');
    hold on;
    plot(cl_dat(cl_start(1,2+index):cl_end(1,2+index), 13+offset), cl_dat(cl_start(1,2+index):cl_end(1,2+index),
15+offset), '-b');
    plot(cl_dat(cl_start(1,3+index):cl_end(1,3+index), 25+offset), cl_dat(cl_start(1,3+index):cl_end(1,3+index),
27+offset), '-.r');
    plot(cl_dat(cl_start(1,4+index):cl_end(1,4+index), 37+offset), cl_dat(cl_start(1,4+index):cl_end(1,4+index),
39+offset), '--g');
    plot(cl_dat(cl_start(1,5+index):cl_end(1,5+index), 49+offset), cl_dat(cl_start(1,5+index):cl_end(1,5+index),
51+offset), ':k');
    xlabel('x/D', 'FontSize', 12); ylabel('Centre-Line Effectiveness', 'FontSize', 12); legend('Single Hole',
'Downstream', 'Upstream', 'Up/Downstream', 'Left/Right', 'FontSize', 12);
    save_name = [hole_type, '-CL-M_020.png'];
    saveas(gcf, save_name);
    close

    % Plot M=0.5 Centreline Effectiveness
```

```
    figure;
    plot(cl_dat(cl_start(2,1+index):cl_end(2,1+index), 4+offset), cl_dat(cl_start(2,1+index):cl_end(2,1+index),
6+offset), '.k');
    hold on;
    plot(cl_dat(cl_start(2,2+index):cl_end(2,2+index), 16+offset), cl_dat(cl_start(2,2+index):cl_end(2,2+index),
18+offset), '-b');
    plot(cl_dat(cl_start(2,3+index):cl_end(2,3+index), 28+offset), cl_dat(cl_start(2,3+index):cl_end(2,3+index),
30+offset), '-.r');
    plot(cl_dat(cl_start(2,4+index):cl_end(2,4+index), 40+offset), cl_dat(cl_start(2,4+index):cl_end(2,4+index),
42+offset), '--g');
    plot(cl_dat(cl_start(2,5+index):cl_end(2,5+index), 52+offset), cl_dat(cl_start(2,5+index):cl_end(2,5+index),
54+offset), ':k');
    xlabel('x/D', 'FontSize', 12); ylabel('Centre-Line Effectiveness', 'FontSize', 12); legend('Single Hole',
'Downstream', 'Upstream', 'Up/Downstream', 'Left/Right', 'FontSize', 12);
    save_name = [hole_type, '-CL-M_050.png'];
    saveas(gcf, save_name);
    close

    % Plot M=1.0 Centreline Effectiveness
    figure;
    plot(cl_dat(cl_start(3,1+index):cl_end(3,1+index), 7+offset), cl_dat(cl_start(3,1+index):cl_end(3,1+index),
9+offset), '.k');
    hold on;
    plot(cl_dat(cl_start(3,2+index):cl_end(3,2+index), 19+offset), cl_dat(cl_start(3,2+index):cl_end(3,2+index),
21+offset), '-b');
    plot(cl_dat(cl_start(3,3+index):cl_end(3,3+index), 31+offset), cl_dat(cl_start(3,3+index):cl_end(3,3+index),
33+offset), '-.r');
    plot(cl_dat(cl_start(3,4+index):cl_end(3,4+index), 43+offset), cl_dat(cl_start(3,4+index):cl_end(3,4+index),
45+offset), '--g');
    plot(cl_dat(cl_start(3,5+index):cl_end(3,5+index), 55+offset), cl_dat(cl_start(3,5+index):cl_end(3,5+index),
57+offset), ':k');
    xlabel('x/D', 'FontSize', 12); ylabel('Centre-Line Effectiveness', 'FontSize', 12); legend('Single Hole',
'Downstream', 'Upstream', 'Up/Downstream', 'Left/Right', 'FontSize', 12);
    save_name = [hole_type, '-CL-M_100.png'];
    saveas(gcf, save_name);
    close

    % Plot M=1.5 Centreline Effectiveness
    figure;
    plot(cl_dat(cl_start(4,1+index):cl_end(4,1+index), 10+offset), cl_dat(cl_start(4,1+index):cl_end(4,1+index),
12+offset), '.k');
    hold on;
    plot(cl_dat(cl_start(4,2+index):cl_end(4,2+index), 22+offset), cl_dat(cl_start(4,2+index):cl_end(4,2+index),
24+offset), '-b');
    plot(cl_dat(cl_start(4,3+index):cl_end(4,3+index), 34+offset), cl_dat(cl_start(4,3+index):cl_end(4,3+index),
36+offset), '-.r');
    plot(cl_dat(cl_start(4,4+index):cl_end(4,4+index), 46+offset), cl_dat(cl_start(4,4+index):cl_end(4,4+index),
48+offset), '--g');
    plot(cl_dat(cl_start(4,5+index):cl_end(4,5+index), 58+offset), cl_dat(cl_start(4,5+index):cl_end(4,5+index),
60+offset), ':k');
    xlabel('x/D', 'FontSize', 12); ylabel('Centre-Line Effectiveness', 'FontSize', 12); legend('Single Hole',
'Downstream', 'Upstream', 'Up/Downstream', 'Left/Right', 'FontSize', 12);
```

```
    save_name = [hole_type, '-CL-M_150.png'];
    saveas(gcf, save_name);
    close

    % Plot M=0.2 Laterally Averaged Effectiveness
    figure;
    plot(lat_avg(lat_start(1,1+index):lat_end(1,1+index), 1+offset),
lat_avg(lat_start(1,1+index):lat_end(1,1+index), 2+offset), '.k');
    hold on;
    plot(lat_avg(lat_start(1,2+index):lat_end(1,2+index), 13+offset),
lat_avg(lat_start(1,2+index):lat_end(1,2+index), 14+offset), '-b');
    plot(lat_avg(lat_start(1,3+index):lat_end(1,3+index), 25+offset),
lat_avg(lat_start(1,3+index):lat_end(1,3+index), 26+offset), '-.r');
    plot(lat_avg(lat_start(1,4+index):lat_end(1,4+index), 37+offset),
lat_avg(lat_start(1,4+index):lat_end(1,4+index), 38+offset), '--g');
    plot(lat_avg(lat_start(1,5+index):lat_end(1,5+index), 49+offset),
lat_avg(lat_start(1,5+index):lat_end(1,5+index), 50+offset), ':k');
    xlabel('x/D', 'FontSize', 12); ylabel('Laterally Averaged Effectiveness', 'FontSize', 12); legend('Single Hole',
'Downstream', 'Upstream', 'Up/Downstream', 'Left/Right', 'FontSize', 12);
    save_name = [hole_type, '-LAT-M_020.png'];
    saveas(gcf, save_name);
    close

    % Plot M=0.5 Laterally Averaged Effectiveness
    figure;
    plot(lat_avg(lat_start(2,1+index):lat_end(2,1+index), 4+offset),
lat_avg(lat_start(2,1+index):lat_end(2,1+index), 5+offset), '.k');
    hold on;
    plot(lat_avg(lat_start(2,2+index):lat_end(2,2+index), 16+offset),
lat_avg(lat_start(2,2+index):lat_end(2,2+index), 17+offset), '-b');
    plot(lat_avg(lat_start(2,3+index):lat_end(2,3+index), 28+offset),
lat_avg(lat_start(2,3+index):lat_end(2,3+index), 29+offset), '-.r');
    plot(lat_avg(lat_start(2,4+index):lat_end(2,4+index), 40+offset),
lat_avg(lat_start(2,4+index):lat_end(2,4+index), 41+offset), '--g');
    plot(lat_avg(lat_start(2,5+index):lat_end(2,5+index), 52+offset),
lat_avg(lat_start(2,5+index):lat_end(2,5+index), 53+offset), ':k');
    xlabel('x/D', 'FontSize', 12); ylabel('Laterally Averaged Effectiveness', 'FontSize', 12); legend('Single Hole',
'Downstream', 'Upstream', 'Up/Downstream', 'Left/Right', 'FontSize', 12);
    save_name = [hole_type, '-LAT-M_050.png'];
    saveas(gcf, save_name);
    close

    % Plot M=1.0 Laterally Averaged Effectiveness
    figure;
    plot(lat_avg(lat_start(3,1+index):lat_end(3,1+index), 7+offset),
lat_avg(lat_start(3,1+index):lat_end(3,1+index), 8+offset), '.k');
    hold on;
    plot(lat_avg(lat_start(3,2+index):lat_end(3,2+index), 19+offset),
lat_avg(lat_start(3,2+index):lat_end(3,2+index), 20+offset), '-b');
    plot(lat_avg(lat_start(3,3+index):lat_end(3,3+index), 31+offset),
lat_avg(lat_start(3,3+index):lat_end(3,3+index), 32+offset), '-.r');
```

```
        plot(lat_avg(lat_start(3,4+index):lat_end(3,4+index), 43+offset),
lat_avg(lat_start(3,4+index):lat_end(3,4+index), 44+offset), '--g');
        plot(lat_avg(lat_start(3,5+index):lat_end(3,5+index), 55+offset),
lat_avg(lat_start(3,5+index):lat_end(3,5+index), 56+offset), ':k');
        xlabel('x/D', 'FontSize', 12); ylabel('Laterally Averaged Effectiveness', 'FontSize', 12); legend('Single Hole',
'Downstream', 'Upstream', 'Up/Downstream', 'Left/Right', 'FontSize', 12);
        save_name = [hole_type, '-LAT-M_100.png'];
        saveas(gcf, save_name);
        close

        % Plot M=1.5 Laterally Averaged Effectiveness
        figure;
        plot(lat_avg(lat_start(4,1+index):lat_end(4,1+index), 10+offset),
lat_avg(lat_start(4,1+index):lat_end(4,1+index), 11+offset), '.k');
        hold on;
        plot(lat_avg(lat_start(4,2+index):lat_end(4,2+index), 22+offset),
lat_avg(lat_start(4,2+index):lat_end(4,2+index), 23+offset), '-b');
        plot(lat_avg(lat_start(4,3+index):lat_end(4,3+index), 34+offset),
lat_avg(lat_start(4,3+index):lat_end(4,3+index), 35+offset), '-.r');
        plot(lat_avg(lat_start(4,4+index):lat_end(4,4+index), 46+offset),
lat_avg(lat_start(4,4+index):lat_end(4,4+index), 47+offset), '--g');
        plot(lat_avg(lat_start(4,5+index):lat_end(4,5+index), 58+offset),
lat_avg(lat_start(4,5+index):lat_end(4,5+index), 59+offset), ':k');
        xlabel('x/D', 'FontSize', 12); ylabel('Laterally Averaged Effectiveness', 'FontSize', 12); legend('Single Hole',
'Downstream', 'Upstream', 'Up/Downstream', 'Left/Right', 'FontSize', 12);
        save_name = [hole_type, '-LAT-M_150.png'];
        saveas(gcf, save_name);
        close
    end
end

% Return to root directory
cd C:\
cd('.\Users\Marc\Documents\Graduate Studies\Research\MATLAB Code');
```

References

[1] Ely M, Jubran B.A. (2008) A Numerical Study on Improving Film Cooling Performance Through the Use of Sister Holes. Proc. ASME Turbo Expo 2008, GT2008-50366

[2] Ely M, Jubran B.A. (2009) A Numerical Study on Improving Large Angle Film Cooling Through the Use of Sister Holes. Num Heat Transf: Part A (Accepted)

[3] Ely M, Jubran B.A. (2009/2010) A Numerical Evaluation on the Effect of Sister Holes on Film Cooling and the Surrounding Flow Field. Heat and Mass Transf (Awaiting Reviewers Comments)

[4] Bogard D, Thole K (2006) Gas Turbine Film Cooling. J Propulsion Power 22:249-270

[5] Sargison J, Oldfield M, Guo S, Lock G, Rawlinson A (2005) Flow Visualizations of the External Flow from a Converging Slot-Hole Film Cooling Geometry. Exp Fluids 38:304-318

[6] Jia R, Sundén B Miron P, Léger B (2005) A Numerical and Experimental Investigation of the Slot Film-Cooling Jet With Various Angles. J. Turbomachinery 127:635-645

[7] Gartshore I, Salcudean M, Hassan I (2001) Film Cooling Injection Hole Geometry: Hole Shape Comparison for Compound Cooling Orientation. AIAA Journal 39:1493-1499

[8] Yuen C, Martinez-Botas R (2003) Film Cooling Characteristics of a Single Round Hole at Various Streamwise Angles in a Crossflow: Part I Effectiveness. Heat Mass Transf 46:221-235

[9] Kohli A, Bogard D (1997) Adiabatic Effectiveness, Thermal Fields, and Velocity Fields for Film Cooling with Large Angle Injection. J. Turbomachinery 119:352-358

[10] Nasir H, Ekkad S, Acharya S (2001) Effect of Compound Angle Injection on Flat Surface Film Cooling with Large Streamwise Injection Angle. Exp. Thermal Fluid Science 25:23-29

[11] Ahn J, Jung I, Lee J (2002) Film Cooling from Two Rows of Holes with Opposite Orientation Angles: Injection Behavior and Adiabatic Film Cooling Effectiveness. Int. J. Heat Fluid Flow 24:91-99

[12] Sargison J, Oldfield M, Guo S, Lock G, Rawlinson A (2005) Flow Visualizations of the External Flow from a Converging Slot-Hole Film Cooling Geometry. Exp. Fluids 38:304-318

[13] Baheri S, Alavi-Tabrizi S.P., Jubran B.A. (2007) Film Cooling Effectiveness from Trenched Shaped and Compound Holes. Heat Mass Transf 44:989-998

[14] Kanani H, Shams M, Ebrahimi R, Ahmadian T (2008) Numerical Simulation of Film Cooling Effectiveness on a Flat Plate. Int. J. Numer. Meth. Fluids 56:1329-1336

[15] Bell C, Hamakawa H, Ligrani P (2000) Film Cooling from Shaped Holes. J. Heat Transf 122:224-232

[16] Roy S (2000) Numerical Investigation of the Blade Cooling Effect Generated by Multiple Jets Issuing at an Angle into an Incompressible Horizontal Crossflow. Num. Heat Transf: Part A 38:701-718

[17] Javadi A, Javadi K, Taeibi-Rahni M, Darbandi M (2003) A New Approach to Improve Film Cooling Effectiveness Using Combined Jets. Proc. Int. Gas Turbine Congress 2003.

[18] Javadi K, Taeibi-Rahni M, Darbandi M (2007) Jet-into-Crossflow Boundary Layer Control: Innovation in Gas Turbine Blade Cooling. AIAA Journal 45:2910-2925

[19] Dhungel A (2007) Film Cooling From a Row of Holes Supplemented with Anti-Vortex Holes. Master's Thesis, Louisiana State University, Baton Rouge, LA

[20] Heidmann D (2008) A Numerical Study of Anti-Vortex Film Cooling Designs at High Blowing Ratio. Proc. ASME Turbo Expo 2008, GT2008-50845

[21] Kusterer K, Bohn D, Sugimoto T, Tanaka R (2007) Double-Jet Ejection of Cooling Air for Improved Film Cooling. J. Turbomachinery 29:809-815

[22] Kusterer K, Bohn D, Sugimoto T (2008) Double-Jet Film-Cooling for Highly Efficient Film-Cooling with Low Blowing Ratios. Proc. ASME Turbo Expo 2008, GT2008-50073

[23] Burd S, Simon T (1997) The Influence of Coolant Supply Plenum Geometry on Coolant Exit Flow and Surface Adiabatic Effectiveness. Proc. ASME Turbo Expo 1997 97-GT-25

[24] Lutum E, Johnson B (1999) Influence of the Hole Length-to-Diameter Ratio on Film Cooling With Cylindrical Holes. J. Turbomachinery 121:209-216

[25] Goldstein R, Eckert E, Burggraf F (1974) Effects of Hole Geometry and Density on Three-Dimensional Film Cooling. Heat Mass Transf 17:595-607

[26] Azzi A, Jubran B.A. (2003) Numerical Modeling of Film Cooling from Short Length Stream-Wise Injection Holes. Heat Mass Transf 39:344-353

[27] Bergeles G, Gosman A.D., Launder, B.E (1978) The Turbulent Jet in a Cross Stream at Low Injection Rates: A Three-Dimensional Numerical Treatment. Num. Heat Transf 1:217-242

[28] Hale C (1999) An Experimental and Numerical Study of the Hydrodynamics and Surface Heat Transfer Associated with Short Film Cooling Holes Fed By a Narrow Plenum. PhD Dissertation, Purdue University, West Lafayette, IN

[29] Plesniak M (2006) Noncanonical Short Hole Jets-in-Crossflow for Turbine Film Cooling. J. Applied Mechanics 73:474-482

[30] Peterson S, Plesniak M (2002) Short-Hole Jet-in-Crossflow Velocity Field and its Relationship to Film-Cooling Performance. Exp. Fluids 33: 889-898

[31] Peterson S, Plesniak M (2004) Evolution of Jets Emanating From Short Holes into Crossflow. J. Fluid Mechanics 53: 57-91

[32] Harrington M, McWaters M, Bogard D, Lemmon C, Thole K (2001) Full-Coverage Film Cooling with

Short Normal Injection Holes. J. Turbomachinery 123:798-805

[33] Kurosaka M (1997) Contoured Holes for Film Cooling: The Effect of Kidney-Shaped Vortices. Technical Report, University of Washington, Seattle, WA

[34]Bernsdorf S, Rose M, Abhari R (2006) Modeling of Film Cooling – Part I: Experimental Study of Flow Structure. J. Turbomachinery 128:141-149

[35] Mayhew J, Baughn J, Byerley A (2003) The Effect of Freestream Turbulence on Film Cooling Adiabatic Effectiveness. Int. J. Heat Fluid Flow 24:669-679

[36] Kapadia S, Roy S, Heidmann J (2003) Detached Eddy Simulation of Turbine Blade Cooling. Proc. 36th Thermophysics Conf, AIAA-2003-3632

[37] Acharya S, Tyagi M, Hoda A, Muldoon F, From RANS to DNS: Application to Film Cooling. Louisiana State University, Baton Rouge, LA

[38] Wilcox D (2006) Turbulence Modeling for CFD. 3rd Ed. Chap 4, DCW Industries, La Cañada

[39] Muldoon F, Acharya S (2004) Direct numerical Simulation of a Film Cooling Jet. Proc ASME Turbo Expo 2004, GT2004-53502

[40] Kalita K, Dewan A, Dass A (2002) Prediction of Turbulent Plane Jet in Crossflow. Num. Heat Transf: Part A 41:101-111

[41] Ajersch P, Zhou J, Ketler S, Salcudean M, Gartshore, I (1997) Multiple Jets in a Crossflow: Detailed Measurements and Numerical Simulations. J. Turbomachinery 119:330-342

[42] Iourokina I, Lele S (2006) Large Eddy Simulation of Film-Cooling Above the Flat Surface with a Large Plenum and Short Exit Holes. Proc. 44th AIAA Aerospace Sciences Meeting and Exhibit, AIAA 2006-1102

[43] Shih T, Liou W, Shabbir A, Yang Z, Zhu J (1995) A New k-ε Eddy-Viscosity Model for High Reynolds Number Turbulent Flows – Model Development and Validation. Computers Fluids 24:227-238

[44] Harrison, K.; Bogard, D.; (2008) Comparison of RANS Turbulence Models for Prediction of Film Cooling Performance, ASME Turbo Expo 2008, GT2008-51423

[45] Roy S, Kapadia S, Heidmann J (2003) Film Cooling Analysis Using DES Turbulence Model. Proc. ASME Turbo Expo 2003, GT-2003-38140

[46] Leylek J, Zerkle R (1994) Discrete-Jet Film Cooling: A Comparison of Computational Results with Experiments. J. Turbomachinery 116:358-368

[47] Thole K, Sinha A, Bogard D, Crawford M (1992) Mean Temperature Measurement of Jets with a Crossflow for Gas Turbine Film Cooling Applications. Rotation machinery Transport Flow Phenomena 69-85

[48] Sinha A, Bogard D, Crawford N (1991) Film Cooling Effectiveness Downstream of a Single Row of Holes with Variable Density Ratio. J. Turbomachinery 113:442-449

[49] Yavuzkurt S, Habte M (2008) Effects of Computational Grid on Performance of Two-Equation Models of Turbulence for Film Cooling Applications, ASME Turbo Expo 2008, GT2008-50153

[50] Launder B, Spalding D (1972) Mathematical Models of Turbulence. Academic Press, London

[51] FLUENT Inc. (2003) Fluent 6.1 Users Guide. FLUENT Inc., Lebanon, NH

[52] Versteeg H, Malalasekera W (1995) An Introduction to Computational Fluid Dynamics: The Finite Volume Method. Longman Scientific & Technical, Essex, England

[53] ANSYS (2009) ANSYS FLUENT flow Modeling Software.
Accessible at: http://www.ansys.com/products/fluid-dynamics/fluent/

[54] Lu Y (2007) Effect of Hole Configurations on Film Cooling From Cylindrical Inclined Holes for the Application to Gas Turbine Blades. PhD Dissertations, Louisiana State University, Baton Rouge, LA

[55] Nemdili F, Abbes A, Theodoridis G, Jubran B (2008) Reynolds Stress Transport Modeling of Film Cooling at the Leading Edge of a Symmetrical Turbine Blade Model. J. Heat Transf. Engineering 29:950-960

[56] Na S, Shih T (2007) Increasing Adiabatic Film-Cooling Effectiveness by Using an Upstream Ramp. J. Heat Transf. 129:464-471